POLITECNICO DI TORINO

Master's Degree in Mechatronic Engineering

High-fidelity modelling of a fuel cell system for shipping industry

Supervisors

prof. Stefano MAURO

prof. Mauro BONFANTI

prof. Matteo MELCHIORRE

Candidate

Alessandro BRUSASCO

A.A. 2023-2024

Acknowledgements

"I want to thank me for believing in me, I want to thank me for doing all this hard work. I wanna thank me for having no days off. I wanna thank me for never quitting." Cit. Snoop Dog. Jokes aside, a special thanks goes to my entire family and my dearest friends who have supported me throughout my university journey. I am incredibly grateful for their unwavering encouragement and belief in me every step of the way. I would also like to express my gratitude to my thesis supervisor, Mauro Bonfanti, for his invaluable guidance and support in the completion of this thesis.

	Break-even point [Years]
Venetian scenario	1,7
Napoli-Ischia scenario	7,3

Abstract

In recent years, both gasoline and diesel engines dominated the maritime sector, having the complete control of the market at any type boat level. Nowadays, the greenhouse gases and pollutant emissions have become significant issues that must be addressed. In this regard, many renewable energy sources have been proposed in order to reduce our dependency on fossil fuels. Among these, the hydrogen-powered fuel cells are definitely a promising solution, due to their zero emissions. This thesis aims to propose an high-fidelity and high-speed modelling of a fuel cell system for shipping industry. In particular, it's modelled an hydrogen-propelled Proton Exchange Membrane (PEM) Fuel Cell with all the auxiliary components that are essential for a correct operation. The hydrogen is stored in a pressurized tank and through a pressure-reducing valve it flows up to the anode gas channels of the fuel cell. Hydrogen reacts with the oxygen of the air, that is drawn by a compressor and then fed to the fuel cell. In order to improve the performance and the efficiency of the system, a moisture humidifier is considered on both anode and cathode side. Finally, a cooling system maintains the suitable fuel cell temperature. The whole system is modelled on MATLAB© and Simulink environment. To validate the model, are carried a thousand simulations in which is compared the model with the PEM Fuel Cell Simscape™ model proposed by Mathworks, Inc. Specifically, the comparison is conducted on all the relevant quantities that govern the system operation. Thus, is performed an error analysis and a performance evaluation of the model. Moreover, it's shown that the proposed model is able to provide very similar result but with a simulation time that is drastically reduced and a easier parameters handling and design changing. Finally, as the model has been validated, are presented possible maritime scenario in which a PEM fuel cell can be adopted as primary energy source. The purpose is to verify which is the most adequate situation for exploiting a fuel cell. This is executed by taking into account several technical factor as fuel cell dynamics, power required, hydrogen consumed and hydrogen refueling. Thus, is provided a straightforward economical analysis on the feasibility of employing a fuel cell for a certain ship route rather than another one.

Contents

List of Tables

List of Figures

Chapter 1

Introduction

1.1 Fuel Cells: a brief overview

The modern technological initiatives require innovative energy frameworks for the progress of our society. A new energy infrastructure is needed in order to improve energy access, economic growth, and to meet current environmental policies. Unfortunately, the most of energy demand is compensated with nonrenewable energy sources, i.e. coal, oil and natural gas[28]. Is required a new power source that is energy efficient, has an unlimited and renewable fuel supply and has low pollutant missions.

One promising possible solution are the Fuel Cells. Their commercialization is still in its dawns, but many different applications already exist and the results fulfill the expectations[31].

A Fuel Cell is an electrochemical device that exploits the oxidation of a fuel to produce DC electricity. Many fuel can be adopted in a fuel cell and they all share the same characteristic of reacting with an oxidant, the oxygen. The products are electricity, heat and reaction compound.

The electrochemical reactions occurs between an oxidizing side (anode) and a reduction side (cathode). The newly generated electron flow is carried by an

external circuit, while between the anode and cathode are transported the ions through an electrolyte. All these form a cell. To improve the generated power, many cell can be connected in series to form a stack.

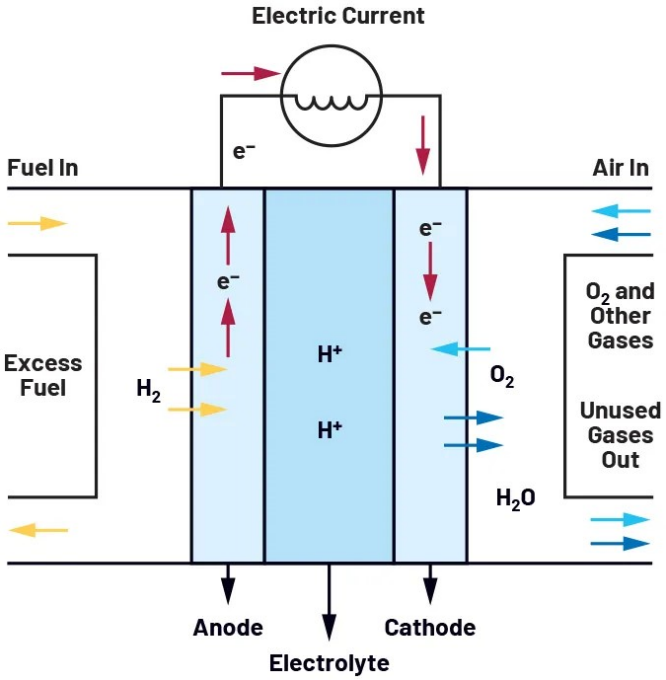

Figure 1.1: General fuel cell scheme

The type of electrolyte strongly depends on the type of fuel used. In fact, exist many different combination of fuel and electrolyte that can be adopted, each with its own characteristics, specific power, operating temperature and efficiency. However, most of fuel cells effectively runs on hydrogen, thanks to its fast oxidation kinetics[36].

According to the type and the nominal power of a fuel cell, some auxiliary components are needed for a proper operation of the FC. These component are referred to as *balance of plant* (BoP). They occupy a big portion of the overall system and are:

- Cooling system. Necessary for large application in which significant amount of heat must be exchanged;

- Humidifiers. In most applications the electrolyte membrane between anode and cathode must be humidified to promote the ions exchange. Humidifiers can be placed on the anode, cathode or on both side;

- Compressor. The oxygen flow coming in the cathode gas channels must be continuous and pressurized, so a compressor is necessary to maintain the correct air supply;

- Power conditioning. The electrical output of a fuel cell is DC power that may be adjusted according to the other devices (batteries or electric motor for example) connected to the line through DC/DC and DC/AC converters;

- Control systems. They are responsible for controlling variable of interest all over the components.

One possible project scheme of fuel cell stack with auxiliaries components it's depicted in figure 1.2.

Sometimes it's also present a fuel processor in the system. This allows to produce hydrogen starting from other fuels such as diesel, natural gas or methanol. Employing a fuel reformer increases cost and complexity, leading also to minor overall efficiency[36].

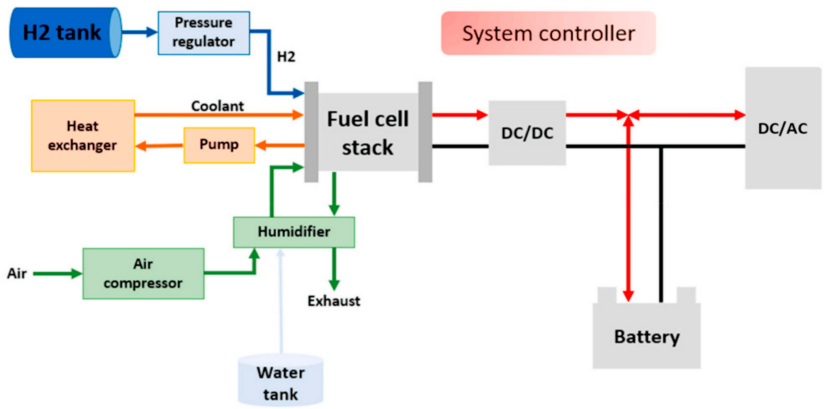

Figure 1.2: A possible scheme of fuel cell stack with auxiliaries components

Indeed, the hydrogen on the market is classified through colors, according to the source and the type of energy used to produce it. The existing types of hydrogen are reported in table 1.1[35]. Each has its own energy requirements and carbon footprint.

Hydrogen color code	**Hydrogen source**	**Energy source**
Black or Brown	Coal	Thermal
Gray	Natural gas	Thermal
Blue	Natural gas	Thermal
Turquoise	Methane	Thermal
Green	Water	Electricity (renewables)
Yellow	Water	Electricity (grid mix)
Purple	Water	Electricity (nuclear)
Pink	Water	Thermal + Electricity (nuclear)
Red	Water	Thermal (nuclear)
Aqua	Oil reservoirs	Thermal
White	Water	Thermal (solar)

Table 1.1: Hydrogen color codes and sources

1.1.1 Types of Fuel Cell

For what concerns types of Fuel Cells, they are commonly classified according to the kind of electrolyte placed between the electrodes. They differs in output power, operating temperature, start-up time and type of application. The most important are[25][29]:

- **Proton Exchange Membrane Fuel Cell (PEMFC).** It's a low-temperature fuel cell (50-100°C, typically around 80°C) with extraordinary features. It's characterised by high power densities and good transient performance. The

low temperature allows not strict material requirements and flexible operations, such as rapid start-up. They use only hydrogen as a fuel and waste products are water and heat, no hazardous material are released. The efficiency is around 50-70%, depending on the operating point. All this features make the PEMFC the most commecialised and promising among the fuel cell, suitable for portable high power devices. They are also called polymeric electrolyte membrane, since use a solid polymer membrane between the electrodes, the perfluorosulfonic acid or Nafion. The main disadvantages are the limited tolerance to impurities in the fuel and the relative high cost, since it's used platinum as catalyst due to the low operating temperatures;

- **Alkaline Fuel Cell (AFC).** They exploit solutions of alkaline metal such as NaOH or KOH in the membrane. These allow the cell to works in a wide range of temperature (100-250°C). Thus, also non precious metal can be used as catalyst reducing significantly the price of the fuel cell. They suffer of electrolyte poisoning, that is if CO_2 in the fuel or in the air reacts with the alkaline solution, the conductivity and so the efficiency drops drastically. Hence, a purification system is required.

- **Direct Methanol Fuel Cell (DMFC).** These fuel cells are another low temperature technology similar to PEMFC, about 50-100°C as operating temperature. The catalyst is made of platinum and ruthenium, since these fuel cells work directly with methanol, without any intermediate transformations. This makes easier handling and storing the fuel. However, they produce CO_2 as waste product and are characterised by low efficiency and power output;

- **High Temperature Proton Exchange Membrane Fuel Cell (HT-PEMFC).** These are a variant of PEMFCs that can work at higher temperatures, from 100 to 200°C. the Nafion of PEMFCs doesn't tolerate these temperatures and so it is replaced by others acid-based polymers. The big

advantage of high-temperature PEMFC is the better resistance to CO poisoning. As a consequence more types of hydrogen can be used;

- **Phosphoric Acid Fuel Cell (PAFC).** The name derives from the phosphoric acid used as electrolyte. They use platinum as catalyst and thanks to the working temperatures (150-200°C), they are not much sensitive to CO poisoning. This characteristic makes them suitable for the adoption of a reformer for producing H_2 starting from liquid natural gas (LNG) or methanol. Of course, this would produce greenhouse gas emissions. They are generally both large and heavy due to low power density;

- **Molten Carbonate Fuel Cell (MCFC).**. These use molten salts as carbonate of alkaline metal as electrolyte. Thus, in order to reach the best conductivity, these fuel cells must be warmed up to 600-700°C. Thanks to high temperatures, the employ of a heat recovery system is indicated to increase the overall efficiency. Moreover, the high temperatures and efficiency and the slow start up make them perfect for stationary applications, as in the energy production systems. They may use a wide range of fuels, since high temperature makes these cells tolerant to impurities;

- **Solid Oxide Fuel Cell (SOFC).** These are one of the most used high-temperature fuel cells. The temperatures are around 800-1000°C. As electrolyte, they make use of a solid-state ceramic. As the MCFCs, they can make use of a heat recovery systems, they run on different fuels by using a reformer and they can be used in power plants or in huge ship.

In table 1.2 are summarized these types of fuel cells and their characteristics[14].

As a conclusion, it worth noticing that this great variety of fuel cells makes possible to choose the most suitable one for the application desired, according to the characteristics of the fuel cell to be exploited. Considering marine applications, it's been made a ranking of the most suitable fuel cells[34], on the basis of different

criteria such as relative costs, power density, lifetime, safety aspect and more. In the evaluation, PEMFC, HT-PEMFC and SOFC received the highest scores and are considered to be the most promising fuel cell for the maritime sector.

FC type	**Operating temperature [°C]**	**Typical fuel**	**Electrical Efficiency**	**Power range [kW]**
PEMFC	80	H_2	50-70%	1-500
AFC	50-250	H_2	60-70%	10-200
DMFC	50-100	CH_4OH	20-30%	1-10
HT-PEMFC	100-200	H_2	50-60%	1-500
PAFC	150-200	H_2, LNG, CH_4OH	30-50%	50-1000
MCFC	600-700	H_2, LNG, C_xH_x	40-60%	10-1000
SOFC	700-1000	H_2, LNG, C_xH_x	50-60%	10-3000

Table 1.2: Main fuel cells technologies

1.2 Focus on PEM Fuel Cells

1.2.1 PEMFC stack structure

As already mentioned, the PEM fuel cell technology is the most promising among all. The studies and research projects on this type of fuel cell are a lot and can be found many different successful applications, such as transportation, portable electronic devices and distributed generation systems[14].

PEMFC is a low temperature fuel cell with operating temperatures around 80°C. They are characterized by great power density and efficiency. Thanks to the low temperatures, good transient performance are guaranteed, but costly catalysts are required to accelerate the reactions. They work with hydrogen and to improve the durability the fuel cell, it must be quite pure[29].

For what concerns the structure of a PEMFC, an exploded view is represented

in figure 1.3. It represent a stack, that is a certain number of fuel cells stacked in series. Stacking is necessary when speaking of FCs, as a single cell is able to create a very low voltage. For a PEMFC is less than 1.5 V. Thus, the cell are stacked in order to reach hundreds of volt.

A stack is formed by an alternation of two components:

- **Membrane Electrode Assembly (MEA);**
- **Bipolar Plates (BP).**

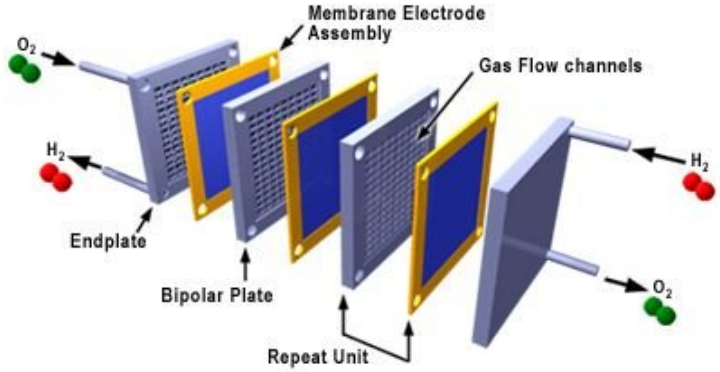

Figure 1.3: Exploded view of a PEMFC stack

The MEA represents the heart of a fuel cell. It's formed by different layers, each with its own function. Inside of it, the gas reactants diffuse and reach the electrodes. Here, they participate to the electrochemical reactions. The ions produced flow through the polymeric membrane and close the electrical circuit. In the next section the components of the MEA are seen in more details.

The bipolar plates are the most expensive and heavy components in a PEM fuel cell. BPs play different roles: first of all they act as separators between two unit cell and provide mechanical strength to the overall stack, moreover the plates are responsible for the transportation of reactants, product, electrons and heat among the cell. For this reason, the constituting material must have high thermal and electrical conductivity, it must be corrosion resistant and impermeable to the

flowing gases[16]. A commonly used material is the Graphite. However, many other materials are proposed that can ensure better mechanical properties such as carbon-based, metals and alloys[26].

As said, the bipolar plates constitute the flow field in which the reactants flow to reach the MEA. Its designing is fundamental for the cell efficiency, water balance, uniform reactant distribution and transport. Many flow field configurations have been proposed, such as parallel, serpentine, parallel-serpentine, interdigitated or pin-type[42], as shown in figure 1.4. It worth noticing that ad the edges of the stack the bipolar plates are replaced by two end plates.

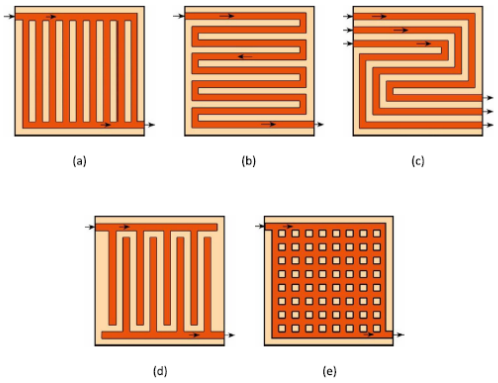

Figure 1.4: Proposed flow-field designs: (a) parallel, (b) serpentine, (c) parallel-serpentine, (d) interdigitated, and (e) pin-type.

Two other components are jointed with the bipolar plates, the current collector and the gaskets. The current collector provides the link between the electrodes and the external circuit, so they have to be characterized by high conductivity and stability. Titanium, aluminum, copper and stainless steel are usually used. Whereas, the gaskets are necessary in order to prevent leakages of reactants, products and coolants. Silicon or PTFE-based materials are suitable for this application[33].

1.2.2 Membrane Electrode Assembly

The membrane electrode assembly is composed of different layers that are "sandwiched" together, as shown in figure 1.5. These are:

- **Proton-exchange membrane**
- **Catalyst layers (CL)**
- **Gas diffusion layers (GDL)**
- **Microporous layer (MPL)**

The last three layer form together the two electrodes, i.e. anode and cathode. Here, the two half-reaction take places. In order to achieve as reaction sites as possible, the electrodes have to be highly porous, so that a large surface area-volume ratio in guaranteed. Indeed, in a PEMFC each reaction site is a three phase boundary (TPB) as shown in figure 1.6, in which gas, solid electrode and solid electrolyte meet each other and make possible the reactions begin[5]. In the gas phase occurs the exchange of gaseous reactants and products, in the solid electrolyte takes place the ions transport while the solid electrode exchanges free electrons.

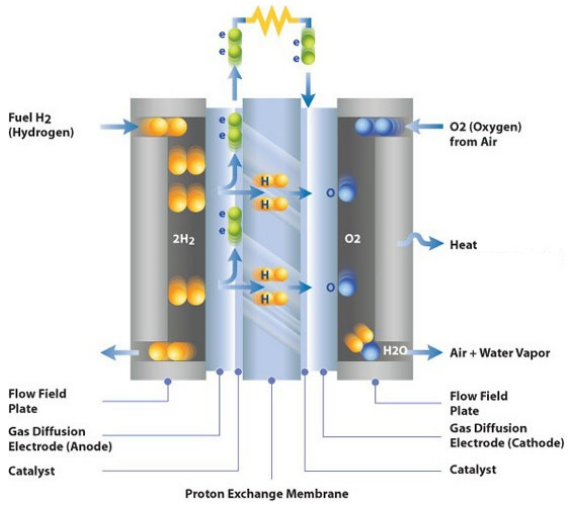

Figure 1.5: Representation of a single PEM cell

To create the highly porous structure of the electrodes, are usually employed carbon black particles (45-90 nm)[30]. They are characterised by good thermal and

electrical conductivity and corrosion resistance. By the way, to have a half-reaction kinetics fast enough, these particle must be coated with precious catalytic metals. The most used is platinum as catalyst, in particular nano-particle of platinum. They coat the surface of the carbon particle and their dimension is around 2-3 nm. This way, the reaction site's area in maximized[24]. This complex, highly porous and nano-sized structure represents the catalyst layer (CL). The overall thickness must be around 5-30 μm, in order to minimize the resistances.

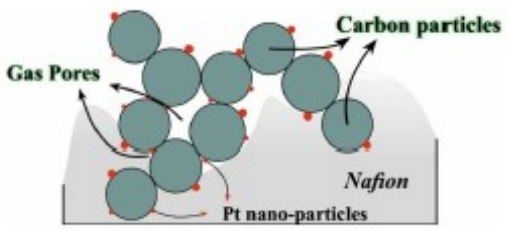

Figure 1.6: Three phase boundary of the nano-structured CL

As a consequence it's required another layer to provide the necessary mechanical strength, that is the gas diffusion layer (GDL). This layer must also be highly porous, permeable and electrical conductive. In fact, it is responsible for the gas diffusion from the flow field plates to the catalyst layer, it mediates the electron flow exchange and protects the CLs from corrosion. The thickness is around 100 μm and is usually made of carbon fiber-based materials[39].

In addition, in order to enhance the water management in both the electrodes and improve the adhesion of the two previous layers, are inserted between the CL and the GDL an highly hydrophobic microporous layers (MPL). It is made of a carbon and PTFE mixture[4].

Finally, between the anode and cathode catalyst layer is positioned the Proton-exchange membrane. The essential role of the membrane is to act as a separator between electrodes, allows the ions flow from anode to cathode and prevent electron transfer. Thus, the membrane material should have mechanical and chemical stability, restrict gas crossover, be a good insulator but at the same time have

high ionic conductivity[14].

The material used nowadays was invented by DuPont in 1967, that is the sulfonated polytetrafluorethylene (PFSA) or Nafion©[12]. The chemical structure is depicted in figure 1.7. This is a copolymer constituted by PTFE (main chain), sulfonic acid group (end chain) and perfluorinated (side chain). The PTFE act as hydrophobic backbone of the membrane while the hydrophilic sulfonic acid group are responsible for proton transfer. The presence of F-atoms along the chain provides higher mechanical and chemical stability, and increases the acidity of sulfonic acid group improving the proton conductivity[23].

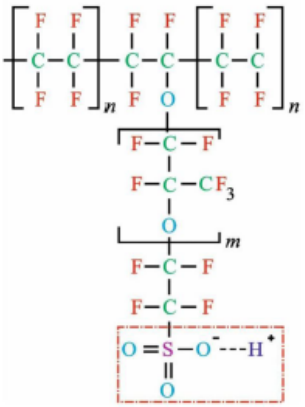

Figure 1.7: Chemical structure of PFSA

However, it's well known that the ions conductivity is mostly affected by the level of hydration of the membrane. A membrane with 100% of relative humidity exhibits the best conductivity, improving significantly the overall efficiency.

1.3 PEM fuel cells working principle

1.3.1 PEMFC Electrochemistry

This technology exploits the electrochemical reaction between H_2 and O_2 to form H_2O. This reaction involves the exchange of free electrons that flow into an external circuit. In particular, focusing on the anode side, the hydrogen flow

coming from the bipolar plates enters the GDL and diffuses up to the catalyst layer. Here, the platinum-based nanoparticles catalyze the anodic semi-reaction:

$$H_2 \longrightarrow 2\,H^+ + 2\,e^- \tag{1.1}$$

The electrons released by Eq. (1.1), by means of the GDL and the BPs flow into in the external circuit and than reach the cathode in order to participate to the cathodic semi-reaction. Meanwhile, the protons flow throughout the polymer membrane and reach the cathode, and here are reduced. A simple schematic is presented in figure 1.8.

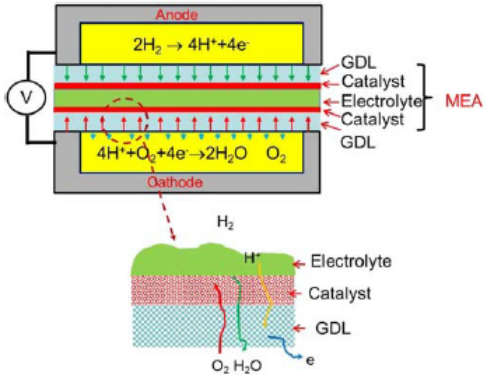

Figure 1.8: Gas diffusion and charge transfer in MEAs

Similarly, on the cathode side the incoming oxygen participates to the reduction semi-reaction to produce water:

$$\frac{1}{2}\,O_2 + 2\,H^+ + 2\,e^- \longrightarrow H_2O \tag{1.2}$$

The overall reaction is the following.

$$H_2 + \frac{1}{2}\,O_2 \longrightarrow H_2O \tag{1.3}$$

Each of the two semi-reactions creates a characteristic potential difference at the CL interface. The difference between these two potential gives the overall cell

potential.

To evaluate this potential, some energy consideration must be addressed. The maximum exploitable energy potential is represented by the Gibbs free energy, that for constant temperature is defined as:

$$\Delta G = \Delta H - T\Delta S \tag{1.4}$$

where T is the temperature, ΔS the entropy variation and ΔH is the enthalpy variation. Considering standard conditions (25°C and 1 atm), the produced water is liquid, hence $\Delta G = -237{,}32$ kJmol^{-1}.

For a constant pressure process, the free energy ΔG represents the maximum electrical work a fuel cell can provide:

$$W_{\text{elec}} = -\Delta G = nFE \tag{1.5}$$

in which E is the electrical potential difference, n is the number of exchanged electrons, 2 e$^-$ in this case, and F is the Faraday's constant equal to 96485 C/mol.

Therefore, starting from this equation can be retrieve the open circuit voltage (OCV) for standard conditions:

$$E^0 = -\frac{\Delta G}{nF} = 1.23V \tag{1.6}$$

This is the maximum theoretical potential that a PEMFC can achieve. In practical application, this potential is never reached due to losses that occur even at zero current[21]. Moreover, the temperature of the cell and the concentrations of reactants and products play a crucial role in changing the output potential. The Nernst's equation shows these correlations:

$$E = E^0 + \frac{RT}{2F} \ln\left(\frac{a_{H_2}\sqrt{a_{O_2}}}{a_{H_2O}}\right) \tag{1.7}$$

R is the universal gas constant and a_i are the activities of each component.

Furthermore, when the current flowing into the cell is not zero, different losses arise resulting in a voltage drop. These considerations are discussed deeply in the next chapter.

1.3.2 PEMFC Thermodynamics

The reaction of hydrogen and oxygen to form water is an exothermic reaction. This means that a certain amount of energy is released that is the reaction enthalpy $\Delta_r H$. This is equal to the water formation enthalpy $\Delta_f H$. Since the water is produced either as gaseous or liquid phase, two values are distinguished for standard conditions[15]:

$$\Delta_r H = \begin{cases} -241{,}8 \text{ kJ/mol} & \text{if } H_2O_{(g)} \\ -285.8 \text{ kJ/mol} & \text{if } H_2O_{(l)} \end{cases} \tag{1.8}$$

The enthalpy of reaction it's the total energy available from the chemical reaction. Yet, not all this energy can be exploited. Due to the irreversibility of the reaction, some of it it's lost in a change of the system entropy. The net useful energy is the Gibbs free energy, defined in eq. (1.4). At standard condition, the produced water is liquid, thus $\Delta G = -237{,}32 \text{ kJmol}^{-1}$.

Using these values, can be retrieved the theoretical fuel cell efficiency. It is defined as the ratio between the total available energy released by the electrochemical reaction, i.e. $\Delta_r H$, and the total output work, which according to eq. (1.5) is equal to ΔG. Therefore, the fuel cell efficiency is:

$$\eta = \frac{\Delta G}{\Delta H} \approx 83\% \tag{1.9}$$

As already mentioned, this is a theoretical efficiency since refers to an open circuit operation, and in standard conditions. In practical condition, the fuel cell efficiency drops due to all the rising losses as a current flows through it.

As a consequence, the actual efficiency of a fuel cell is evaluated defining the

ratio between the output electrical power and the total energy of the fuel. As said before, are distinguished two energy types depending on the state of the produced water. In case of liquid water, it's used the *higher heating value* of hydrogen (HHV). Instead, for water vapour is used the *lower heating value* (LHV). The HHV is the energy of the chemical reaction starting from 25 °C and ending at 25 °C. This implies that the latent heat of water vaporization is considered. In the LHV is not counted, instead.

Considering, a PEM fuel cell working at 80 °C is reasonable to use the HHV:

$$\eta = \frac{W_{\text{elec}}}{W_{\text{H}_2}} = \frac{I_{\text{stack}} V_{\text{stack}}}{n_{\text{H}_2} HHV} \tag{1.10}$$

Where, n_{H2} is the consumed hydrogen in mol/s.

1.4 Fuel Cells in maritime sector: State of Art

The maritime transportation sector is responsible for a significant portion of global greenhouse gas emissions. For this reason, reducing its carbon footprint has become a pressing issue.

According IEA data[**?**], the marine industry accounts for a 3% of the total global emissions, and it is increasing. Today, the 99% of the ships currently in operation use oil derived fuels for propulsion and onboard energy generation through huge internal combustion engines (ICEs). It's clear that this creates a considerable impact in terms of CO2, NO_x, SO_x and particulate matter emissions. For this reason, different strategies must be pursued, combining solution such as[**?**]:

- use of renewable energy sources;
- waste heat recovery for cogeneration and reduction of primary energy consuption;
- use of more energy efficient devices;
- use of alternative fuel with a lower emission impact.

An hydrogen Fuel Cell-based propulsion system is nowadays one of the most promising strategies able to deal with these issues. Indeed, H_2 fuel cells only have water as waste product, no greenhouse gases or pollutants are released. Another benefit of H_2 fuel cells is their efficiency, that is higher compared to the traditional propulsion systems. This means that more power is produced using the the same amount of fuel. Considering the huge drivelines that power marine vessels and ships, this would be a significant advantage for the shipping companies.

However, the adoption of hydrogen as a fuel brings relevant challenges to overcome. Hydrogen is a highly inflammable gas, which requires a special attention during its live cycle, from the production to the distribution and storage. The development of networks and infrastructures is needed to transport and store hydrogen on ships, but requires important investment and technological advancements.

Another issues is the safety related to hydrogen transport, handling and storage on a ship. This involves the employment of specialized personnel as well as the definition of protocols that standardize the hydrogen usage. Despite of these concerns, many successful projects of hydrogen fuel cells-powered vessels and ships can be found all around the world[9]. These involve usually fuel cell only or as part of a fuel cell-battery hybrid systems[36].

In table 1.3 are summed up the most relevant advantages of using H_2 Fuel Cells in maritime application[9].

Environmental benefits	Significant reduce of greenhouse gas emissions and pollutants. The only products are water and heat. Moreover, hydrogen is a renewable source that can be produced starting from electricity, natural gas or biomass.
Efficiency	Fuel Cells are more efficient and cost-effective that traditional engines. They convert directly chemical energy into electrical one, without the typical energy loss of the mechanical parts of an engine. This is surely essential in a world in which the waste of energy has become a crucial point.
Weight and space	Hydrogen Fuel Cells are lighter and take up less space than engines of the same power, making them an interesting alternative for small applications.
Improved reliability	Hydrogen Fuel Cells require less maintenance and are less susceptible to breakdowns than traditional engines. This means longer vessels up time with all the related benefits.
Noise and vibration reduction	Both noise and vibrations are minimized, since the working principle of a fuel cell itself is quiet and there are not present any rotating moving part.

Table 1.3: Most relevant advantages of Hydrogen Fuel Cells

As said before, using Fuel cells also has some issues that must be taken into account. The most relevant ones are listed in table 1.4.

Looking to the past and to the present of fuel cells-powered applications in the marine sector, may be found several different research projects applied to many ship types. They all have in common the use of fuel cells technologies, but exploiting different types of fuel cell or logistic fuel. Some are still employed, while others terminated their operations. Below are listed some relevant applications

Lack of infrastructure	Hydrogen refueling infrastructures are required to satisfy the fuel demand, but this means investing in production of hydrogen, storage and distribution facilities and logistics to support the fuel cells implementation.
Safety	Hydrogen is very dangerous if it is not handled with care. Any leakages, malfunctions or improper use may lead to catastrophic accidents. Thus, must be defined clear safety protocols and control systems in order to ensure safety.
Cost	Nowadays, use of hydrogen fuel cells is not affordable compared to the traditional technologies. Fuel Cell and hydrogen production is still not optimized for large scale commercialization, as well as the infrastructure are not sufficient. This lead to higher cost that curbs the growth of the fuel cell industry.
Limited range	Fuel Cell technology is not ready for long-distance or long-duration trips, since hydrogen is not able to provide the necessary energy density. It must be highly compressed or liquefied, with all the related problems.

Table 1.4: Most relevant disadvantages of Hydrogen Fuel Cells

that demonstrated the successfully employment of fuel cell technology. Are not considered those projects that have not already tested a fuel cell plant on a ship and are still working only on the powertrain.

The use of fuel cells for maritime applications began in the early 1980s with the development of PEMFC based AIP systems and finally the production of the Class 212 submarines by Howaldtswerke-Deutsche in 1998. So far, over thirty such submarines have been commissioned[34].

Moving to more recent years, it worth noticing that Norway became the leader in green shipping around the world. Since 2015, over 150 millions dollars were invested in marine fuel cells applications[38].

In 2003, was established a project named "FellowSHIP", in which a 320 kW, LNG-propelled MCFC was installed on-board of the "Viking Lady", an offshore supply vessel. The fuel cell propulsion run successfully for 18,500 hours.[38]. An imagine is presented in the figure 1.9

Figure 1.9: The offshore supply ship "Viking Lady"

A second important application was the 120-meter-long ferry "MF Hydra". It uses two 200 kW PEMFCs that run with liquefied hydrogen assisted by batteries and two diesel generators. It is still used in Norway for both passengers and goods shipping[35].

In 2006, was built the first inland-river tourist ship, the "FCS Alsterwasser". A 25.5 m long ship powered by two 48 kW PEMFCs and twelve hydrogen storage

tanks of 50 kg in total that was operated successfully for two seasons[10].

In another German project called "Pa-X-ell2", two 30 kW HT-PEMFC was adopted on a cruise ship named "MS Mariella". The fuel cells supply only a part of the requested power, but this attempt lays the foundation for using more powerful cells[17].

In 2006, the "METAPHU" project tested a 20 kW SOFC fueled with methanol on the car carrier "Undine". 5 month and 700 hours of operation validated the test and provided important basis of SOFC utilization[37].

In the Netherlands, the Dutch corporation Boat Amsterdam operated a canal cruise ship, the "Nemo H2". It is propelled with a 70 kW PEMFC system hybridised with a 55 kW lead acid battery pack. It can ship up to 87 passengers and has a lifetime of 9 h at cruise speed. Unfortunately, the lack of hydrogen refueling stations made impossible an active service[11].

In 2009, a 50 kW SOFC was integrated in the powertrain of the multipurpose cargo ship "MS Forester". Diesel was used as fuel and the fuel cell behaviour was good. In the following years, The leading project "SchiBZ" developed these fuel cells for operation with LNG[37].

In 2017, the project "Maranda" developed and tested a marine powertrain based on 2 x 82.5 kW PEMFC fuelled with hydrogen. These powered a research ship called Aranda, that operated in arctic conditions. The project was successful and overcame the problem of hydrogen infrastructure by adopting a mobile storage container which can be easily refueled[13].

An additional important European project is the "FLAGSHIP". The aims was to implement two zero emission cargo ship powered by fuel cell systems in France and Netherlands. The first ship, "ZULU", operated in France exploiting two 200 kW hydrogen PEM fuel cells. The other one employed a hybrid system composed of PEMFC and batteries[**?**].

Considering Italian projects, an interesting one is the "TecBIA" project. It succeeded in developing and testing the "ZEUS", a research vessel powered by two

71 kW PEMFC fueled by hydrogen hybridized with 150 kWh capacity batteries. The project, started in 2018, ended successfully in the summer of 2022, giving an interest in the PEMFC-battery hybridization[2].

Moving to US projects, it worth mentioning the "SF Breeze" project, launched in 2018. Eventually, in 2021 was built the "Sea Change", a 75 passengers ferry that used 3 x 120 kW PEMFC only, becoming the first commercial passenger ship that employs only PEMFCs in the world[8]. It is shown in figure 1.10

Figure 1.10: The passenger vessel "Sea Change"

There also exist fuel cell applications for small boat and the achieved result are interesting. One first example is the 30-meter-long yacht named "Energy Observer", that exploits a 22 kW PEMFC to navigate. At present, it is still sailing around the world[38].

A second one is the "Hydrogenia", a South Korean 10 meter long boat powered by PEMFC.

Finally, in may 2021 was unveiled the "HYNOVA 40", shown in figure 1.11. It exploits a PEMFC that delivers 70 kW power, able to move this 12 m and 12 passenger boat[8].

In table 1.5, all these mentioned applications are listed.

As can be seen above, in the first decades of the 21^{th} centuries occurred a significant increase in fuel cells applications. Both as research project and as real ships implementations. Many of these implementations are not on duty today,

Figure 1.11: The small boat "HYNOVA 40"

Ship Name	Project Name	Time Period	Fuel Cell type	Fuel Type	Application
-	Class 212	1980-1998	PEMFC	H_2	Submarine AIP
Viking Lady	FellowSHIP	2003-2018	MCFC	LNG	Offshore supply
MF Hydra	-	2020-present	PEMFC	Liquid H_2	Passengers ferry
Alsterwasser	ZEMSHIP	2006-2014	PEMFC	H_2	Inland passengers ship
MS Mariella	Pa-X-ell 2	2019-2022	HT-PEMFC	MEOH	Cruise ship
MV Undine	METAPHU	2006-2010	SOFC	MEOH	Car carrier
NEMO H_2	-	2009-2011	PEMFC	H_2	canal cruise ship
MS Forester	SchiBZ	2009-2018	SOFC	Diesel	Multipurpose ship
Aranda	Maranda	2017-2022	PEMFC	H_2	Arctic researcher
ZULU	FLAGSHIP	2019-present	PEMFC	H_2	Cargo ship
FPS Waal	FLAGSHIP	2019-present	PEMFC	H_2	Cargo ship
ZEUS	TecBIA	2018-2022	PEMFC	H_2	Research vessel
Sea Change	SF-BREEZE	2018-2022	PEMFC	H_2	Passengers ferry
Energy Observer	-	2017-present	PEMFC	H_2	Catamaran
Hydrogenia	-	2019-2021	PEMFC	H_2	Small boat
Hynova 40	-	2021-present	PEMFC	H_2	Small boat

Table 1.5: Some relevant marine applications of fuel cells technologies

but they has been experimentally tested and validated. The point was to prove that fuel cells can be employed in marine applications and that the technology is mature enough to be widely implemented all over round the world. However,

the fundamental problems is that there not exist the sufficient infrastructures to support hydrogen as a fuel, and that the fuel cell industry is not optimised yet for the global market.

Anyway, it's clear that PEMFC is the most mature technology. It has been tested in many different applications and conditions providing promising results. Moreover, the most used fuel is Hydrogen, since PEMFCs require this fuel. It worth noticing that in some application it's preferred to use other fuel such as LNG, MEOH or Diesel and exploit a reformer to produce hydrogen from them, as hydrogen handling and storing is still a challenging issues.

Chapter 2

PEM Fuel Cell Model

In this chapter is described the model of a Proton Exchange Membrane (PEM) fuel cell stack. Are presented all the equations that govern the operation of the cell and all the auxiliaries components (BOP).

These equation are then exploited to create a model of the PEMFC in MATLAB© and Simulink environment, in order to simulate its behaviour in different working conditions. In figure 2.1 is presented the overall scheme.

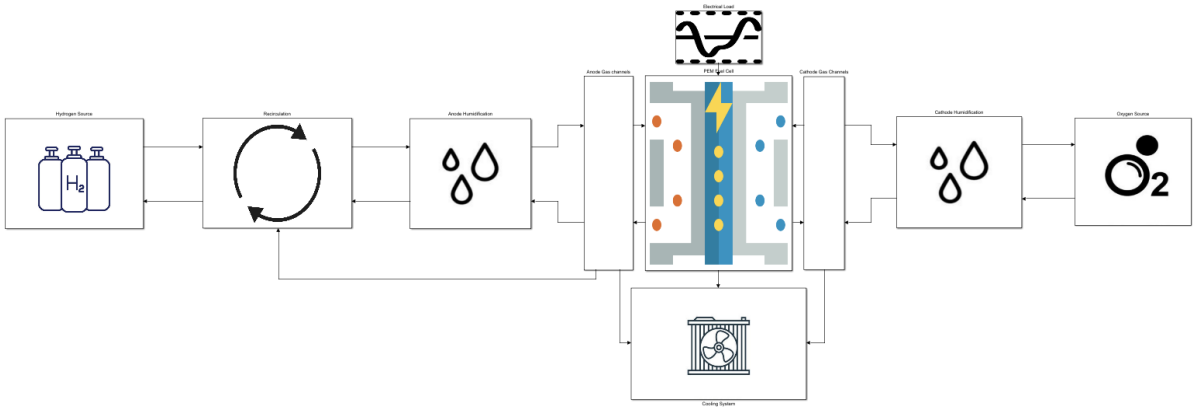

Figure 2.1: PEM Fuel Cell stack Simulink model

The building blocks are:

- **PEM Fuel Cell** → Equations of electrochemitry and thermodynamics of the fuel cell;
- **Hydrogen Source** → Hydrogen tank and pressure valve;
- **Recirculation** → Recirculation pipe;
- **Anode Humidification** → Humidification pipe and humidification control;
- **Anode Gas Channels**;
- **Cathode Gas Channels**;
- **Cathode Humidification** → Humidification pipe and humidification control;
- **Oxygen source** → Air intake and air compressor;
- **Cooling System** → Fuel cell coolant channels and radiator.

For this purpose, has been taken a case study of a 110 kW fuel cell stack. It is made of 400 unit cells. The hydrogen is stored into a 120 l fuel tank at a pressure of 70 MPa. A pressure valve connected to the tank and a back-pressure relief valve at the cathode exhaust are responsible for maintaining the pressure in the stack at around 0.16 MPa. The air compressor brings air into the stack at a controlled rate so that a predefined stoichiometric ratio in achieved. The consumed hydrogen at the anode is recirculated back so that the overall efficiency is increased.

The two humidifiers aims to bring the relative humidity as close as possible to 100%. Finally, the cooling system is responsible for keeping the operating temperature around 80 °C.

2.1 PEM Fuel Cell

In this section are presented all the equations that govern the working principles of a PEM fuel cell. From the voltage creation to the reactant utilization and the membrane's water management.

2.1.1 FC Voltage Model

As already mentioned in the introduction, the voltage produced by a fuel cell is defined by the Nernst's equation:

$$E = E^0 + \frac{RT}{2F} \ln\left(\frac{a_{H_2}\sqrt{a_{O_2}}}{a_{H_2O}}\right) \tag{2.1}$$

Where, E_0=1,23 V is the open circuit voltage, R is the universal gas constant, T is absolute stack temperature, F is the Faraday's constant and a_i are the activities of each component. For hydrogen and oxygen, $a_i = p_i/p_0$ where p_i is the gas partial pressure and p_0 is a reference pressure, i. e. environment pressure. For water, the activity is evaluated as the ratio of its partial pressure to the saturation pressure at T_{stack}[31].

As soon as the a current flow into a the cell, it's observed a voltage drop due to three types of losses: the activation losses, the concentration losses and the ohmic losses. In figure 2.2 is proposed a typical polarization curve of a PEM fuel cell. It's visible the voltage drop as the current increases and the three different contribution of the losses.

The first losses that are dominant at low current are the **Activation Losses.** They are the result of the inertia to start and maintain the reactions at the electrodes due to breaking a forming of chemical bonds. In fact, to overcome the reactions energy barrier is required an overpotential that is the activation polarization. This occurs both at anode and cathode[31].

These losses are described by the Tafel's equation:

$$V_{\text{act}} = \frac{RT}{2\alpha F} \ln\left(\frac{i_{\text{cell}}}{i_0}\right) \tag{2.2}$$

where i_{cell} is the fuel cell stack current density, α is the charge transfer coefficient that represents the velocity at which the electrons are transferred at the electrode-electrolyte interface. The exchange current density i_0 is the current that flows equally in both directions.

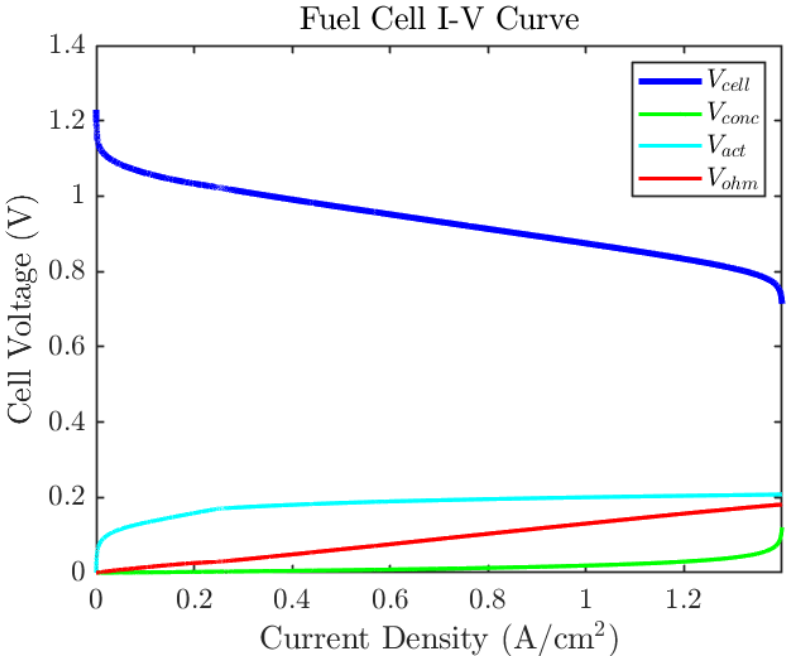

Figure 2.2: General Fuel Cell Polarization curve

The second type of losses are the **Concentration Losses**. As the reactants are consumed at the electrodes, a change in concentrations is recorded leading to a drop in partial pressures. This affects the cell voltage (eq. (2.1)) and the voltage reduction can be calculated using[22]:

$$V_{\text{conc}} = \frac{RT}{2F} \ln\left(1 - \frac{i_{\text{cell}}}{i_L}\right) \tag{2.3}$$

in which, i_L is the max limiting current density, at which the voltage drop drastically.

These losses become relevant at high current density as shown in figure 2.2, where large amount of reactants is requested at the reaction sites but the diffusivity of them is limited by construction.

Lastly, there exist the **Ohmic Losses**. Here, are taken into account all the resistance that arise in the MEA: resistance of the polymer membrane, resistance at the electrode-electrolyte interface and resistance in the electrodes. The voltage drop is proportional to this overall resistance, that is defined as the integral over the membrane thickness t_m of the reciprocal of the conductivity:

$$V_{\text{ohm}} = I_{\text{stack}} R_{\text{membrane}} \qquad R_{\text{membrane}} = \int_0^{t_m} \frac{dz}{\sigma(\lambda)} \tag{2.4}$$

The membrane conductivity in $(\Omega/cm)^{-1}$ is a function of the membrane water content λ,which is defined as the ratio of water molecules to the sulfonated sites, and stack temperature T_{stack}[32]:

$$\sigma = \sigma_{30} \exp\left[1268\left(\frac{1}{303.15} - \frac{1}{T_{\text{stack}}}\right)\right] \tag{2.5}$$

$$\sigma_{30} = \begin{cases} 0.005139\lambda - 0.00326 & \text{if } \lambda > 1 \\ 0.005139 - 0.00326 & \text{if } \lambda < 1 \end{cases} \tag{2.6}$$

The membrane water content λ is a function of the water activity at the anode and cathode catalyst layers $a_{w,cl}$[7]:

$$\lambda = \begin{cases} 0.043 + 17.81 a_{w,cl} & \text{if } \mathrm{a}_{w,cl} < 0 \\ 0.043 + 17.81 a_{w,cl} - 39.85 a_{w,cl}^2 + 36 a_{w,cl}^3 & \text{if } 0 \leq \mathrm{a}_{w,cl} \leq 1 \\ 14.003 + 1.4(a_{w,cl} - 1) & \text{if } \mathrm{a}_{w,cl} > 1 \end{cases} \tag{2.7}$$

Practically, is evaluated the water content at anode and cathode catalyst layer, than is made the mean value and is put in eq. (2.5). The final integration in made

considering the conductivity to be not a function of the membrane thickness.

Thus, the output voltage of the fuel cell stack is given by:

$$V_{\text{stack}} = N_{\text{cell}}(E - V_{\text{act}} - V_{\text{conc}} - V_{\text{ohm}}) \tag{2.8}$$

where N_{cell} is the number of fuel cells.

2.1.2 Water Management Model

The membrane water content strongly depends on water concentrations at anode and cathode and on the water vapour flow from one to the other. In a PEM fuel cell there are three phenomena that defines the water flow across the membrane:

- **Electro-osmotic drag.** The hydrogen protons drag water molecules from anode to cathode. The resulting molar flow in [mol/(s·cm^2)] is a function of the current density[7]:

$$N_{osmotic} = n_d \frac{i}{F} \tag{2.9}$$

  where F is the Faraday's constant and n_d is the electro-osmotic drag coefficient:

$$n_d = \begin{cases} 0.0029\lambda^2 + 0.05\lambda & \text{if } \lambda \geq 0 \\ 0.05\lambda & \text{if } \lambda < 0 \end{cases} \tag{2.10}$$

  where λ is evaluated at anode catalyst layer by means of eq. (2.7)

- **Back-diffusion.** Differences of water concentrations at anode and cathode catalyst layers creates a flow in order to balance the concentrations. This gradient is due to differences in humidity in anode and cathode. This water flow is usually from cathode to anode, since the water is produced at the cathode. It is defined as[27]:

$$N_{diff} = \frac{D_{w,diff}}{t_{mem}} (C_{w,acl} - C_{w,ccl}) \tag{2.11}$$

where t_{mem} is the membrane thickness, $D_{w,diff}$ is the water back-diffusion coefficient, $C_{w,acl}$ and $C_{w,ccl}$ are respectively the water concentration at anode and cathode catalyst layer:

$$C_{w,acl} = \frac{\rho_{m,dry}}{M_{m,dry}}\lambda_{acl} \qquad C_{w,ccl} = \frac{\rho_{m,dry}}{M_{m,dry}}\lambda_{ccl} \tag{2.12}$$

in which $\rho_{m,dry}$ is the dry membrane density and $M_{m,dry}$ is the membrane molar mass. The water content is calculated again using (2.7). Whereas, the water back-diffusion coefficient is defined as[7]:

$$D_{w,diff} = 1.25 \cdot 10^{-6} \exp\left[2416\left(\frac{1}{303.15} - \frac{1}{T_{\text{stack}}}\right)\right] \tag{2.13}$$

$D_{w,diff}$ is expressed in [cm^2/s]

- **Pressure Gradient.** When the pressure of anode and cathode are not equal, it creates a water flow based on Darcy's law:

$$N_{hydr} = \begin{cases} p_{an} K_d \frac{(p_{an} - p_{cat}) y_{w,acl}}{R T_{stack} \mu_w t_{mem}} & \text{if } p_{an} > p_{cat} \\ p_{cat} K_d \frac{(p_{an} - p_{cat}) y_{w,acl}}{R T_{stack} \mu_w t_{mem}} & \text{if } p_{an} < p_{cat} \end{cases} \tag{2.14}$$

p_{an} and p_{cat} are respectively the pressure at anode and cathode, K_d is the Darcy's constant equal to 1,58·10^{-14} cm^2, μ_w is the dynamic viscosity of water and t_{mem} is the membrane thickness.

Therefore, the overall water flow through the membrane is the sum of these three phenomena. Since the result is expressed in [mol/(s·cm^2)], the total water mass flow is:

$$W_{w,membrane} = M_w A_{cell} N_{cell} (N_{osmotic} + N_{dif} + N_{hydr}) \tag{2.15}$$

in which A_{cell} is the active area of the fuel cell, N_{cell} is the number of cells in the stack and M_w is the water molar mass.

In the following table are presented the fuel cell parameters that have been chosen for the simulations of the fuel cell stack.

Symbol	Variable	Value	Unit
N_{cell}	Number of cell in the stack	400	[-]
i_0	Exchange current density	$1{\cdot}10^{-4}$	[A/cm^2]
i_L	Max limiting current density	1,4	[A/cm^2]
α	Charge transfer coefficient	0.7	[-]
A_{cell}	Fuel cell active area	280	[cm^2]
t_{mem}	Membrane thickness	125	[μm]
t_{GDL}	Gas diffusion layer thickness	250	[μm]
$M_{m,dry}$	Dry membrane equivalent weight	1.1	[kg/mol]
$\rho_{m,dry}$	Dry membrane density	2000	[kg/m^3]

Table 2.1: Fuel Cell stack parameters

2.1.3 Reactants Consumption

The hydrogen and oxygen rate of consumption in a fuel cell can be retrieved based on Faraday's laws[15]. The mass flows [kg/s] for reactants consumption are defined as follows:

$$W_{H_2,cons} = N_{cell} M_{H_2} \frac{I_{stack}}{2F} \qquad W_{O_2,cons} = N_{cell} M_{O_2} \frac{I_{stack}}{4F} \tag{2.16}$$

where M_i are the molar mass expressed in [kg/mol], F is the Faraday's constant and N_{cell} is the number of fuel cell in the stack.

Likewise, the produced water is calculated as:

$$W_{H_2O,cons} = N_{cell} M_{H_2O} \frac{I_{stack}}{2F} \tag{2.17}$$

When designing a fuel cell stack is fundamental that the stack is never starved of oxygen or hydrogen. Otherwise, there would be voltage and efficiency drops and could also shorten the FC life time[18].

The stoichiometric ratio λ (or reactant utilization) defines the ratio between the reactant fed to the fuel cell and the actual reactant consumption:

$$\lambda = \frac{W_{fed}}{W_{consumed}} > 1 \tag{2.18}$$

As shown, this ratio must be always greater than one. This is achieved on the anode side by using a recirculation system, while at the cathode side by exploiting a control algorithm on the air compressor.

2.1.4 FC Thermodynamics

The energy balance for a generic fuel cell it's defined by equating the incoming energies and the output energies[31]:

$$\sum_i (h_i)_{in} = \sum_i (h_i)_{out} + W_{el} + Q_{gen} \tag{2.19}$$

As inputs, there are the enthalpies of the hydrogen, oxygen and water vapour, while as output there are the gases enthalpies exiting the cell, the electrical energy produced and the heat released. The enthalpies are directly defined by multiplying the specific enthalpies by eq. (2.16) and eq. (2.17) respectively. For hydrogen is considered the LHV. The specific enthalpies are defined through Look up Table at the temperature of the stack. The W_{el} is simply the stack voltage multiplied by the current. Thus, can be retrieved the heat produced, that is both dissipated to the surroundings and taken away from the cooling system.

Moreover, as already mentioned in the introduction, the fuel cell efficiency is defined as:

$$\eta = \frac{Power_{\text{elec}}}{Power_{\text{H}_2}} = \frac{I_{\text{stack}} V_{\text{stack}}}{N_{\text{H}_2} HHV} \tag{2.20}$$

where N_{H_2} is the molar flux of hydrogen consumed. By substituting in eq. (2.20) the definition of N_{H_2}:

$$\eta = \frac{V_{\text{stack}} 2F}{HHV} \tag{2.21}$$

In case of water in gaseous state as product, HHV is replaced by LHV.

2.2 Anode Network

The anode network is constituted by the anode gas channels, the humidifier, the recirculation and the hydrogen tank. These components are basically all described by the same equation of a moist air. Indeed, they are considered as pipe or chamber containing moist air composed of hydrogen, water vapour and nitrogen. It's modelled also the nitrogen dynamics, since nitrogen can diffuse through the membrane and reach the anode networks. The phenomenon entity may varies and sometimes may be needed a purge valve to vent out the nitrogen[19].

For constructing the equation of gas mixture dynamics in the pipes are made the following assumption, that are valid for all the next sections:

- Pipe wall perfectly rigid;
- No friction losses considered;
- Supersonic flow not considered;
- Fluid inertia negligible;
- Gravity effect negligible.

For matter of convenience, is used the notation showed in table 2.2

inlet	outlet	H_2	O_2	H_2O	N_2
in	out	g	g	w	n

Table 2.2: Notation

Firstly are defined the mass and energy balance for a 3 gases mixture pipe:

$$\frac{dm}{dt} = \dot{m}_{in} - \dot{m}_{out} - \dot{m}_{condense} \tag{2.22}$$

$$\frac{d\Phi}{dt} = \Phi_{in} - \Phi_{out} - \Phi_{condense} + Q \tag{2.23}$$

$$\frac{dm_w}{dt} = \dot{m}_{w,in} - \dot{m}_{w,out} - \dot{m}_{condense} \tag{2.24}$$

$$\frac{dm_g}{dt} = \dot{m}_{g,in} - \dot{m}_{g,out} \tag{2.25}$$

where Q is the heat exchanged between the pipe wall and the internal volume, $\dot{m}_{condense}$ is the rate of water condensation and $\Phi_{condense}$ is the rate of energy loss due to condensation.

In order to calculate the outlet flow of each pipe, the nozzle flow equations are considered. According to these equations the flow rate is generally a function of the nozzle cross-sectional area, density and the upstream and downstream pressure[41]. Moreover, depending on the pressure ratio, the flow can be chocked or unchocked, as shown in figure 2.3.

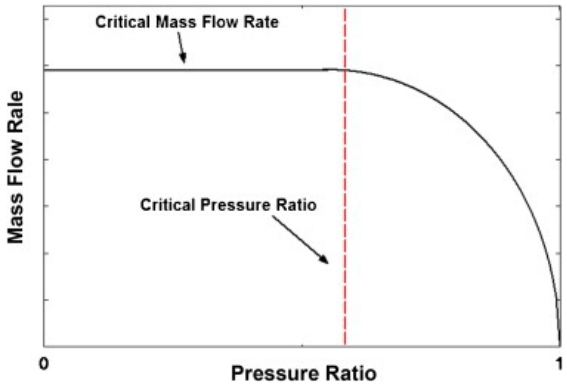

Figure 2.3: Nozzle flow rate over the pressure ratio

Therefore, if the pressure ratio is very small, the flow is subcritical and can be linearized as[27]:

$$\dot{m}_{out} = k_{flow}(p - p_{out}) \tag{2.26}$$

in which, k is the nozzle constant, p is the pipe internal pressure and p_{out} is the downstream pressure.

The energy flow associated is defined as:

$$\Phi_{out} = \dot{m}_{out}\left(h + \frac{1}{2}\left(\frac{\dot{m}_{out}}{\rho S}\right)^2\right) \tag{2.27}$$

where h is the mixture specific enthalpy, S is the pipe cross-sectional area and ρ is the moist air density.

Considering the gases flow rates, they are simply for each species i:

$$\dot{m}_{i,out} = x_i \dot{m}_{out} \tag{2.28}$$

where x_i is the mass fraction of species i.

Combining eq.2.25 and eq.2.22, and explicating the mass fraction of gas x_g, can be retrieved the dynamics of the gas in the moist air volume:

$$\frac{dx_g}{dt}\rho V + x_g\frac{dm}{dt} = \frac{dm_g}{dt} \tag{2.29}$$

Similarly, the dynamics of water vapour is defined as:

$$\frac{dx_w}{dt}\rho V + x_w\frac{dm}{dt} = \frac{dm_w}{dt} \tag{2.30}$$

in which V is the internal volume of the pipe.

The dynamics of the nitrogen mass fraction is easily derived considering that:

$$x_n = 1 - x_g - x_w$$

Furthermore, from eq.(2.23) it's derived the dynamics of the internal temperature[41]:

$$\rho c_v V\frac{dT}{dt} = \frac{d\Phi}{dt} - (u_w - u_n)(\frac{dm_w}{dt} - x_w\frac{dm}{dt}) + (u_g - u_n)(\frac{dm_g}{dt} - x_g\frac{dm}{dt}) - u\frac{dm}{dt} \tag{2.31}$$

where, c_v is the mixture specific heat at constant volume, u_i are the specific internal energy of the gases and u is the mixture internal energy.

Finally, the mixture mass conservation allows to derive the relationship between temperature and pressure dynamics:

$$\rho V(\frac{dp}{dt}\frac{1}{p} - \frac{dT}{dt}\frac{1}{T}) = \frac{dm}{dt} - \frac{R_n - R_w}{R}(\frac{dm_w}{dt} - x_w\frac{dm}{dt}) - \frac{R_n - R_g}{R}(\frac{dm_g}{dt} - x_g\frac{dm}{dt}) \tag{2.32}$$

In which R_i is each specific gas constant and R is the mixture specific gas constant.

The mixture quantities are defined as:

$$R = x_g R_g + x_w R_w + x_n R_n$$

$$u = x_g u_g + x_w u_w + x_n u_n$$

$$c_v = x_g c_{v,g} + x_w c_{v,w} + x_n c_{v,n}$$

$$p = \rho R T$$

For what concerns the wall heat transfer, it is given by both convective and conductive contributions, $Q = Q_{conv} + Q_{cond}$. These two are defined as[3]:

$$Q_{cond} = \frac{kS_{surf}}{D_h}(T_{wall} - T) \tag{2.33}$$

It's assumed an exponential distribution of the temperature along the pipe, so:

$$Q_{conv} = |\dot{m}_{avg}|c_{p,avg}(T_{wall} - T_{in})(1 - exp(-\frac{hS_{surf}}{|\dot{m}_{avg}|c_{p,avg}})) \tag{2.34}$$

where:

- T_{wall} is the temperature of pipe walls;
- T_{in} is the inlet temperature, according to the flow direction;
- $\dot{m}_{avg} = (m_{in} + m_{out})/2$
- $c_{p,avg}$ is the mixture specific heat evaluated at the average temperature between inlet and outlet;

- k is the mixture thermal conductivity;
- D_h is the hydraulic diameter of the pipe;
- S_{surf} is the pipe surface area.

While, $h = N_u \frac{k_{avg}}{D_h}$ is the heat transfer coefficient. N_u is the Nusselt number, that for a laminar flow is constant, whereas for turbulent flow is defined using the Gnielinki's correlation[6].

Finally, are modelled also the equations that account for water condensation on pipe walls:

$$\dot{m}_{condense} = \begin{cases} 0 & \text{if } x_w \leq x_w s \\ \frac{x_w - x_{ws}}{\tau_{condense}} \rho V & \text{if } x_w > x_w s \end{cases} \tag{2.35}$$

where, $\tau_{condense}$ is the condensation time constant, that is always considered equal to 10^{-3} [1/s]. Whereas, x_{ws} is defined as the specific humidity at saturation:

$$x_{ws} = \phi_{ws} \frac{R}{R_w} \frac{p_{ws}}{p} \tag{2.36}$$

in which, ϕ_{ws} is the relative humidity at saturation, equal to 1, and p_{ws} is the water saturation pressure evaluated at the pipe temperature.

The energy loss associated to the condensed water vapor is:

$$\Phi_{condense} = \dot{m}_{condense}(h_w - \Delta h_{vap}) \tag{2.37}$$

where, Δh_{vap} is the specific enthalpy of vaporization calculated at the pipe temperature.

2.2.1 Hydrogen source

The hydrogen source is composed of a hydrogen tank and a pressure valve. The hydrogen tank is modeled using the equation previously described with the following additional assumptions:

- It's stored almost pure hydrogen (molar fraction y_{H_2}=0.9997);
- The chamber is isolated, no heat exchanged → Q=O;
- Only one port, that is the outlet;
- No condensation.

Connected to the hydrogen tank is placed a pressure reducing valve with a variable cross-sectional area. It's assumed an unidirectional subsonic flow that undergoes an adiabatic transformation. This valve is assumed to be controlled through an algorithm that exploits a reference pressure p_{ref}=0.16 MPa and a feedback of the downstream pressure. The pressure difference is then multiplied by a proportional constant. This forms the command for the valve actuator:

$$S_{R,desired} = k_p(p_{ref} - p_{out}) \tag{2.38}$$

Thus, the mass flow rate exiting the tank is:

$$\dot{m}_{out} = S_{R,des} C_d \sqrt{2\rho_{tank}(p_{tank} - p_{out})} \tag{2.39}$$

where C_d is the discharge coefficient.

In table 2.3 are listed the chosen parameters for the simulations.

Symbol	Variable	Value	Unit
V_{tank}	Hydrogen tank volume	120	[l]
$p_{tank,0}$	Initial tank pressure	70	[MPa]
$T_{tank,0}$	Initial tank temperature	293,15	[K]
S_{tank}	Cross-sectional area of outlet	$7{,}854 \cdot 10^{-5}$	[m^2]
$y_{H_2,tank}$	Hydrogen tank mole fraction	0,9997	[-]
C_d	Discharge coefficient	0.64	[-]
p_{ref}	Reference Anode pressure	0.16	[MPa]
k_p	Control law proportional constant	$-1.5708 \cdot 10^{-8}$	[m^2/Pa]

Table 2.3: Hydrogen source parameters

2.2.2 Recirculation

This block is modelled as a square chamber with two inlet and one outlet, one from the hydrogen tank and one from the anode gas channels. The pipe is considered thermally isolated.

The mass flow rate coming from the anode gas channels is assumed to be defined by a proportional controller based on the stack current density:

$$\dot{m}_{rec} = k_p(c_1 + c_2 I_{stack}/(i_L A_{cell})) \tag{2.40}$$

where, i_L is the fuel cell max limiting current density and A_{cell} is the active fuel cell area.

In table 2.4 are listed the chosen parameters for the simulations.

Symbol	Variable	Value	Unit
V_{rec}	Chamber volume	0.05^3	[m^3]
S_{rec}	Cross-sectional area of the chamber	$7{,}854{\cdot}10^{-5}$	[m^2]
c_1	Recirculation control constant	0,2	[-]
c_2	Recirculation control constant	0,8	[-]
k_p	Control law proportional constant	0,01	[kg/s]
k_{flow}	Outlet flow constant	$4{\cdot}10^{-5}$	[kg/(s·Pa)]

Table 2.4: Recirculation parameters

2.2.3 Anode Humidifier

Here, is modelled a pipe in which is added water vapour in order to reach 100% of relative humidity. The pipe is considered thermally isolated. The injection of water vapour is controlled by a proportional controller that works on the difference between the reference relative humidity (equal to 1) and the measured one:

$$\dot{m}_{w,inj} = k_p(RH_{set} - RH_{meas}) \tag{2.41}$$

Thus, the energy of water vapour injected is:

$$\Phi_{w,inj} = \dot{m}_{w,inj} h_w \tag{2.42}$$

The water specific enthalpy is evaluated at the temperature of the stack, since it's assumed that the water produced by the fuel cell is reused for the humidification.

In table 2.5 are listed the chosen parameters for the simulations.

Symbol	Variable	Value	Unit
$V_{hum,a}$	Pipe volume	$4{,}91 \cdot 10^{-4}$	[m^3]
$S_{hum,a}$	Pipe cross-sectional area	0,00196	[m^2]
$L_{hum,a}$	Pipe length	0,25	[m]
RH_{set}	Relative humidity setpoint	1	[-]
k_p	Control law proportional constant	0,1	[kg/s]
k_{flow}	Outlet flow constant	$6 \cdot 10^{-5}$	[kg/(s·Pa)]

Table 2.5: Anode humidification parameters

2.2.4 Anode Gas Channel

The anode gas channels are modelled as a pipe with three ports, one where it exchange gases with the membrane electrode assembly. The flows rate exchanged are the hydrogen consumed (eq. (2.16)) and the water vapour that diffuses thorughout the membrane (eq.(2.15)). Here, the pipe is not considered isolated, instead it exchanges heat with the MEA through the pipe walls.

The outlet flow rate is fixed by the recirculation control (eq.(2.40)). The development of the mixture dynamics is crucial in this point, since the partial pressures, molar and mass fractions of the gas components determine the fuel cell behaviour.

In table 2.6 are listed the chosen parameters for the simulations.

Symbol	Variable	Value	Unit
V_{an}	Pipe volume	0,0535	[m^3]
S_{an}	Pipe cross-sectional area	0,32	[m^2]
D_{an}	Hydraulic diameter	0,01	[m]
L_{an}	Pipe length	0,167	[m]
$w_{ch,an}$	Gas channels width	0,01	[m]
$n_{ch,an}$	Number of gas channels per cell	8	[-]
Nu_{lam}	Nusselt number for laminar heat transfer	3,66	[kg/s]
ϵ	Internal surface absolute roughness	$15{\cdot}10^{-6}$	[m]

Table 2.6: Anode gas channels parameters

2.3 Cathode Network

As in the anode network, the components are modelled using the general balance equations for a gas mixture, that are from eq.(2.22) to eq.(2.37). Of course, instead of hydrogen is considered oxygen.

2.3.1 Oxygen Source

In this block is modelled the air compressor that takes air from the environment and vents it into the network. This compressor is regulated through a control law that defines the correct flow that the compressor must provided to the cathode.

It's assumed that the compressor vacuums air with a RH=50% , p=101325 Pa and T=293,15 K, and performs an isentropic transformation to the air. The water vapour condensation is not considered.

The controller is a PI (proportional-integral) that works on the difference between a flow rate setpoint, i.e. the flow rate that the compressor has to provide, and a measured one. The setpoint is defined considering the Oxygen Excess Ratio (OER), that is the ratio between the oxygen flow into the cathode $W_{O_2,in}$ and the

oxygen consumption $W_{O_2,react}$[18]. It's chosen a value equal to 2,5:

$$\lambda_{O_2} = \frac{W_{O_2,in}}{W_{O_2,react}} = 2{,}5 \tag{2.43}$$

This is crucial, since the fuel cell must never be starved of oxygen.

Thus, the flow rate setpoint is

$$W_{set} = \frac{\lambda_{O_2} W_{O_2,react}}{x_{O_2,env}} \tag{2.44}$$

where $x_{O_2,env}$ is the oxygen mass fraction in ambient air, equal to 0,234.

The output of the PI controller is the command for the compressor. It is expressed in [rpm]. This command and pressure difference at the compressor edges are then fed to a compressor map, that provides the flow rate that the compressor reaches.

The power added to the flow is:

$$\Phi_{work} = \dot{m}(h_{t,out} - h_{t,in}) \tag{2.45}$$

where h_t is the total enthalpy of the flow and $\dot{m}$ is the compressor flow rate.

In table 2.7 are listed the chosen parameters for the simulations.

Symbol	**Variable**	**Value**	**Unit**
V_{comp}	Compressor volume	0,0003	[m^3]
$S_{comp,in}$	Compressor inlet cross-sectional area	0.00196	[m^2]
$S_{comp,out}$	Compressor outlet cross-sectional area	0.00196	[m^2]
k_p	Control proportional constant	5	[s/kg]
k_i	Control integral constant	0.5	[s^2/kg]

Table 2.7: Oxygen source parameters

2.3.2 Cathode Humidifier

In this block, is modelled a pipe in which is injected water vapour in order to reach 100% or relative humidity, as happens for the anode humidifier. It's considered as a thermal isolated pipe. A proportional controller defines the injected flow rate:

$$\dot{m}_{w,inj} = k_p(RH_{set} - RH_{meas}) \tag{2.46}$$

As a consequence, the energy of water vapour injected is:

$$\Phi_{w,inj} = \dot{m}_{w,inj} h_w \tag{2.47}$$

where h_w is the water specific enthalpy evaluated at the temperature of the stack.

In table 2.8 are listed the chosen parameters for the simulations.

Symbol	Variable	Value	Unit
$V_{hum,c}$	Pipe volume	$4{,}91 \cdot 10^{-4}$	[m^3]
$S_{hum,a}$	Pipe cross-sectional area	0,00196	[m^2]
$L_{hum,a}$	Pipe length	0,25	[m]
RH_{set}	Relative humidity setpoint	1	[-]
k_p	Control law proportional constant	0,1	[kg/s]
k_{flow}	Outlet flow constant	$4 \cdot 10^{-3}$	[kg/(s·Pa)]

Table 2.8: Cathode humidification parameters

2.3.3 Cathode Gas Channels

This component is modelled at the same way of the anode gas channels. Yet, here oxygen diffuse to the membrane while the water produced and the water coming from the membrane converge into the pipe. Moreover, the pipe exchange heat with the MEA through the pipe walls.

The outlet flow rate is fixed by the back-pressure relief valve. This valve has a variable cross-sectional area that is controlled through a proportional controller

that works on the pressure difference between the reference pressure and the cathode pressure:

$$S_{R,desired} = c_1 + k_p(p_{ref} - p) \tag{2.48}$$

The p_{ref} is the desired pressure of the cathode, and p is the actual cathode pressure. The constant c_1 ensures a minimum opening of the valve. Then, this command is used to define the outlet flow rate:

$$\dot{m}_{out} = S_{R,des} C_d \sqrt{2\rho(p - p_{env})} \tag{2.49}$$

where C_d is the discharge coefficient, ρ and p are respectively the internal pipe density and pressure of the mixture.

In table 2.9 are listed the chosen parameters for the simulations.

Symbol	**Variable**	**Value**	**Unit**
V_{cat}	Pipe volume	0,0535	[m^3]
S_{cat}	Pipe cross-sectional area	0,32	[m^2]
D_{cat}	Hydraulic diameter	0,01	[m]
L_{cat}	Pipe length	0,167	[m]
$w_{ch,an}$	Gas channels width	0,01	[m]
$n_{ch,an}$	Number of gas channels per cell	8	[-]
Nu_{lam}	Nusselt number for laminar heat transfer	3,66	[kg/s]
ϵ	Internal surface absolute roughness	$15{\cdot}10^{-6}$	[m]
k_p	Control law proportional constant	$-2.513{\cdot}10^{-7}$	[m^2/Pa]
c_1	Control law constant	$1.964{\cdot}10^{-11}$	[m^2]

Table 2.9: Cathode gas channels parameters

2.4 Cooling System

The cooling system is responsible for the heat dissipation coming from the stack. It's assumed water as coolant and it flows through channels all around the stack, absorbing the heat coming from the MEA and the anode and cathode gas

channels. The overall heat produced by the stack heat up the stack itself, until its temperature reaches around 80 °C. Here, the cooling system starts working and dissipate the excess of heat in order to maintain that temperature.

The absorbed heat by the stack is defined as:

$$Q = c_{p,MEA}\rho_{MEA}V_{MEA}\frac{dT}{dt} \tag{2.50}$$

in which $c_{p,MEA}$, ρ_{MEA} and V_{MEA} are respectively the overall specific heat, density and volume of the membrane electrode assembly.

In table 2.10 are listed the chosen parameters.

Symbol	Variable	Value	Unit
ρ_{MEA}	Overall density of MEA	1800	[kg/m^3]
$c_{p,MEA}$	Overall specific heat of MEA	870	[J/(kg·K]
V_{MEA}	Overall MEA volume	0,007	[m^3]

Table 2.10: MEA thermal mass parameters

The cooling system is composed by:

- **Fuel Cell coolant channels**
- **Coolant tank**
- **Pump**
- **Radiator**

2.4.1 FC coolant channels

The fuel cell coolant channels are modelled as a pipe with a fixed volume of liquid. To model the equations, the following assumptions have been made:

- Rigid pipe wall;

- Liquid compressibility is modelled;
- Liquid inertia not considered;
- Viscous friction not considered;
- Gravity effects negligible.

The pipe absorbs the heat produced by the stack through the wall and consequently the liquid, i.e. water, heats up.

As the dynamic compressibility of the liquid is considered, the mass conservation equation in the pipe become[40]:

$$V\rho(\frac{1}{\beta}\frac{dp}{dt} - \alpha\frac{dT}{dt}) = \dot{m}_{in} - \dot{m}_{out} \tag{2.51}$$

where p, T and ρ are respectively the liquid pressure, temperature and density, V is the pipe volume, α is the liquid isobaric thermal expansion coefficient and β is the isothermal bulk modulus. As in the moist air networks, the outlet flow rate $\dot{m}_{out}$ is defined through a linear relation with the pressure difference:

$$\dot{m}_{out} = k_{flow}(p - p_{out}) \tag{2.52}$$

Similarly, the energy conservation equation depends on the inlet energy flow rate Φ_{in}, the outlet energy flow rate Φ_{out} and the heat Q exchanged through the pipe walls:

$$V\frac{d(\rho u)}{dt} = \Phi_{in} - \Phi_{out} + Q \tag{2.53}$$

where u in the liquid internal energy.

The energy flow rate are defined as:

$$\Phi_{out} = \dot{m}_{out}h \tag{2.54}$$

where h in the liquid enthalpy calculated at the liquid temperature in the pipe.

For what concerns the wall heat transfer, are modelled both convective and conductive contributions, $Q = Q_{conv} + Q_{cond}$. These two are defined as[3]:

$$Q_{cond} = \frac{kS_{surf}}{D}(T_{wall} - T) \tag{2.55}$$

It's assumed an exponential distribution of the temperature along the pipe, so:

$$Q_{conv} = |\dot{m}_{avg}|c_{p,avg}(T_{wall} - T_{in})(1 - exp(-\frac{hS_{surf}}{|\dot{m}_{avg}|c_{p,avg}})) \tag{2.56}$$

where:

- T_{wall} is the temperature of pipe walls;
- T_{in} is the inlet temperature, according to the flow direction;
- $\dot{m}_{avg} = (m_{in} + m_{out})/2$
- $c_{p,avg}$ is the liquid specific heat evaluated at the average temperature between inlet and outlet;
- k is the liquid thermal conductivity;
- D is the diameter of the pipe.
- S_{surf} is the pipe surface area.

While, $h = N_u \frac{k_{avg}}{D}$ is the heat transfer coefficient. N_u is the Nusselt number, that for a laminar flow is constant, whereas for turbulent flow is defined using the Gnielinki's correlation[6].

In table 2.11 are listed the chosen parameters for the simulations.

2.4.2 Coolant tank

This block models the tank in which is contained the thermal liquid. It is both connected to the FC coolant channels and to the pump. It is modelled as a variable

Symbol	Variable	Value	Unit
V_{cool}	Pipe volume	0,004	[m^3]
S_{cool}	Pipe cross-sectional area	0,002	[m^2]
D_{cool}	Hydraulic diameter	0,01	[m]
L_{cool}	Pipe length	2,008	[m]
n_{layers}	N. of layers in stack	20	[-]
n_{passes}	N. of coolant channels per layer	12	[-]
Nu_{lam}	Nusselt number for laminar heat transfer	3,66	[kg/s]
ϵ	Internal surface absolute roughness	$15{\cdot}10^{-6}$	[m]
k_{flow}	Outlet flow constant	$1{\cdot}10^{-4}$	[kg/(s·Pa)]

Table 2.11: FC coolant channels parameters

volume chamber with one inlet. One side is free to move, so the internal pressure is constant equal to the environment pressure and the liquid compressibility is considered negligible. Moreover, the chamber is considered rigid, the resistances are negligible and the chamber is considered isolated.

In particular, the mass conservation is:

$$\dot{m} = \rho S v \tag{2.57}$$

where v is the translational velocity of the free-moving side and S is the cross-sectional area. It worth noticing that a positive flow rate (incoming flow) causes a positive velocity, that is an increase in volume.

Finally the energy conservation equation is:

$$V\frac{d(\rho u)}{dt} = \Phi + Q - pSv \tag{2.58}$$

where u in the liquid internal energy, V is the chamber volume, p is the chamber pressure and Φ is the energy associated to the flow rate.

In table 2.12 are listed the chosen parameters for the simulations.

Symbol	Variable	Value	Unit
$V_{tank,0}$	Chamber initial volume	0,0081	[m^3]
S_{tank}	Pipe cross-sectional area	0,1	[m^2]

Table 2.12: Coolant tank parameters

2.4.3 Coolant pump

The coolant pump is modelled as an ideal flow rate source that maintain a specified mass flow rate, regardless of the external conditions. The work spent by the pump is considered isentropic and it's added to the liquid energy flow[40]:

$$\Phi_{work} = \frac{\dot{m}(p_{out} - p_{in})}{\rho_{avg}} \tag{2.59}$$

where ρ_{avg} is the mean density between inlet and outlet and $\dot{m}$ is the flow rate imposed by the control algorithm. The control law chosen exploits a PI controller, a reference stack temperature of 80°C and a feedback of the stack temperature.

In table 2.13 are shown the chosen parameters of the PI controller.

Symbol	Variable	Value	Unit
k_p	Control proportional constant	0.1	[kg/(s·K]
k_i	Control integral constant	0.01	[kg/(·K]

Table 2.13: Coolant pump control parameters

2.4.4 Radiator

This component is responsible for refrigerating the coolant through an heat exchange with the environment. It is modelled using the same equations adopted for the FC coolant channels, from eq.(2.51) to eq.(2.56). Moreover, for a better

modelling is also taken into account the heating of the radiator itself:

$$Q = c_{p,rad} m_{rad} \frac{dT}{dt} \tag{2.60}$$

The heat exchange with the environment is considered convective and occurs at the fins level:

$$Q_{conv} = k_{rad} A_{rad} (T_{wall} - T_{env}) \tag{2.61}$$

where k_{rad} is the radiator convective heat transfer coefficient, A_{rad} is the radiator active surface area for convective heat transfer.

In table 2.14 are listed the chosen parameters for the simulations.

Symbol	**Variable**	**Value**	**Unit**
V_{rad}	Radiator volume	$9{,}38 \cdot 10^{-4}$	[m^3]
A_{rad}	Radiator active surface area	9,31	[m^2]
D_{rad}	Hydraulic diameter	0,0028	[m]
L_{rad}	Radiator overall length	1	[m]
H_{rad}	Radiator overall height	0,5	[m]
w_{rad}	Radiator overall width	0,025	[m]
η_{fin}	Fins efficiency	0,7	[-]
n_{cools}	N. of coolant tubes	25	[-]
$c_{p,rad}$	Radiator specific heat	910	[J/(kg·K)]
$cmrad$	Radiator mass	3,45	[kg]
Nu_{lam}	Nusselt number for laminar heat transfer	3,66	[kg/s]
ϵ	Internal surface absolute roughness	$15 \cdot 10^{-6}$	[m]
k_{flow}	Outlet flow constant	$1 \cdot 10^{-3}$	[kg/(s·Pa)]

Table 2.14: Radiator parameters

Chapter 3

PEM Fuel Cell validation

In this chapter are presented the simulations that have been conducted in order to validate the model behaviour in different working conditions. In particular the aim of this thesis is to present a high speed, very accurate and complete PEM Fuel Cell stack model that can be used for designing a propulsion system for maritime applications.

According to this purpose, the model is validated through simulations comparison with the PEM Fuel Cell stack Simscape^{TM} model presented by Mathworks, Inc[20]. The two models are built using the same parameters, those listed in the previous chapter. The inputs also is the same, that are the input currents that emulate an electrical load. Then, the two models are compared in terms of

- Simulation times;
- Time histories difference of the variable of interest.

This way, it's shown how the presented Simulink model is able to produce the same results of the Simscape model but with a lower level of complexity and a overall time of simulation that is drastically reduced. Moreover, the Simulink model provides a easier parameters handling and design changing.

The simulations are carried using different load shapes, that are represented

by input currents. Particularly, have been chosen 3 current shapes, and for each other 3 current profiles with different magnitude. This way, the fuel cell is tested in different maritime scenarios, where the required output power can either constant or variable.

In the next sections will be presented the these output demands and for each are shown the relevant quantities time history of the presented Simulink model compared to the Simscape model. Afterwards, it follows an error analysis of these variables and then a simulation times comparison.

3.1 Simulations results comparison

3.1.1 Constant step load

The first set of simulations aims to show a possible scenario in which the fuel cell powers a ship that travels at constant speed for all the working period. The 3 load current profiles are shown in figure 3.1.

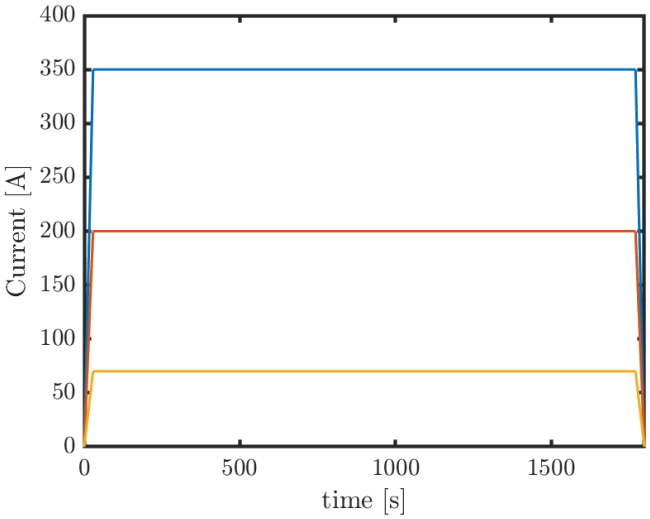

Figure 3.1: 3 load current profiles

Essentially, they both are constituted by a ramp up to the target current and

then a ramp down to zero. The period of time considered is 30 minutes. The point is to test the fuel cell in 3 different operating points and compare the results by means of a graphical comparison and error analysis. Figure 3.2 depicts the three operating point chosen.

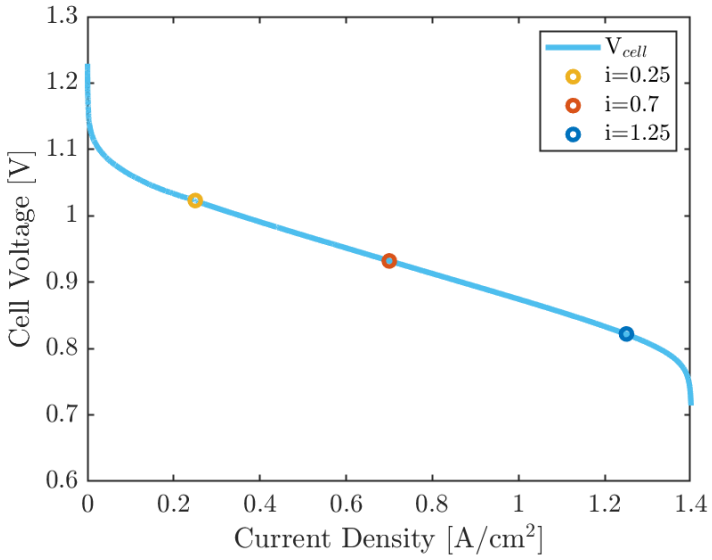

Figure 3.2: The three operating point chosen

Firstly, in the following graphs are depicted the time history of the most relevant quantities for each current profile, that are the output voltage (fig.3.3), the output power (fig.3.4), the HHV efficiency (fig.3.5), the consumed hydrogen (fig.3.6), the stack temperature (fig.3.7), the heat produced (fig.3.8) and the air compressor power (fig.3.9)

In figure 3.5 is presented only the HHV efficiency since the trend of the LHV efficiency is exactly the same. These images shows that the results are very similar in values and shape. The small differences are more visible when considering high input current as in the thirds graphs, where the input currents are very near to the max limiting current of the fuel cell.

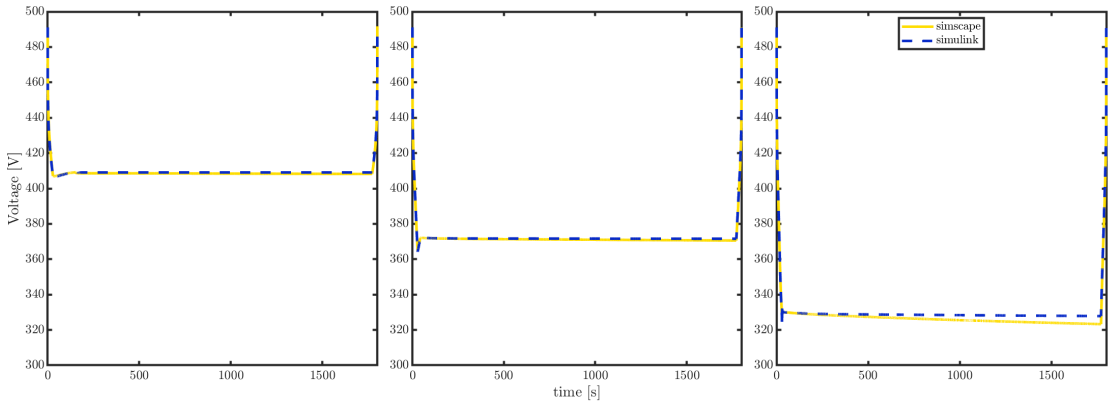

Figure 3.3: Fuel cell stack output voltage

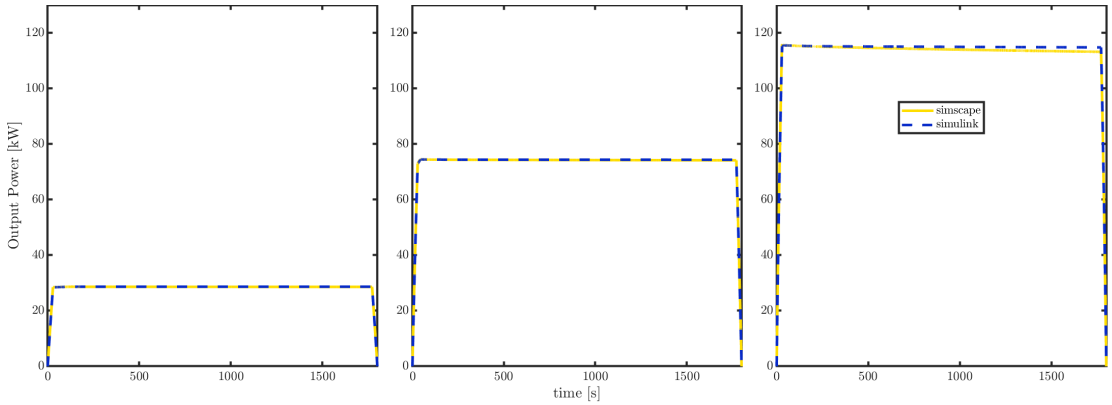

Figure 3.4: Fuel cell stack output power

The comparison of the two models is performed also taking into account all the relevant quantities that defines the gas mixture dynamics of each building block of anode and cathode networks. Particularly, has been made the comparison and the error analysis on the temporal evolution of four quantities for each block, that are the internal pressure, temperature, hydrogen or oxygen mass fraction and relative humidity.

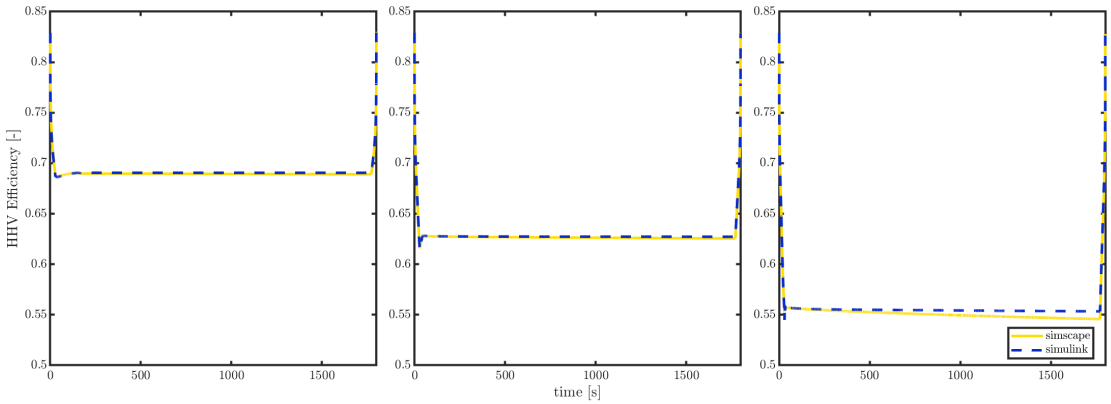

Figure 3.5: Fuel cell stack efficiency

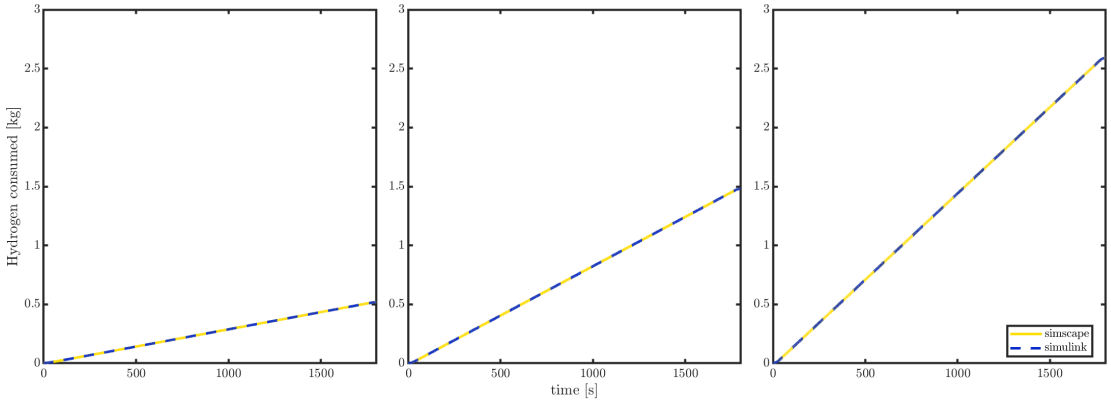

Figure 3.6: Hydrogen consumed

For matter of convenience and clarity are presented only the graphs of the anode and cathode gas channels variables time history when the second input current is applied, that is the 200 A current step, the red line of figure 3.1.

The anode gas channels quantities are reported in (fig.3.10), while the cathode gas channels ones in (fig.3.11).

Finally, in figure 3.12 are reported the pressure and temperature of the hydrogen tank.

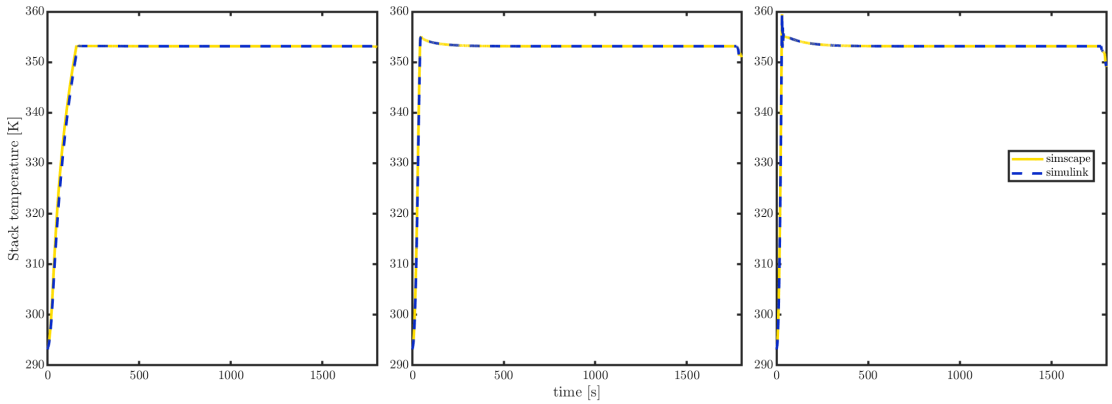

Figure 3.7: Fuel cell stack temperature

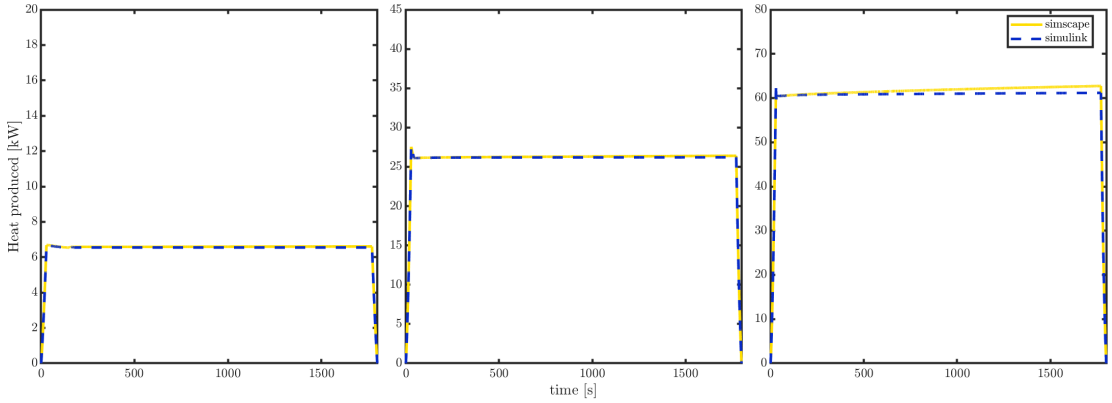

Figure 3.8: Fuel cell heat produced

Once the graphical comparison is conducted, a error analysis is made on each relevant variable of the system. To compare the two system is chosen to employ three different error formulation:

- **Mean absolute error (MAE);**

$$\mathrm{MAE} = \frac{1}{n}\sum_{i=1}^{n}|x_i - y_i|$$

- **Root mean square error (RMSE);**

$$\mathrm{RMSE} = \sqrt{\frac{\sum_{i=1}^{n}(x_i - y_i)^2}{n}}$$

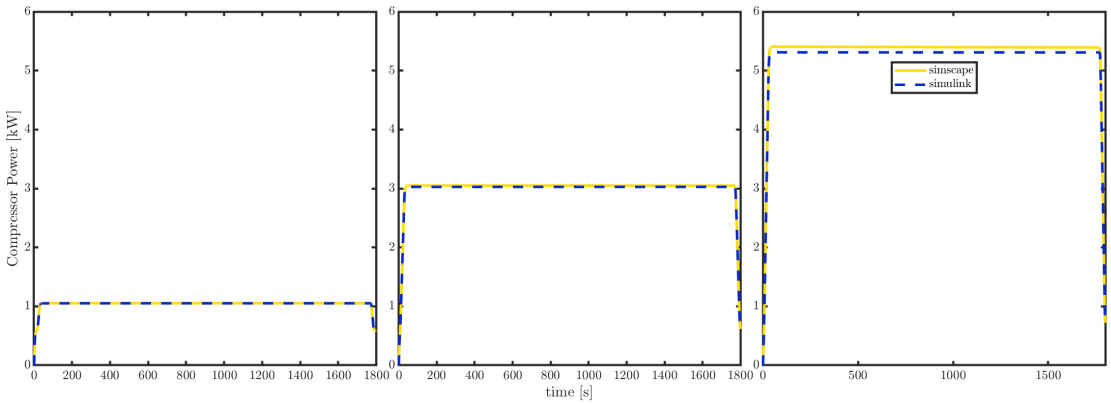

Figure 3.9: Air compressor power

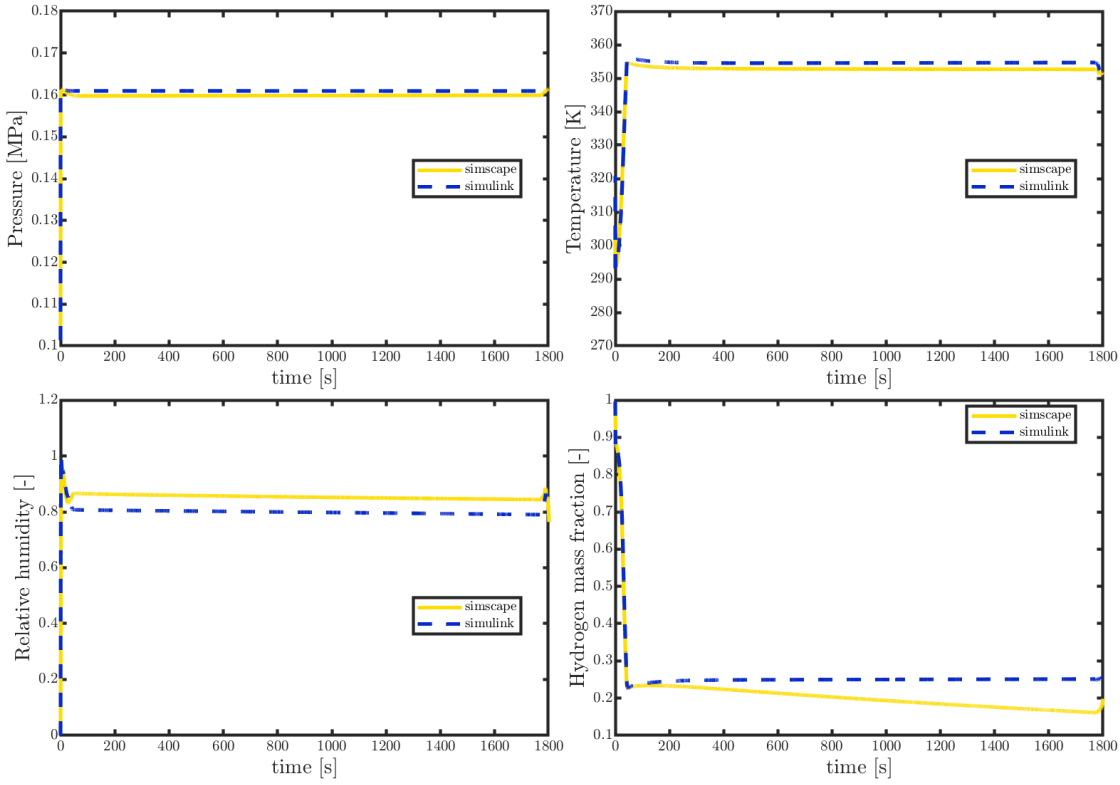

Figure 3.10: Anode gas channels relevant quantities

- **MEAN relative error (MRE)**.

$$\mathrm{MRE} = \frac{1}{n}\sum_{i=1}^{n}\left(\frac{|x_i - y_i|}{y_i}\right)\cdot 100\%$$

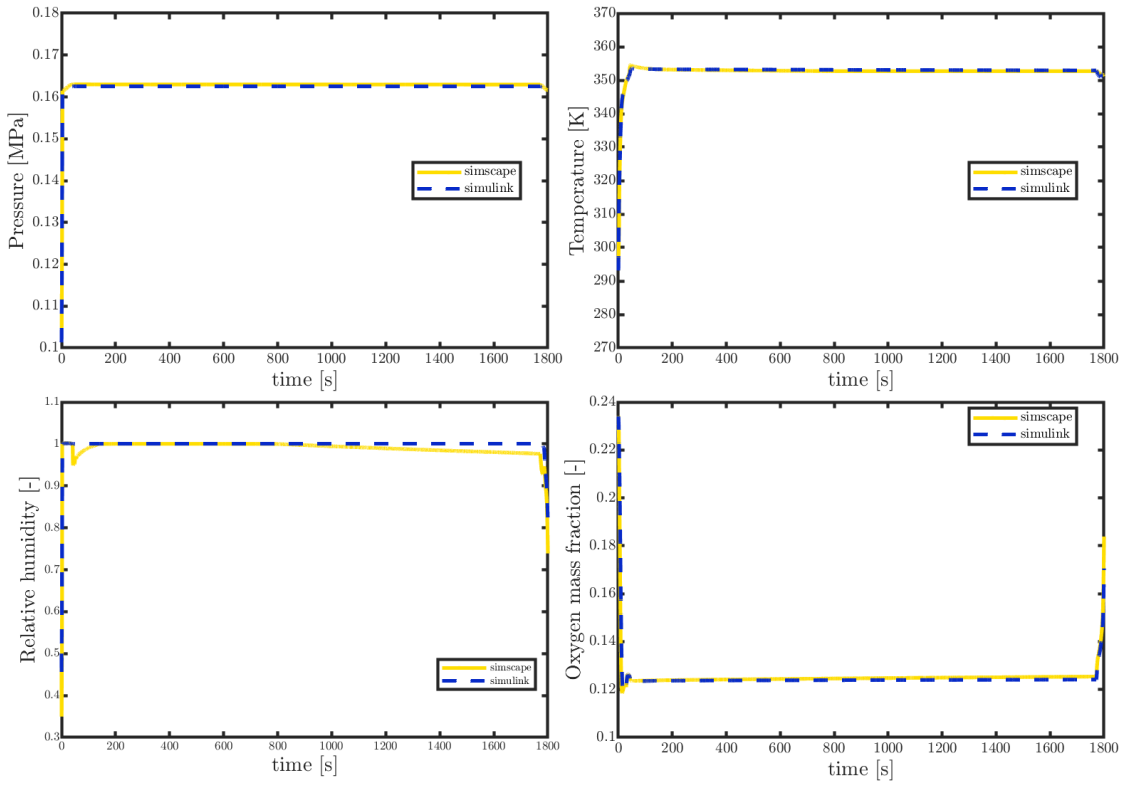

Figure 3.11: Cathode gas channels relevant quantities

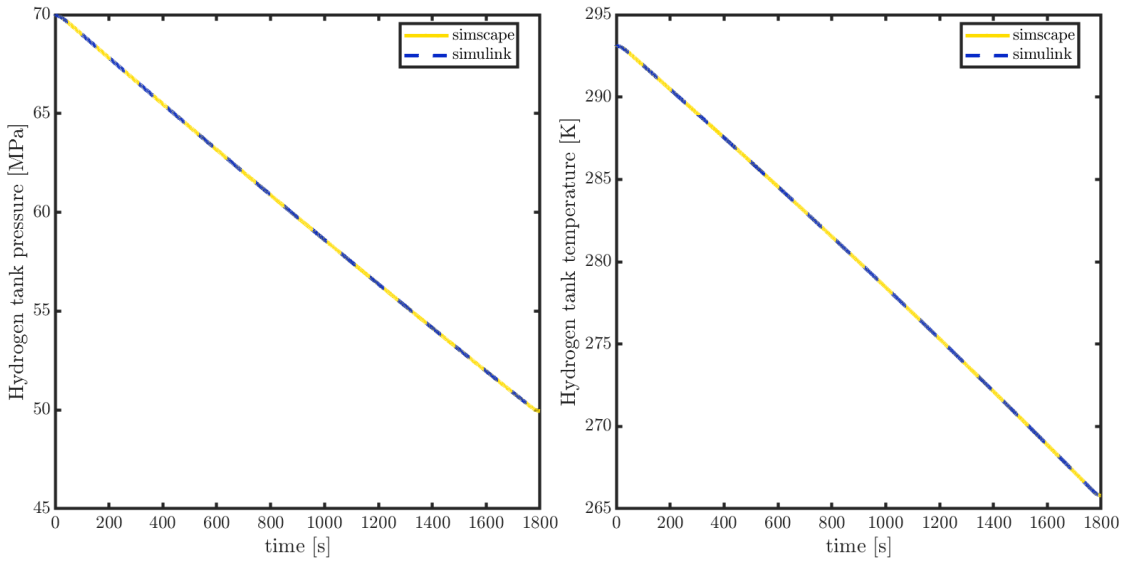

Figure 3.12: Hydrogen tank pressure and temperature

where x_i is the general output variable of the Simulink model, y_i is the general output variable of the Simscape model and n is the number of simulation.

These errors are evaluated averaging the output variable over all the 100 simulation for each current profile, obtaining a error value for each time instant. Then, these errors are averaged over the time, retrieving a total mean error for each variable.

It's chosen to display only the MRE, since provides the best clear comparison of the results. The obtained values are presented in table 3.1. The table is structured so that three columns shows the MRE for each variable of interest and in the last column it's reported the mean over all the three current profiles.

Variable	**1^{th} Current**	**2^{nd} Current**	**3^{rd} Current**	**Mean**
Output voltage	0,15	0,16	0,74	0,35
Output power	0,15	0,16	0,74	0,35
Energy produced	0,10	0,09	0,37	0,18
Heat produced	0,68	0,43	1,36	0,82
Stack temperature	0,05	0,01	0,01	0,02
HHV efficiency	0,15	0,16	0,74	0,35
LHV efficiency	0,15	0,16	0,74	0,35
H_2 mass consumed	0,13	0,06	0,08	0,09
Tank pressure	0,0027	0,0018	0,0025	0,0024
Tank temperature	0,0008	0,0003	0,0007	0,0006
Recirculation pressure	0,15	0,87	2,33	1,12
Recirculation temperature	0,19	0,38	0,94	0,50
Recirculation RH	0,28	0,55	2,38	1,07
Recirculation H_2 mass fraction	4,60	15,48	26,51	15,53
Anode humidifier pressure	0,10	0,77	2,18	1,02
Anode humidifier temperature	0,22	0,59	1,38	0,73
Anode humidifier RH	0,07	0,49	2,04	0,86
Anode humidifier H_2 mass fraction	3,22	8,90	10,20	7,44
Anode gas channels pressure	0,06	0,69	2,02	0,92
Anode gas channels temperature	0,32	0,51	0,18	0,34
Anode gas channels RH	2,98	6,32	4,03	4,45

Anode gas channels H_2 mass fraction	6,44	26,79	52,03	28,42
Air compressor pressure	0,07	0,31	0,73	0,37
Air compressor temperature	0,03	0,10	0,22	0,11
Air compressor RH	1,17	0,67	0,52	0,79
Air compressor O_2 mass fraction	$2{,}7 \cdot 10^{-10}$	$5{,}4 \cdot 10^{-10}$	$1{,}2 \cdot 10^{-10}$	$3{,}1 \cdot 10^{-10}$
Air compressor power	0,18	0,73	1,65	0,85
Cathode humidifier pressure	0,07	0,29	0,68	0,35
Cathode humidifier temperature	0,01	0,07	0,19	0,09
Cathode humidifier RH	0,07	0,14	0,05	0,09
Cathode humidifier O_2 mass fraction	0,26	0,17	0,03	0,15
Cathode gas channels pressure	0,07	0,27	0,63	0,33
Cathode gas channels temperature	0,12	0,09	0,22	0,14
Cathode gas channels RH	0,36	0,92	0,10	0,46
Cathode gas channels O_2 mass fraction	0,57	0,69	1,23	0,83
FC coolant channels temperature	0,21	0,06	0,04	0,10
Radiator temperature	0,009	0,010	0,032	0,017

Table 3.1: Relevant variables MRE [%]

Concerning the simulation times comparison, the figure 3.13 shows all the 100 simulation times for each current profile.

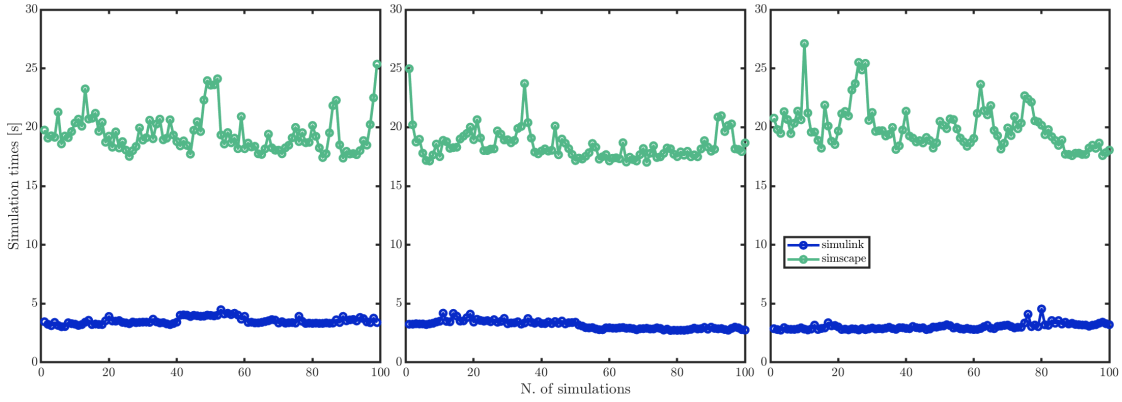

Figure 3.13: Simulation times

Therefore, it's computed the mean simulation time and the respective standard deviation for each current profile. The results are reported in table 3.2, also with

the relative difference between the two models.

The outcomes reveal that for a constant input current profile, the presented model is able to conduct simulations that are about 6 times faster than the Simscape model, that is a reduction of time equal to 83%.

	Mean simulation time [s]		Standard deviation [s]		Δ_{rel} [%]
	Simulink	Simscape	Simulink	Simscape	
1^{st} Current	3,53	19,43	0,3	1,62	81,69
2^{nd} Current	3,17	18,39	0,35	1,09	82,73
3^{rd} Current	3,03	19,94	0,27	1,82	84,63

Table 3.2: Mean simulation time, standard deviation and time relative difference for each current profile

3.1.2 Piecewise constant load

The second set of simulations aims to show another possible scenario in which the fuel cell powers a ship that basically travels at constant speed, but that as a consequence of a stormy sea the ship performs rapid accelerations and breaking. The three "base" currents chosen are the same of the first case (fig. 3.2), so that the fuel cell is tested on three distinct points of the characteristic. In figure 3.14 are reported the current profiles used.

As shown, during the operation of 30 minutes, many step changes of input current occur. This way is tested the fuel cell behaviour in condition of instant load variation. As in the first scenario, 100 simulations are conducted for each current profile and are compared the results by means of graphs comparison and error analysis.

Firstly, in the following graphs are depicted the time history of the most relevant quantities for each current profile, that are the output voltage (fig.3.15), the output power (fig.3.16), the HHV efficiency (fig.3.17), the consumed hydrogen

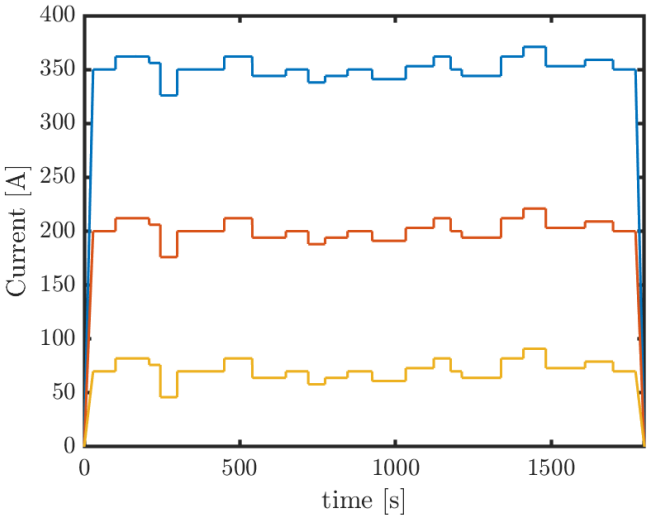

Figure 3.14: 3 load current profiles

(fig.3.18), the stack temperature (fig.3.19), the heat produced (fig.3.20) and the air compressor power (fig.3.21)

In figure 3.17 is presented only the HHV efficiency since the trend of the LHV efficiency is exactly the same. These images shows that the results are very similar in values and shape. The small differences become more visible when considering high input current near to the max limiting current, as in the third current profile.

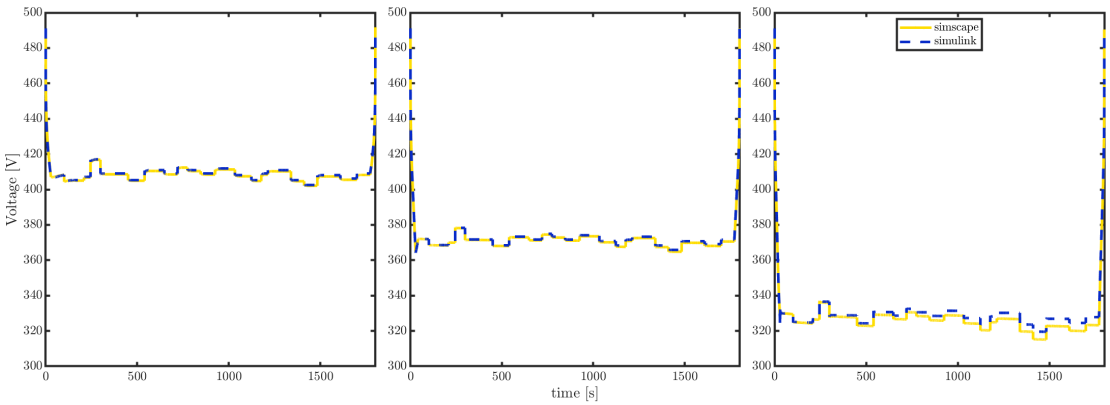

Figure 3.15: Fuel cell stack output voltage

The comparison of the two models is performed also taking into account all the

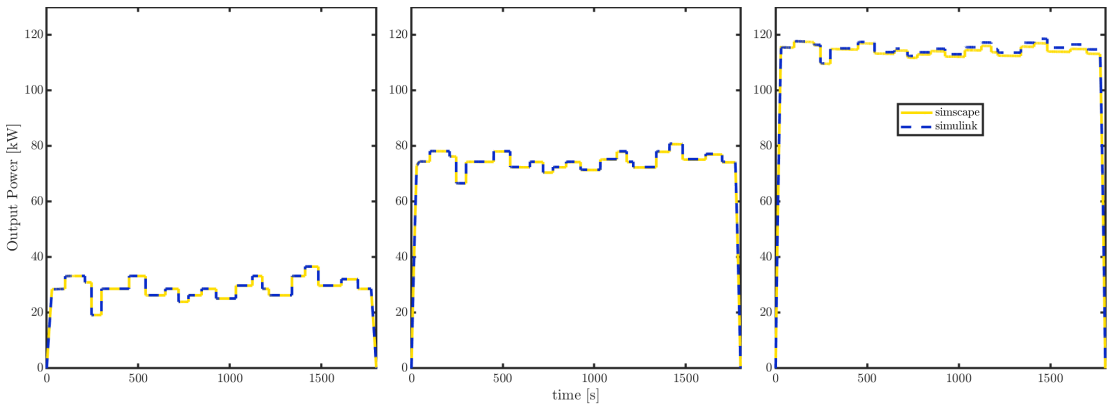

Figure 3.16: Fuel cell stack output power

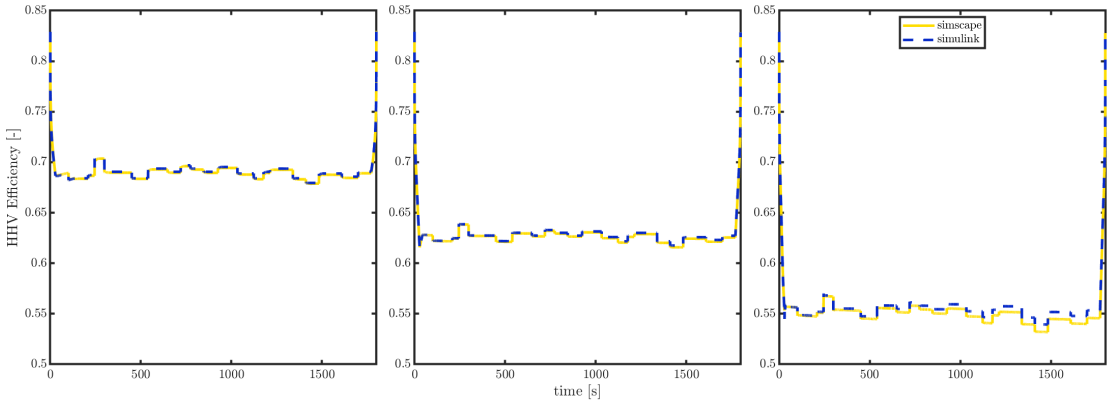

Figure 3.17: Fuel cell stack efficiency

relevant quantities that defines the gas mixture dynamics of each building block of anode and cathode networks. Particularly, has been made the comparison and the error analysis on the temporal evolution of four quantities for each block, that are the internal pressure, temperature, hydrogen or oxygen mass fraction and relative humidity.

For matter of convenience and clarity are presented only the graphs of the anode and cathode gas channels variables time history when the second input current is applied, that is the red line of figure 3.14.

The anode gas channels quantities are reported in (fig.3.22), while the cathode gas channels ones in (fig.3.23).

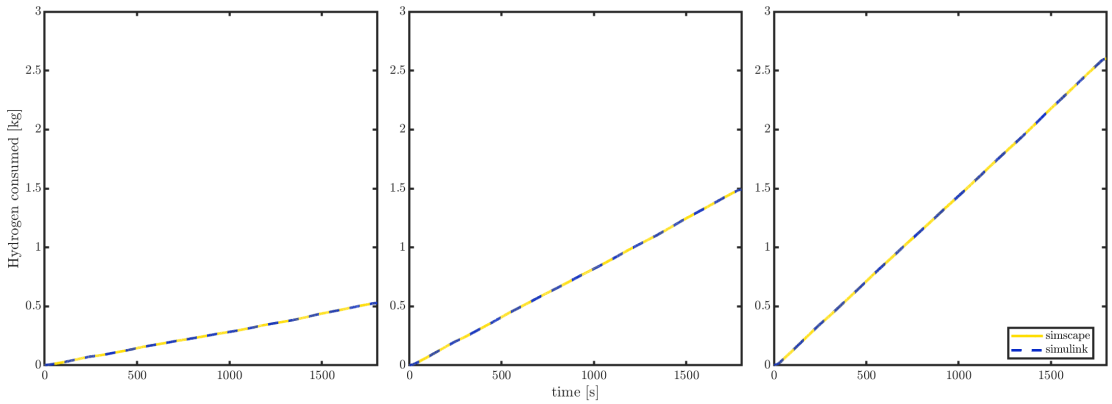

Figure 3.18: Hydrogen consumed

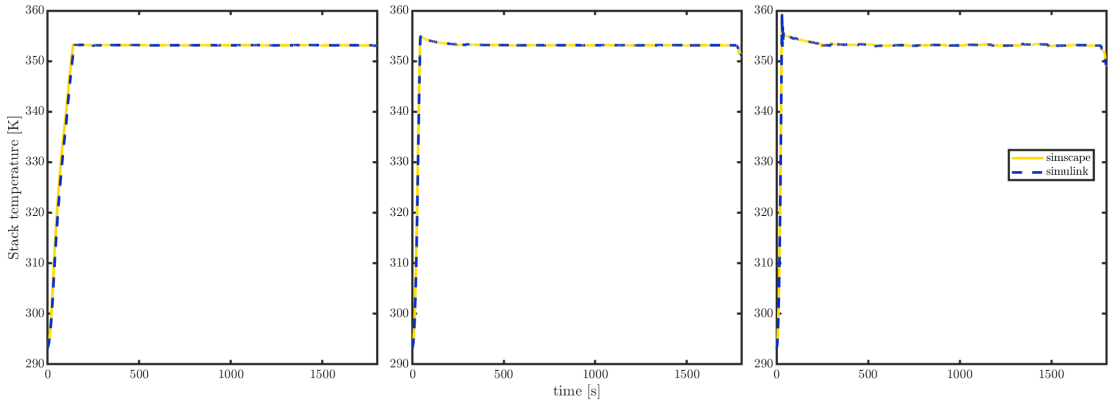

Figure 3.19: Fuel cell stack temperature

Finally, in figure 3.24 are reported the pressure and temperature of the hydrogen tank.

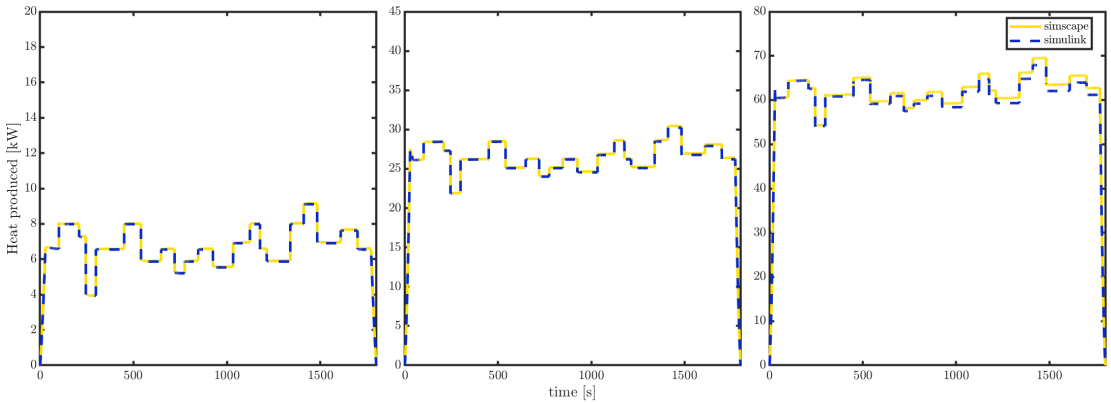

Figure 3.20: Fuel cell heat produced

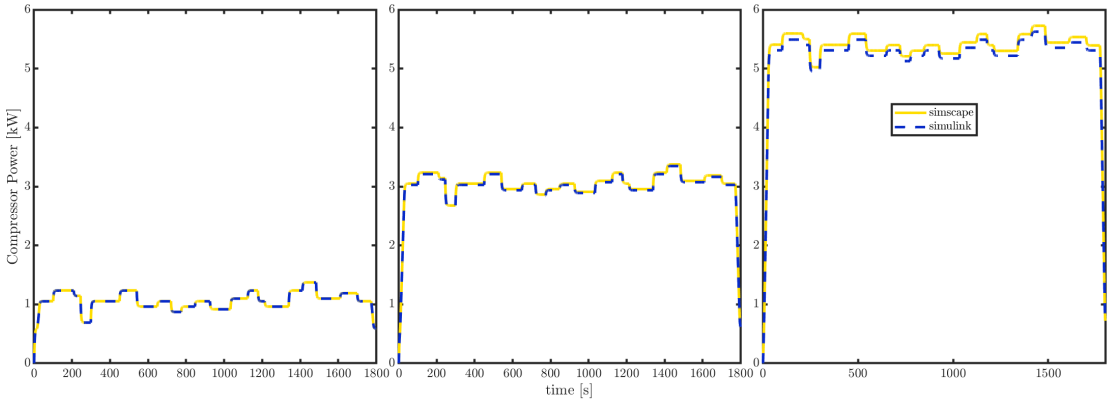

Figure 3.21: Air compressor power

Once the graphical comparison is conducted, a error analysis is performed on each relevant variable of the system. To compare the two system is chosen to employ three different error formulation: the Mean absolute error (MAE), the Root mean square error (RMSE) and the Mean relative error (MRE).

These errors are evaluated averaging the output variable over all the 100 simulation for each current profile, obtaining a error value for each time instant. Then, these errors are averaged over the time, retrieving a total mean error for each variable.

It's chosen to display only the MRE, since provides the best clear comparison of the results. The obtained values are presented in table 3.3. The table is structured

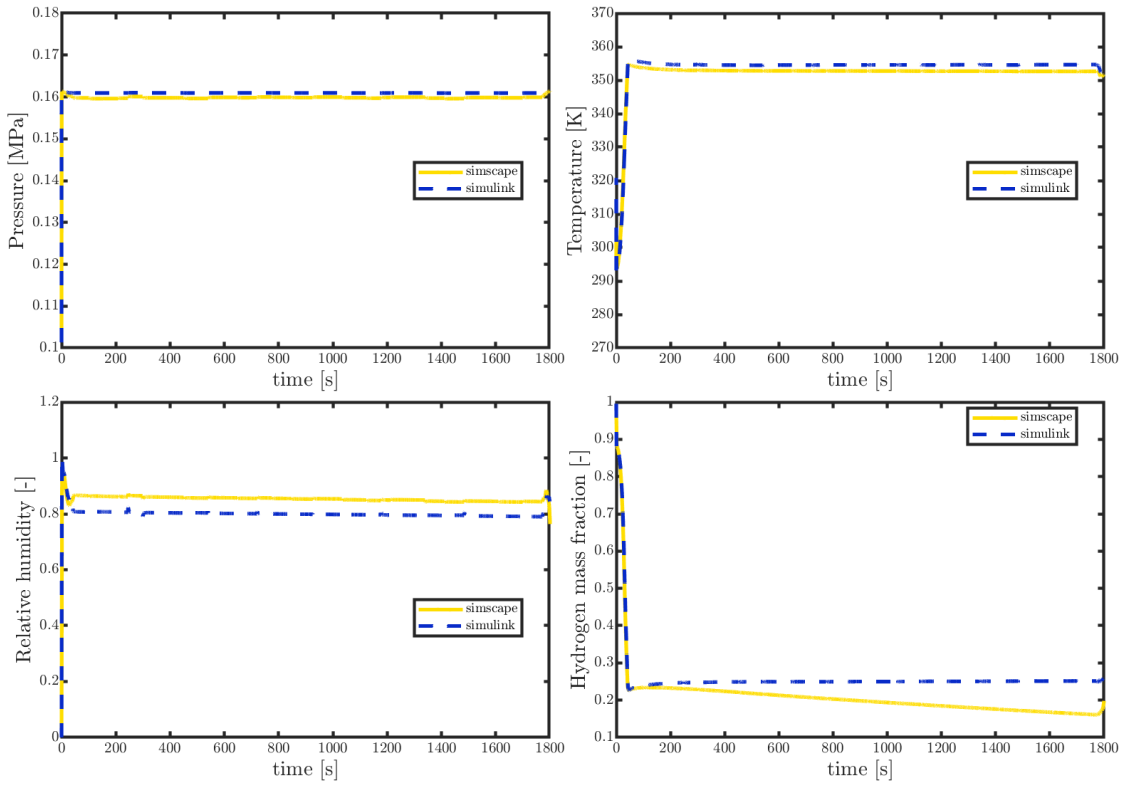

Figure 3.22: Anode gas channels relevant quantities

so that three columns shows the MRE for each variable of interest and in the last column it's reported the mean over all the three current profiles.

Variable	**1^{th} Current**	**2^{nd} Current**	**3^{rd} Current**	**Mean**
Output voltage	0,13	0,16	0,75	0,35
Output power	0,13	0,16	0,75	0,35
Energy produced	0,09	0,09	0,37	0,18
Heat produced	0,59	0,44	1,35	0,8
Stack temperature	0,05	0,01	0,01	0,02
HHV efficiency	0,13	0,16	0,75	0,35
LHV efficiency	0,13	0,16	0,75	0,35
H_2 mass consumed	0,13	0,06	0,08	0,09
Tank pressure	0,0027	0,0015	0,0022	0,0021
Tank temperature	0,0008	0,0004	0,0006	0,0006
Recirculation pressure	0,15	0,88	2,34	1,13

Recirculation temperature	0,18	0,39	0,95	0,51
Recirculation RH	0,28	0,56	2,40	1,08
Recirculation H_2 mass fraction	4,72	15,49	26,48	15,56
Anode humidifier pressure	0,09	0,78	2,19	1,08
Anode humidifier temperature	0,21	0,59	1,38	0,73
Anode humidifier RH	0,07	0,5	2,06	0,88
Anode humidifier H_2 mass fraction	3,22	8,83	10,01	7,38
Anode gas channels pressure	0,06	0,69	2,03	0,93
Anode gas channels temperature	0,33	0,51	0,18	0,34
Anode gas channels RH	3,23	6,25	4,23	4,57
Anode gas channels H_2 mass fraction	6,67	26,83	51,99	28,5
Air compressor pressure	0,07	0,31	0,73	0,37
Air compressor temperature	0,03	0,10	0,22	0,11
Air compressor RH	1,16	0,66	0,53	0,78
Air compressor O_2 mass fraction	$1{,}47 \cdot 10^{-9}$	$1{,}47 \cdot 10^{-9}$	$1{,}2 \cdot 10^{-9}$	$1{,}38 \cdot 10^{-9}$
Air compressor power	0,19	0,73	1,66	0,86
Cathode humidifier pressure	0,07	0,29	0,68	0,35
Cathode humidifier temperature	0,01	0,07	0,19	0,09
Cathode humidifier RH	0,07	0,14	0,05	0,09
Cathode humidifier O_2 mass fraction	0,26	0,17	0,03	0,15
Cathode gas channels pressure	0,07	0,27	0,64	0,33
Cathode gas channels temperature	0,11	0,09	0,22	0,14
Cathode gas channels RH	0,62	0,88	0,10	0,53
Cathode gas channels O_2 mass fraction	0,62	0,69	1,23	0,85
FC coolant channels temperature	0,21	0,06	0,04	0,10
Radiator temperature	0,008	0,01	0,032	0,017

Table 3.3: Relevant variables MRE [%]

Taking into account the simulation times comparison, the figure 3.25 shows all the 100 simulation times for each current profile.

Therefore, it's computed the mean simulation time and the respective standard deviation for each current profile. The results are reported in table 3.4, also with the relative difference between the two models.

The outcomes reveal that for a piecewise constant load, the presented model

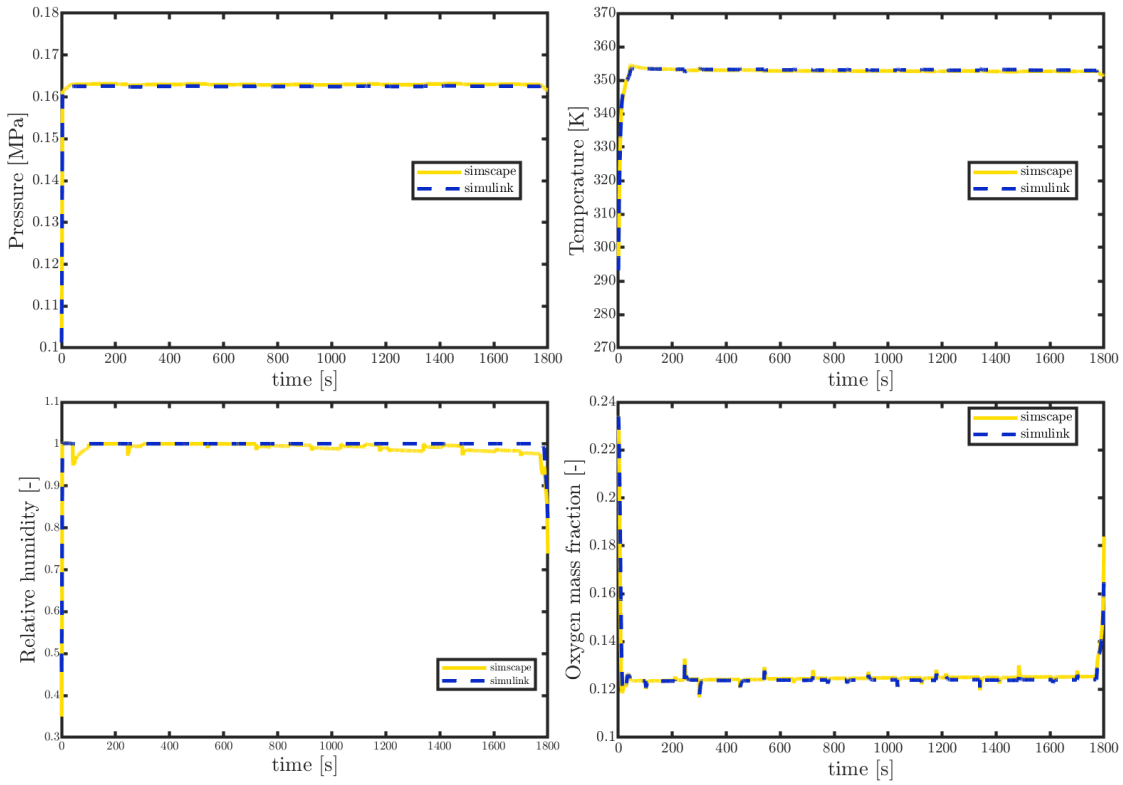

Figure 3.23: Cathode gas channels relevant quantities

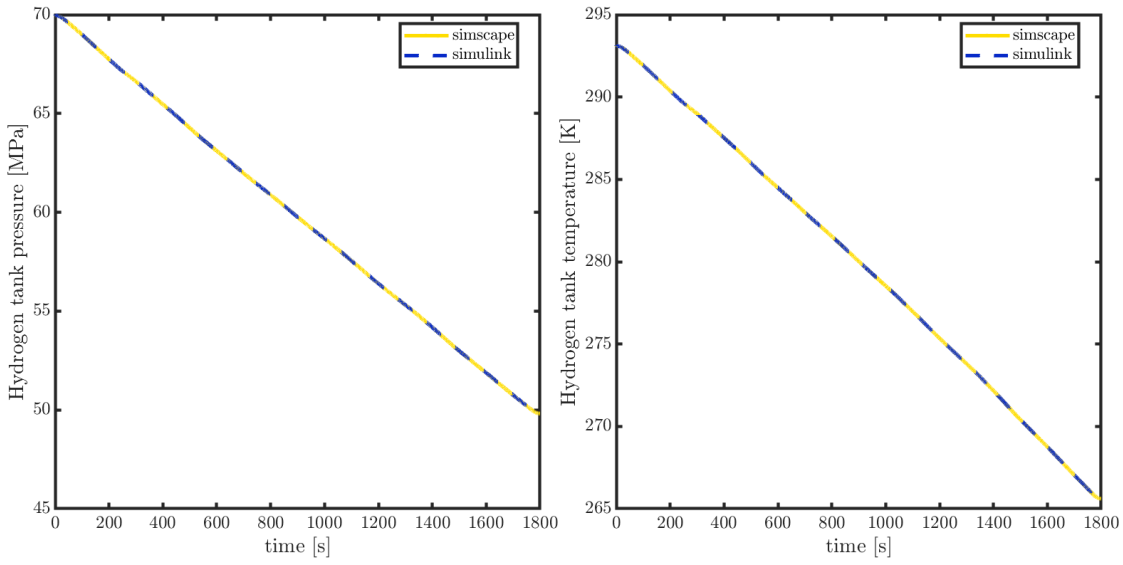

Figure 3.24: Hydrogen tank pressure and temperature

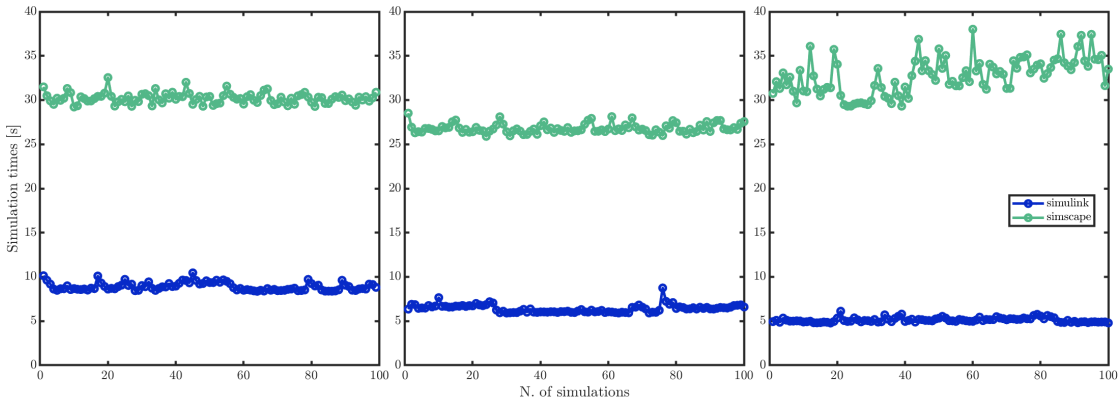

Figure 3.25: Simulation times

is able to conduct simulations that are about 5 times faster than the Simscape model, that is a reduction of time equal to 76,9%.

	Mean simulation time [s]		Standard deviation [s]		Δ_{rel} [%]
	Simulink	Simscape	Simulink	Simscape	
1^{st} Current	8,9	30,21	0,46	0,60	70,48
2^{nd} Current	6,42	26,77	0,44	0,5	76,03
3^{rd} Current	5,12	32,75	0,25	2,07	84,26

Table 3.4: Mean simulation time, standard deviation and time relative difference for each current profile

3.1.3 Irregular load

The third set of simulations aims to show different scenario in which the fuel cell powers a ship that travels at many different velocities that change continuously during the working operation, alternating also period of zero load. This way is tested the fuel cell behaviour in a scenario that emulates a passengers ferry operation.

Again, three irregular load profile have been used, so that the fuel cell is tested

on three distinct RMS values. In figure 3.26 are reported the current profiles used.

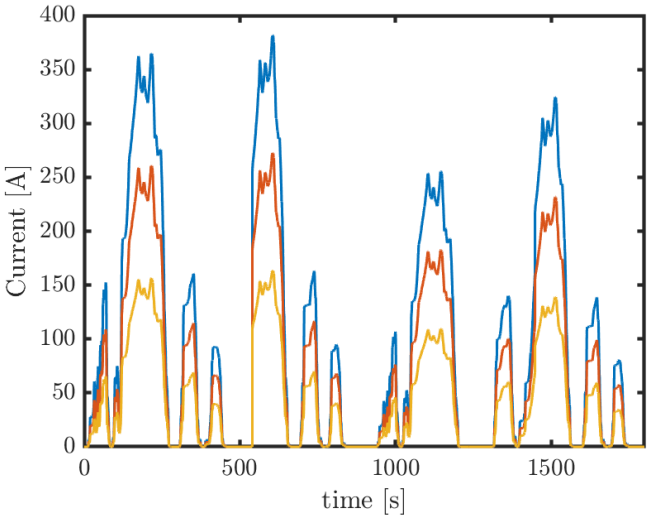

Figure 3.26: 3 load current profiles

As in the others scenarios, 100 simulations are conducted for each current profile and are compared the results by means of graphs comparison and error analysis.

Firstly, in the following graphs are depicted the time history of the most relevant quantities for each current profile, that are the output voltage (fig.3.27), the output power (fig.3.28), the HHV efficiency (fig.3.29), the consumed hydrogen (fig.3.30), the stack temperature (fig.3.31), the heat produced (fig.3.32) and the air compressor power (fig.3.33).

These images shows that the results are very similar in values and shape. Very small differences can be seen.

The comparison of the two models is performed also taking into account all the relevant quantities that defines the gas mixture dynamics of each building block of anode and cathode networks. Particularly, has been made the comparison and the error analysis on the temporal evolution of four quantities for each block, that are the internal pressure, temperature, hydrogen or oxygen mass fraction and relative humidity.

For matter of convenience and clarity are presented only the graphs of the anode

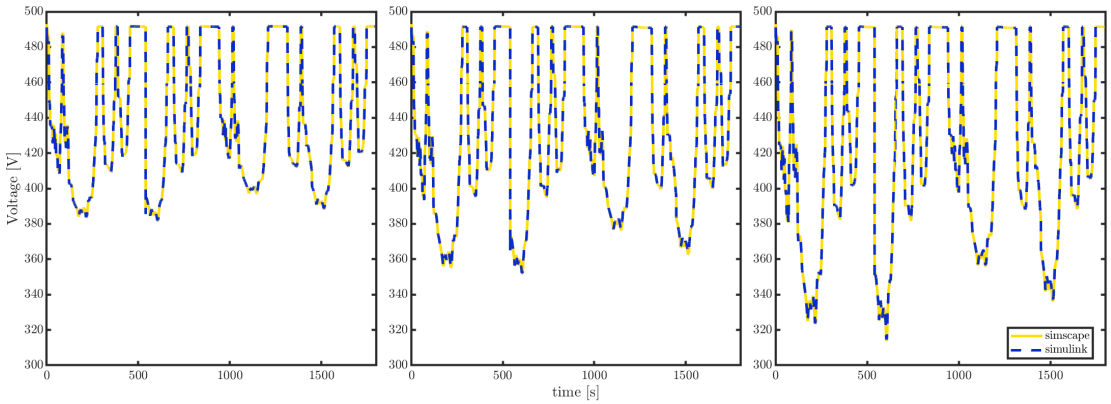

Figure 3.27: Fuel cell stack output voltage

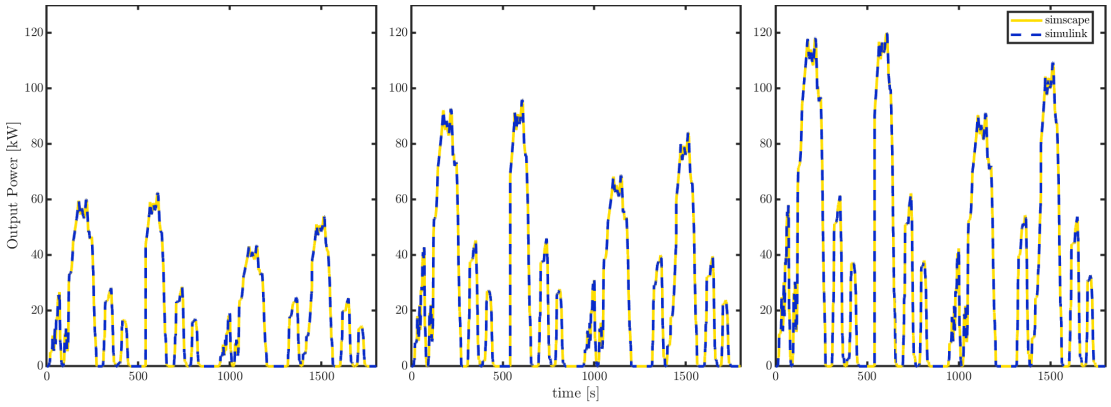

Figure 3.28: Fuel cell stack output power

and cathode gas channels variable time history when the second input current is applied, the red line of figure 3.26.

The anode gas channels quantities are reported in (fig.3.34), while the cathode gas channels ones in (fig.3.35).

Finally, in figure 3.36 are reported the pressure and temperature of the hydrogen tank.

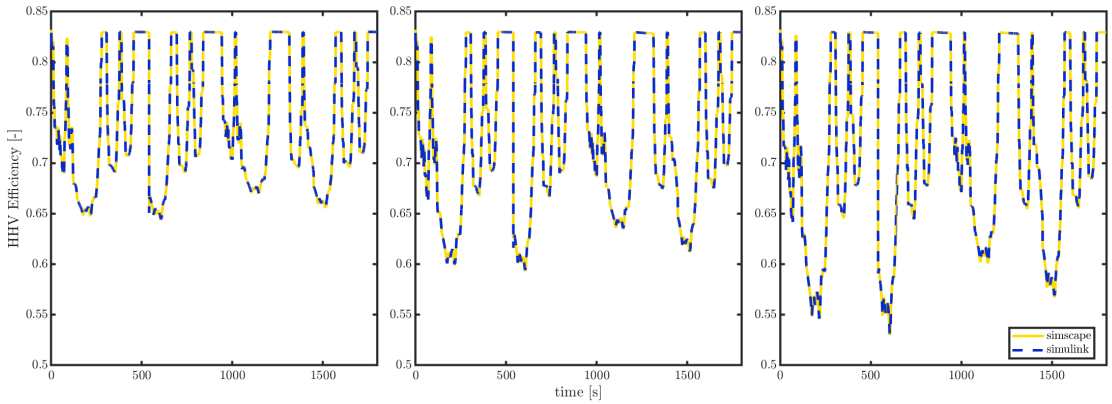

Figure 3.29: Fuel cell stack efficiency

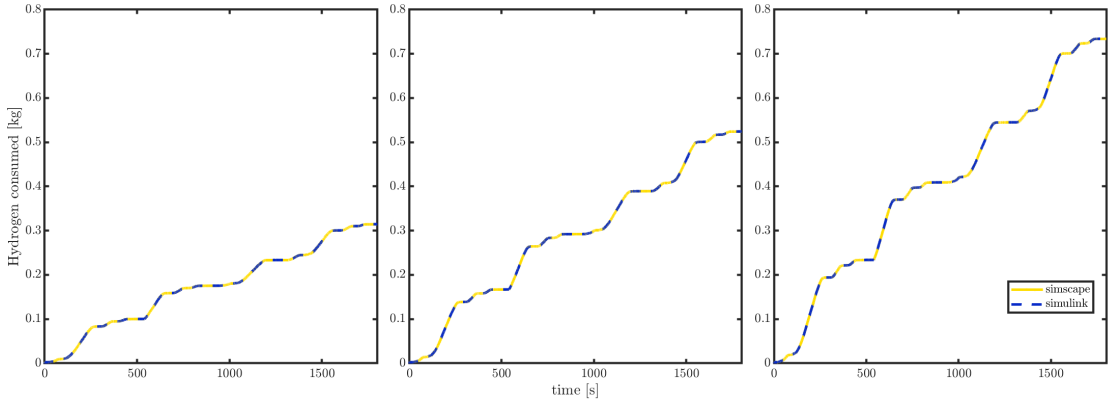

Figure 3.30: Hydrogen consumed

Once the graphical comparison is conducted, a error analysis is made on each relevant variable of the system. To compare the two system is chosen to employ three different error formulation: the Mean absolute error (MAE), the Root mean square error (RMSE) and the Mean relative error (MRE).

These errors are evaluated averaging the output variable over all the 100 simulation for each current profile, obtaining a error value for each time instant. Then, these errors are averaged over the time, retrieving a total mean error for each variable.

It's chosen to display only the MRE, since it provides the best clear comparison of the results. The obtained values are presented in table 3.5. The table is

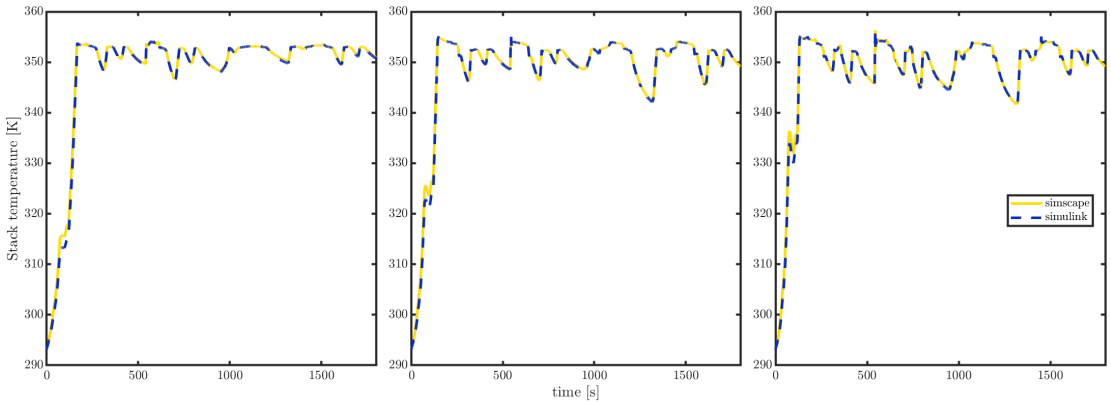

Figure 3.31: Fuel cell stack temperature

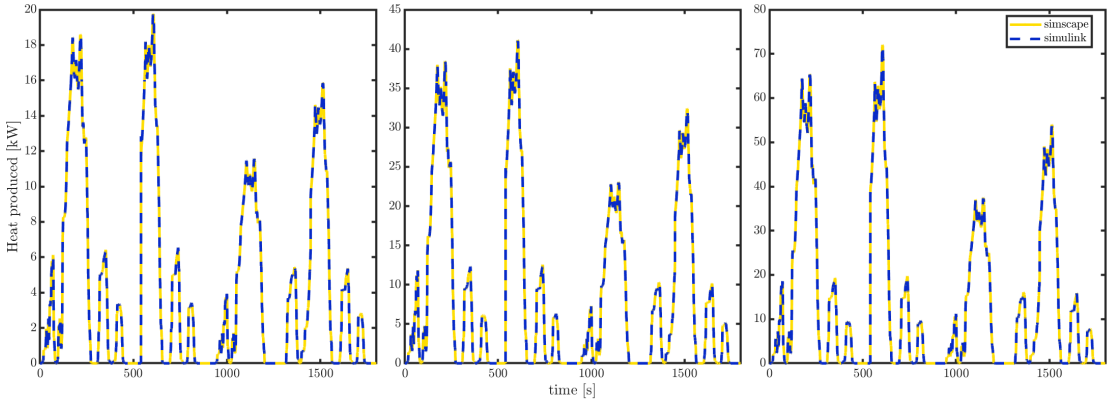

Figure 3.32: Fuel cell heat produced

structured so that three columns shows the MRE for each variable of interest and in the last column it's reported the mean over all the three current profiles.

Variable	**1^{th} Current**	**2^{nd} Current**	**3^{rd} Current**	**Mean**
Output voltage	0,06	0,06	0,08	0,07
Output power	0,06	0,06	0,08	0,07
Energy produced	0,04	0,04	0,06	0,05
Stack temperature	0,08	0,07	0,06	0,07
HHV efficiency	0,06	0,06	0,08	0,07
LHV efficiency	0,06	0,06	0,08	0,07
H_2 mass consumed	0,17	0,12	0,11	0,13
Tank pressure	0,0025	0,0021	0,0022	0,0023

Tank temperature	0,0007	0,00076	0,0007	0,0007
Recirculation pressure	0,14	0,29	0,51	0,31
Recirculation temperature	0,17	0,18	0,20	0,18
Recirculation RH	1,53	2,54	2,66	1,58
Recirculation H_2 mass fraction	3,67	6,48	9,62	6,59
Anode humidifier pressure	0,13	0,26	0,45	0,29
Anode humidifier temperature	0,18	0,20	0,24	0,21
Anode humidifier RH	0,06	0,09	0,14	0,1
Anode humidifier H_2 mass fraction	3,43	5,65	8,39	5,82
Anode gas channels pressure	0,13	0,25	0,44	0,27
Anode gas channels temperature	0,22	0,24	0,22	0,23
Anode gas channels RH	3,19	3,57	6,3	3,35
Anode gas channels H_2 mass fraction	4,55	8,11	12,28	8,31
Air compressor pressure	0,06	0,11	0,18	0,12
Air compressor temperature	0,03	0,04	0,06	0,04
Air compressor RH	1,16	1,05	0,97	1,06
Air compressor O_2 mass fraction	$2{,}6 \cdot 10^{-9}$	$7{,}8 \cdot 10^{-9}$	$2{,}2 \cdot 10^{-8}$	$1{,}08 \cdot 10^{-8}$
Air compressor power	0,17	0,29	0,44	0,30
Cathode humidifier pressure	0,06	0,11	0,17	0,12
Cathode humidifier temperature	0,02	0,03	0,05	0,03
Cathode humidifier RH	0,06	0,07	0,07	0,07
Cathode humidifier O_2 mass fraction	0,24	0,23	0,2	0,2
Cathode gas channels pressure	0,06	0,10	0,16	0,11
Cathode gas channels temperature	0,13	0,13	0,13	0,13
Cathode gas channels RH	1,95	1,69	1,43	1,69
Cathode gas channels O_2 mass fraction	1,88	2,02	2,12	2,01
FC coolant channels temperature	4,29	2,45	1,60	2,78
Radiator temperature	0,009	0,010	0,015	0,011

Table 3.5: Relevant variables MRE [%]

Taking into account the simulation times comparison, the figure 3.37 shows all the 100 simulation times for each current profile.

Therefore, it's computed the mean simulation time and the respective standard deviation for each current profile. The results are reported in table 3.6, also with

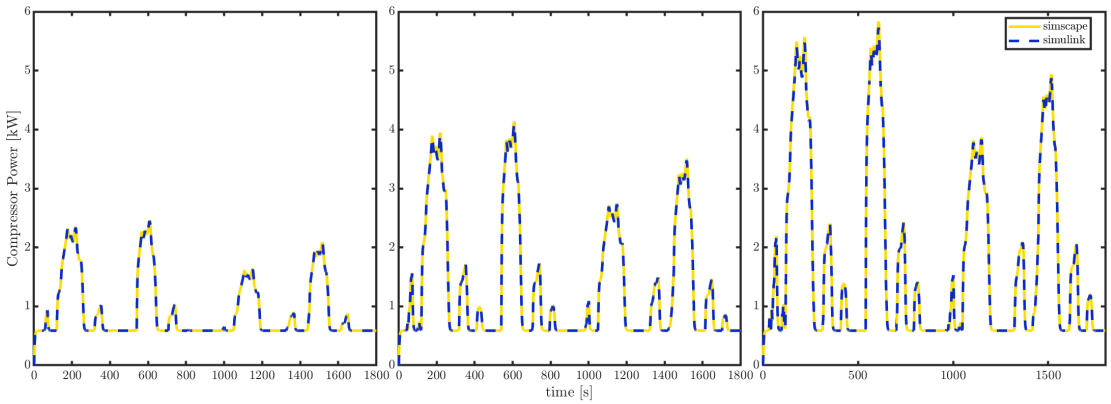

Figure 3.33: Air compressor power

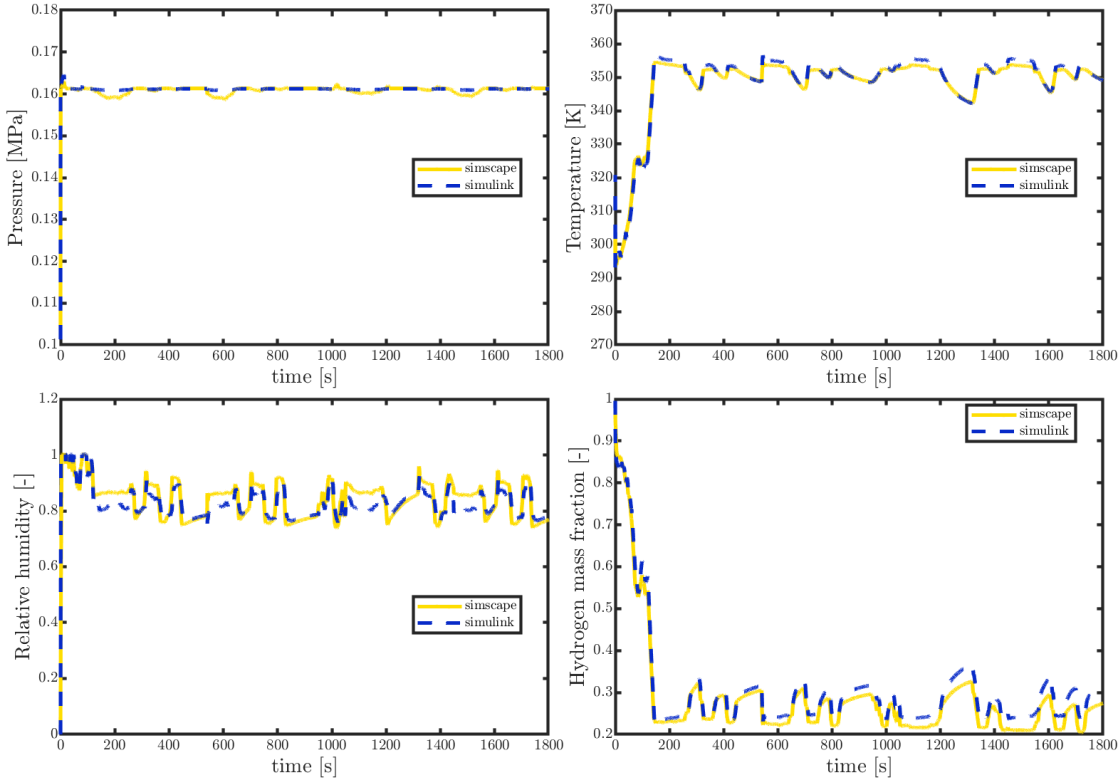

Figure 3.34: Anode gas channels relevant quantities

the relative difference between the two model.

The outcomes reveal that for a irregular load, the presented model is able to conduct simulations that are about 5 times faster than the Simscape model, that

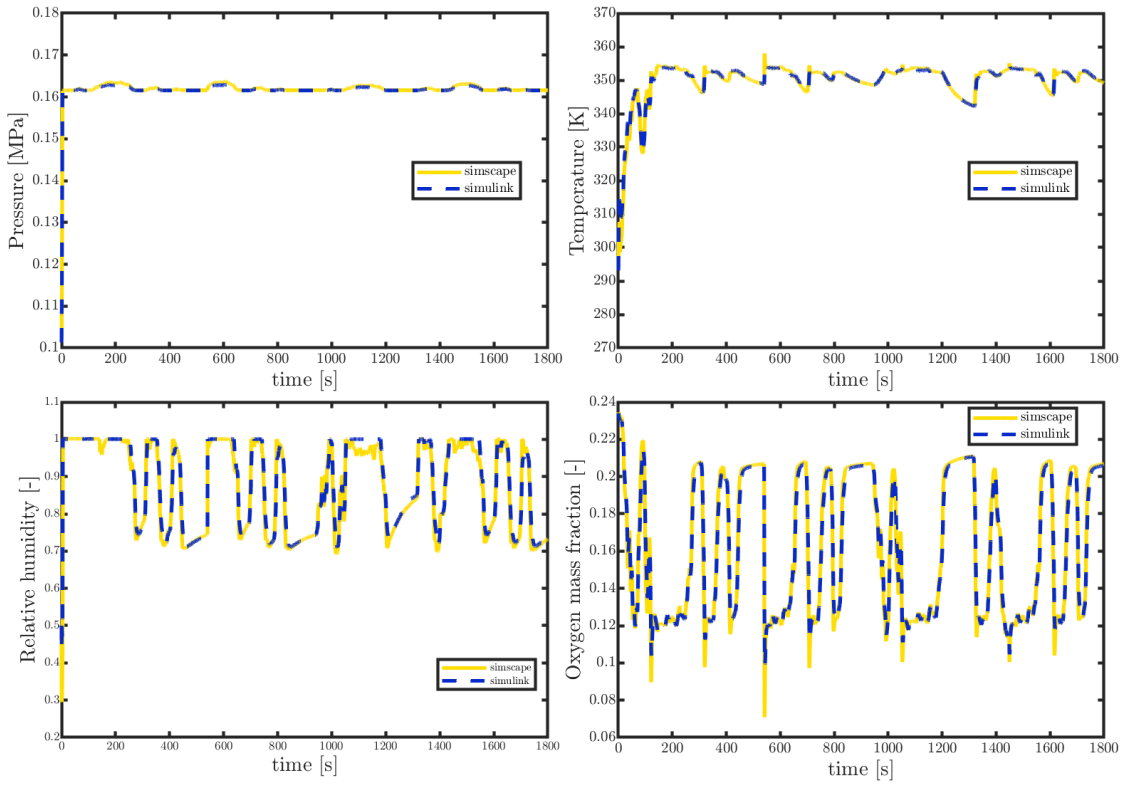

Figure 3.35: Cathode gas channels relevant quantities

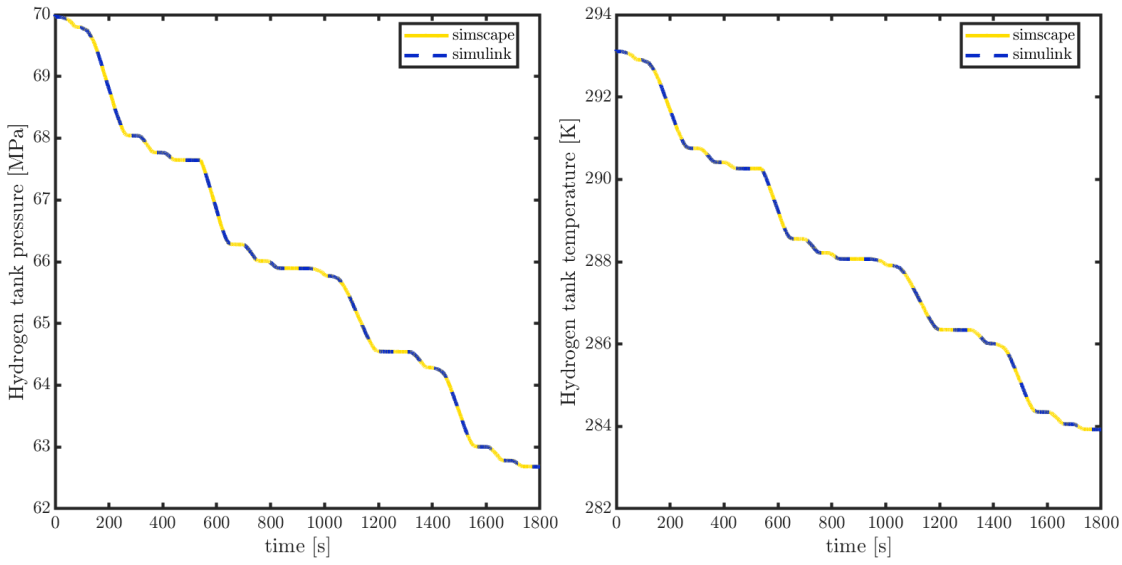

Figure 3.36: Hydrogen tank pressure and temperature

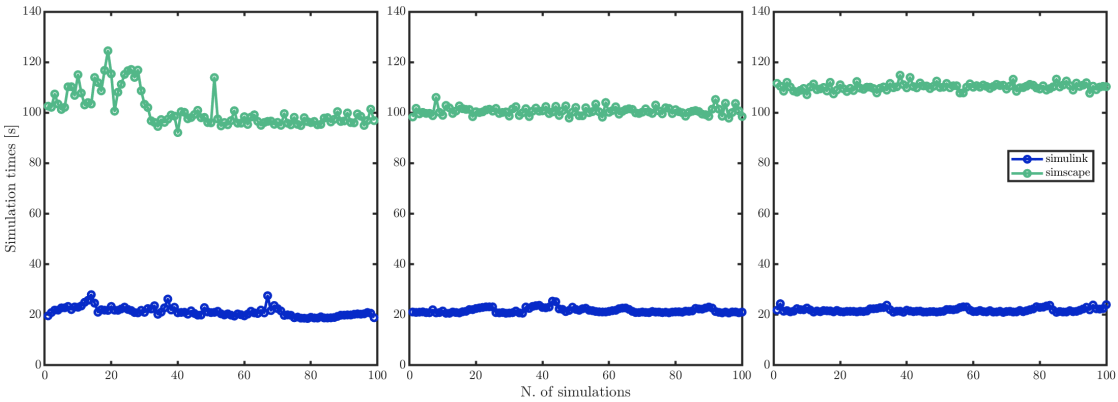

Figure 3.37: Simulation times

correspond to a reduction of time equal to 79,2%.

	Mean simulation time [s]		Standard deviation [s]		Δ_{rel} [%]
	Simulink	Simscape	Simulink	Simscape	
1^{st} Current	21,19	101,04	1,85	6,86	78,98
2^{nd} Current	21,70	100,66	0,98	1,54	78,43
3^{rd} Current	21,82	110,19	0,78	1,35	80,19

Table 3.6: Mean simulation time, standard deviation and time relative difference for each current profile

Chapter 4

PEM Fuel Cell performance analysis

Once the model has been validated, this works aims to test the fuel cell system in two specific maritime scenarios in which it is used as primary energy source. Indeed, the point is to discover which is the most suitable application in which the fuel cell is able to provide an efficient and feasible solution, taking into account also economic aspects.

For this purpose, two important ship routes have been chosen to test the fuel cell:

- **Venetian scenario.** It's taken the route of a passengers ferry that travels in the Venice lagoon, that brings people from one stop to another during the whole day. Thus, here is tested the fuel cell behaviour in a scenario characterized of continuous load variations within a short period of time;
- **Napoli-Ischia scenario.** In this situation a hydrofoil carries passengers from Napoli to Ischia island, completing about ten travel a day. Each trips features almost constant load profile.

The fuel cell system is defined by the same sizing parameters described in the

previous chapters, except for the hydrogen tank volume. The main features are listed below:

- 110 kW PEM fuel cell stack;
- 800 l H_2 tank at 700 Bar;
- 6 kW air compressor.

Considering the load profile that have been created to emulate the two scenarios, it's considered that downstream the fuel cell system are connected the suitable power conditioning units so that the load current flowing into the fuel cell correspond to points in the I-V characteristic that guarantee a sufficient efficiency.

4.1 Venice's lagoon scenario

The Venice lagoon is served by many passengers ferry lines that cover different ares of the lagoon, each with a fixed number of stops. As case study, has been chosen the route that follows the Line 1 ferry. It is shown in figure 4.1. It's one of the most critical situation, since there are many nearby stops in Canal Grande, the most crowded channel.

Figure 4.1: Venice's Line 1 route

In order to create the load profile for this type of route, has been chosen one ferry and has been evaluated the time it takes to travel from one stop to another all over the day. Moreover, it's assumed that some periods of the day are more crowded than other and that certain areas are more frequented that others, leading to a load request variations.

In figure 4.2 it's depicted the load profile, defined as current request. For matter of clarity, the period of the day from 00:00 to 5:00 is not shown, since the ferry is out of service.

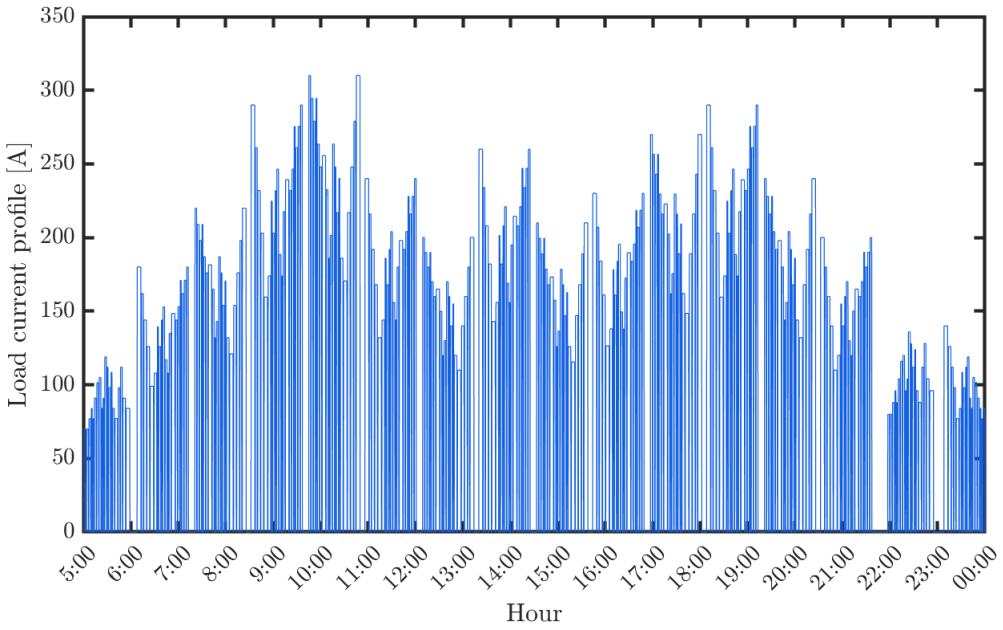

Figure 4.2: *Ad hoc day.* Venice's lagoon scenario load current

In the following graphs are depicted the obtained results. Looking at figure 4.3, it is visible that this type of load profile defines a continuously changing output voltage, so that almost all the points of the I-V characteristic are visited during the daily operation. This is confirmed by the efficiency time history (fig.4.5).

In figure 4.4 are plotted the relevant powers and heat dissipated by the fuel cell system. It's displayed clearly that the air compressor power and the coolant pump power are very small compared to the output electrical power. Instead, the heat

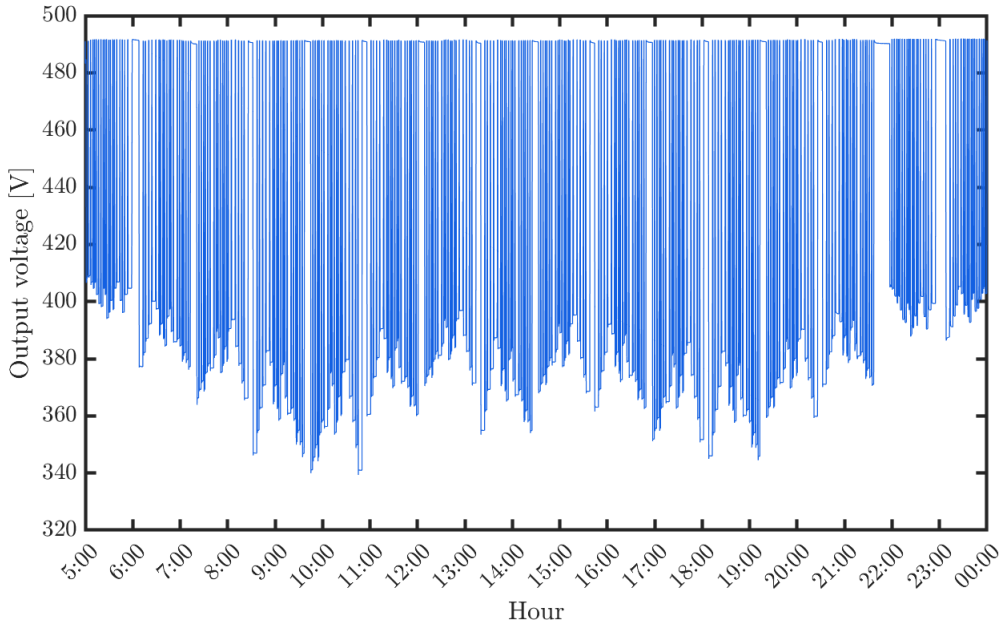

Figure 4.3: *Ad hoc day.* Venice lagoon's scenario output voltage

produced is important, being about the 25% of the electrical power. Finally, in figure 4.6 are represented some relevant temperatures of the system.

4.2 Napoli-Ischia scenario

For what concerns the Napoli-Ischia scenario, some different shipping companies offer services that allow to travel from one place to the other. In order to create the load current profile, has been chosen the route that the Alilauro's hydrofoil makes. The trip is shown in figure 4.7. It's a one way trip that last about 50 minutes without any intermediate stops. During a normal day operation, the hydrofoil makes this trip 8 times back and forth. Consequently, a possible daily load profile is shown in figure 4.8. As in the previous case, it's represented only the period of the day in which the hydrofoil is on operation, that is from 6:00 to 22:00.

Considering a sea route like that, the ferry travels at constant speed for most of the time. Instead, before and after reaching cruise speed the ferry crosses the

ports and here its speed is limited. In addition some periods of the day may be more crowded that others. Thus, this is considered in the current profile.

The model is simulated using this type of input. In figure 4.9 is shown the output voltage all over the day. Analogously, are presented the relevant powers of the system (4.10), the efficiencies (4.11) and relevant temperatures of the system (4.12).

4.3 Performance analysis

For what concerns the performance comparison between the two scenarios, an entire year of service was taken into account for this analysis. This allowed for the evaluation of the fuel cell behavior in various situations. Indeed, the influx of people along these routes varies depending on the time of year, as it is closely linked to the number of tourists present. According to information released by the Municipality of Venice, the highest tourist influx occurs between the months of

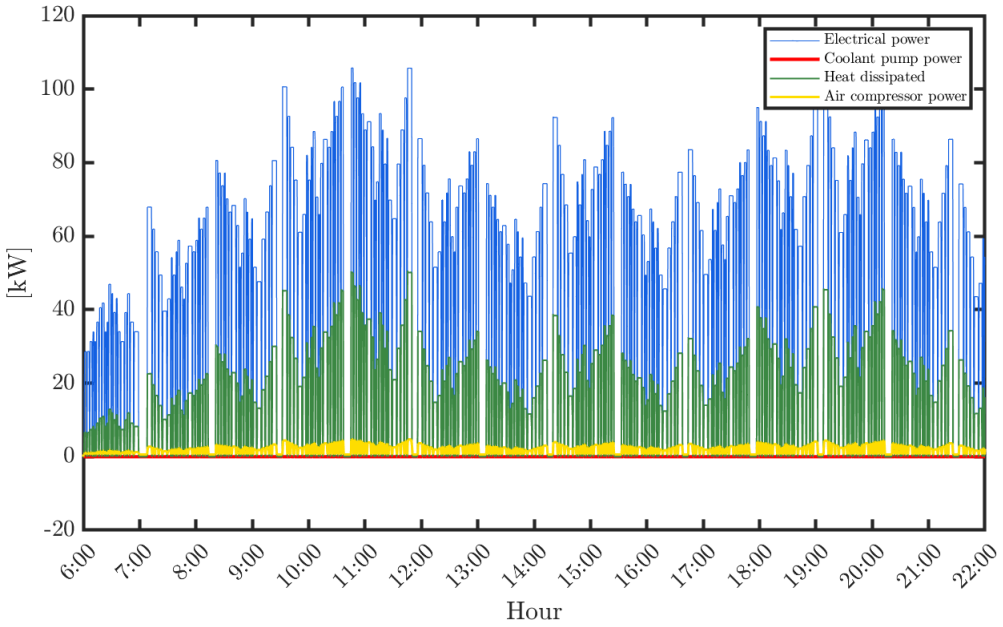

Figure 4.4: *Ad hoc day.* Venice lagoon's scenario output power, air compressor power, coolant pump power and heat dissipated

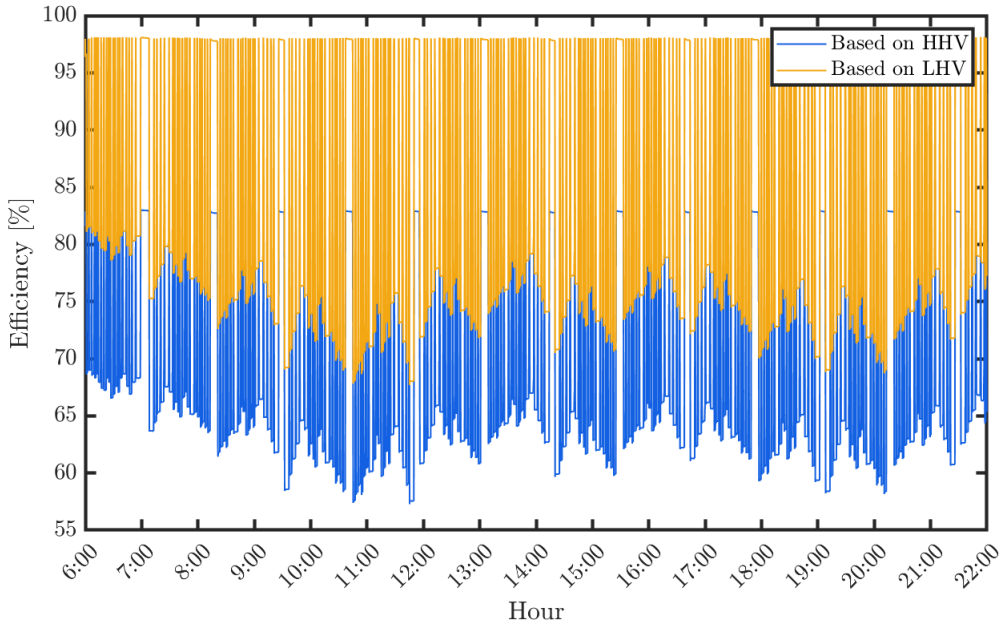

Figure 4.5: *Ad hoc day.* Venice lagoon's scenario HHV and LHV efficiencies

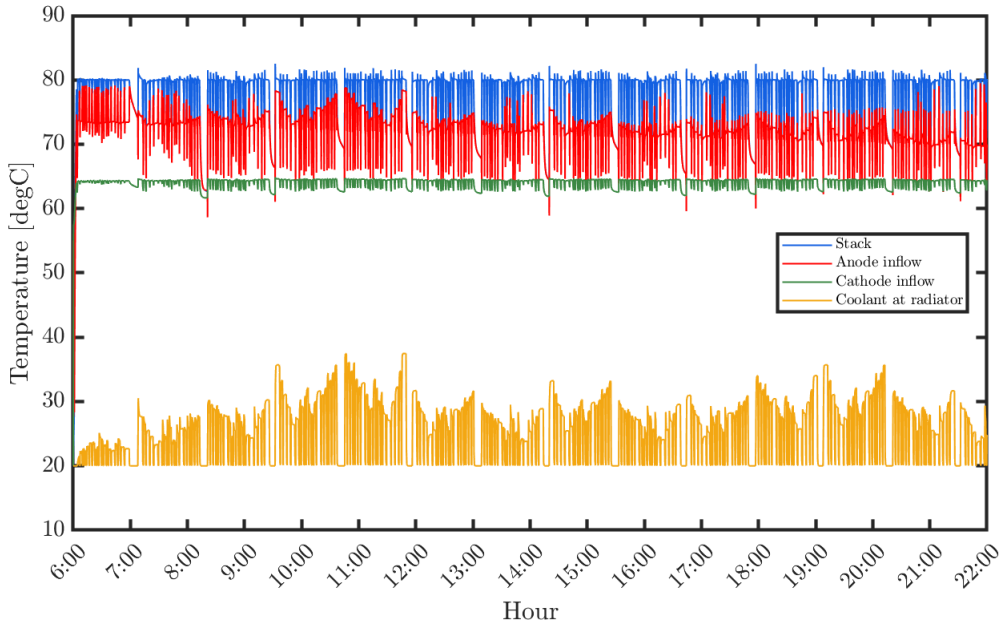

Figure 4.6: *Ad hoc day.* Venice lagoon's scenario relevant system temperatures

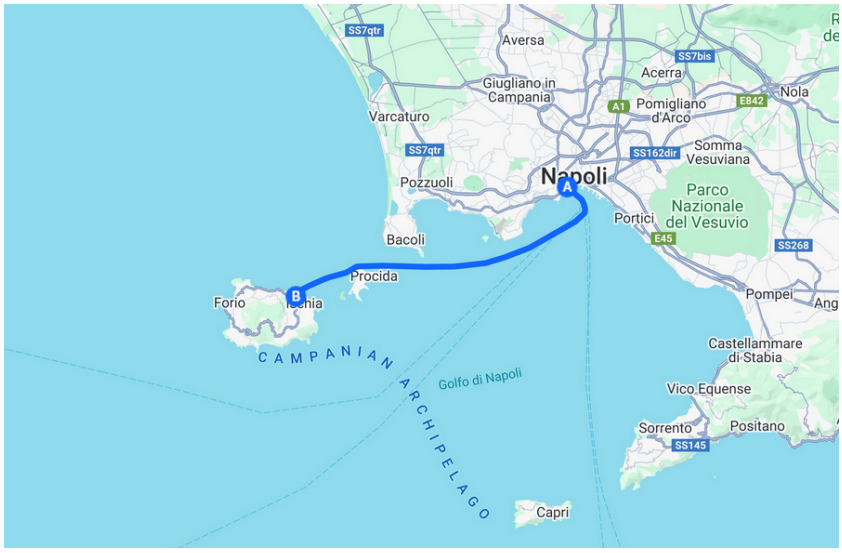

Figure 4.7: Alilauro's hydrofoil route

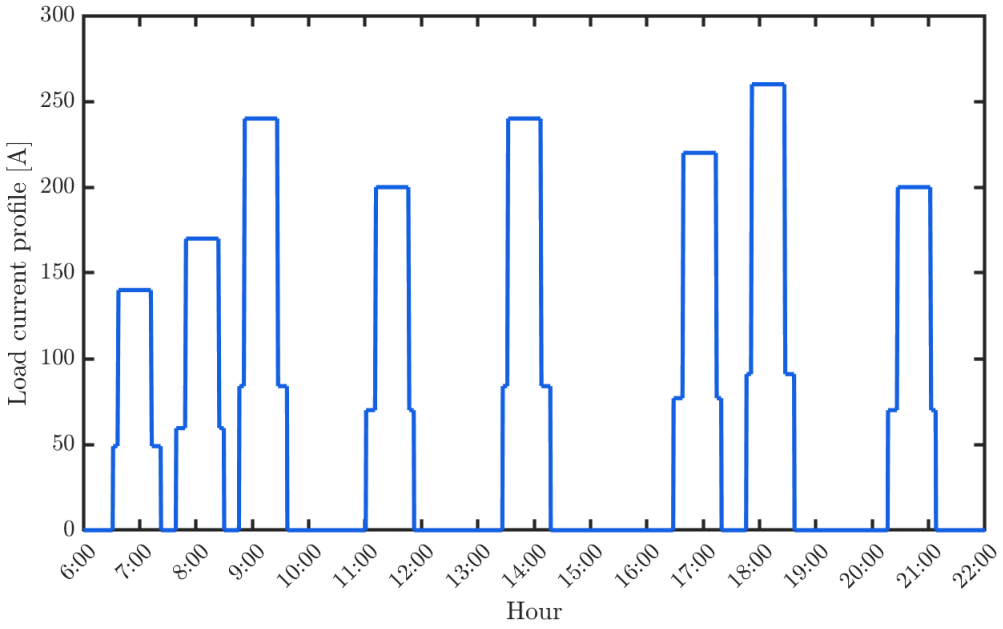

Figure 4.8: *Ad hoc day.* Napoli-Ischia's scenario load current

May and October, with peaks in July and August. During the winter, the number of people decreases[1]. By the way, the total number is still quite high during all the year. A similar trend can be observed on the island of Ischia, although there is

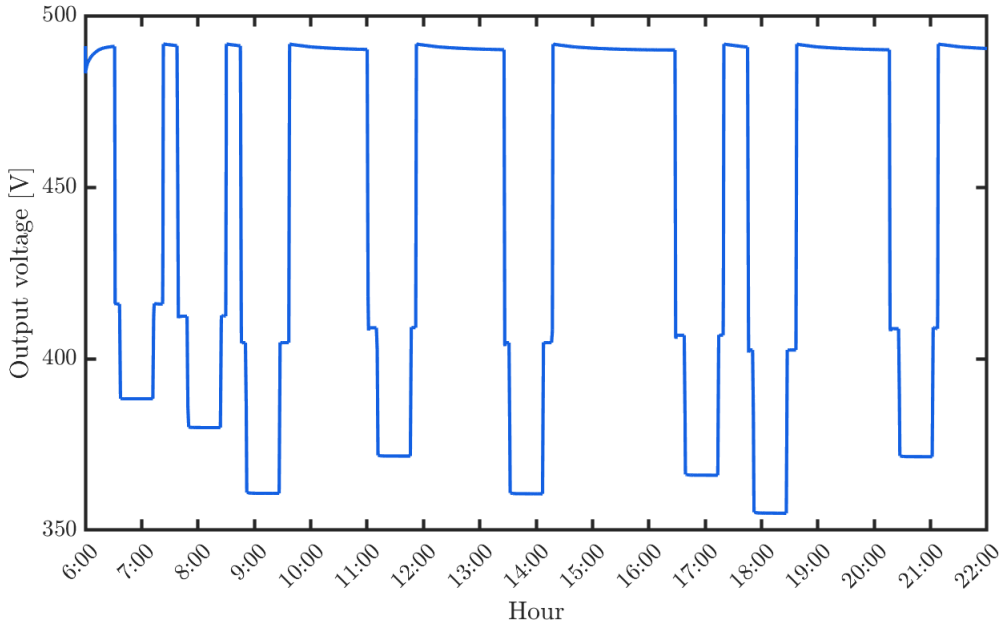

Figure 4.9: *Ad hoc day.* Napoli-Ischia's scenario output voltage

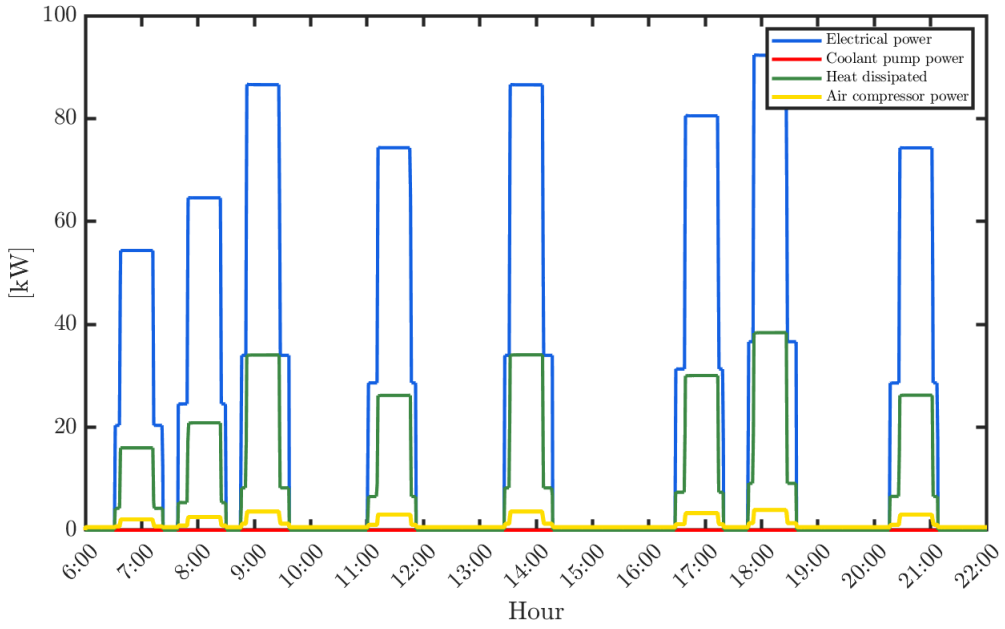

Figure 4.10: *Ad hoc day.* Napoli-Ischia's scenario output power, air compressor power, coolant pump power and heat dissipated

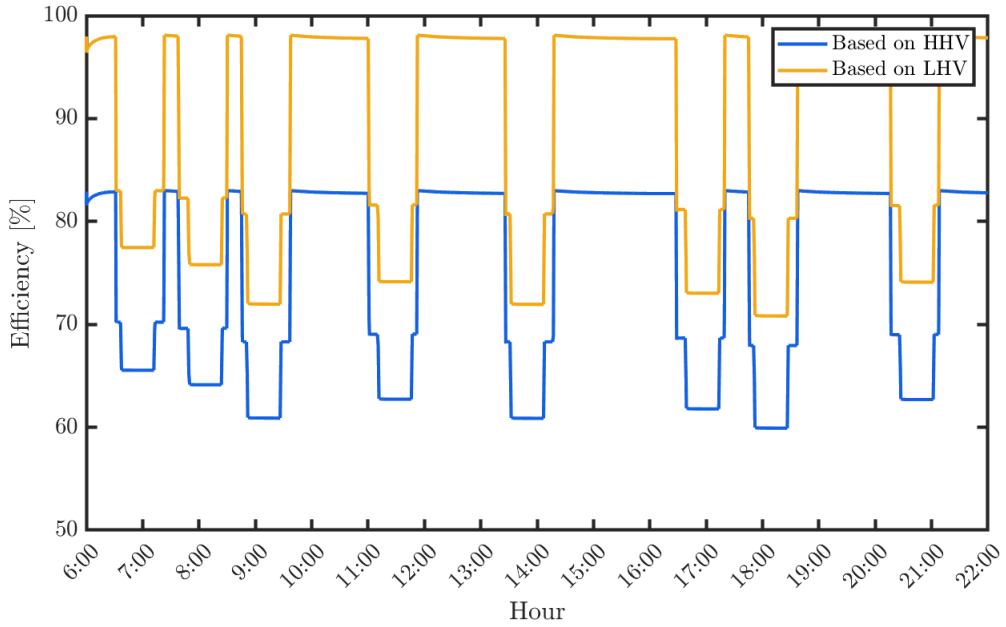

Figure 4.11: *Ad hoc day.* Napoli-Ischia's scenario HHV and LHV efficiencies

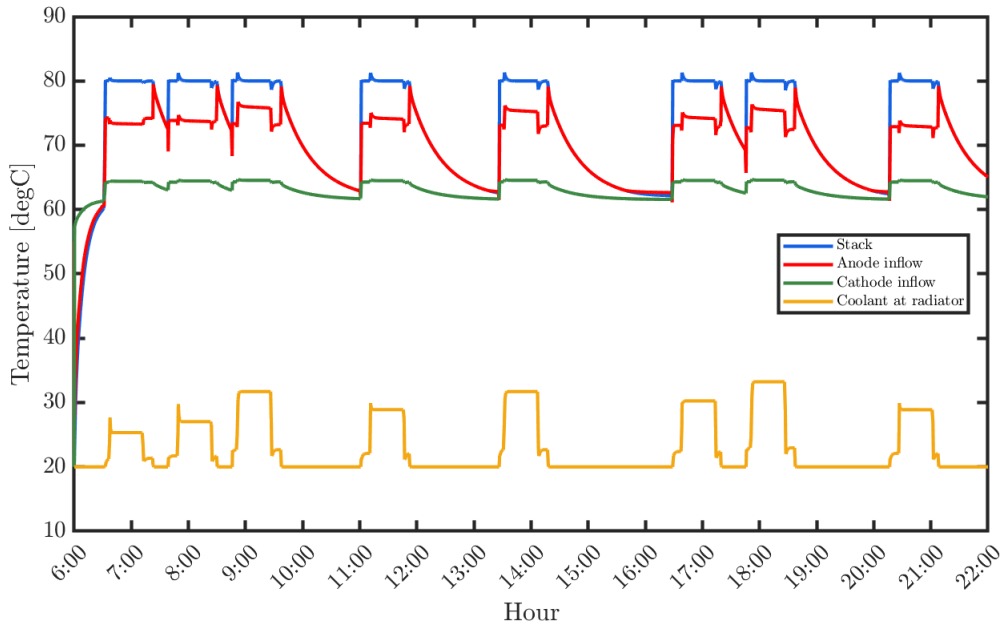

Figure 4.12: *Ad hoc day.* Napoli-Ischia's scenario relevant system temperature

a greater difference in the number of visitors throughout the year, as it is primarily a summer destination.

Therefore, in order to consider these influx variations, the load requests have been adjusted according to the number of passengers using these routes at different times of the year.

Consequently, is performed a weighted average of the variables of interest all over the year, so that a more reliable analysis is carried out. The obtained result considering a year operation are shown in tale 4.1. Here are listed the RMS values of current, voltage and power and the mean efficiency evaluated considering one year of operation.

	$\mathbf{I}_{rms}$ [A]	$\mathbf{V}_{rms}$ [V]	$\mathbf{P}_{rms}$ [kW]	η_{mean} [%]
Venice's lagoon scenario	159,6	387,2	59,6	**65,4**
Napoli-Ischia scenario	145,1	392,4	54,6	**66,2**

Table 4.1: RMS values of relevant quantities for the two scenarios

It is visible that, even though the two scenario's load request are very different, similar results arise. The Napoli-Ischia scenario provides a slightly greater efficiency, about 1%. This means that in terms of efficiency, there are no such marked differences that can justify the use of the cell in one situation rather than another. It can be said that the cell performs admirably in both cases, maintaining a fairly high efficiency value. In figure 4.13 there is a graphical representation of the two mean operating points.

Furthermore, other considerations can be made. First of all, it's rightful speak about the hydrogen consumed in the two scenario. Since the two fuel cells work almost at the same RMS values of current, and since the consumption of hydrogen is proportional to the load current, it worth noticing that the specific consume of hydrogen is also almost the same. In figure 4.14 is depicted the average daily hydrogen consumption in kg.

Looking at the graph, it's clear that in a day the fuel cell of the first scenario consumes much more fuel that the other. It's almost doubled the utilization. This

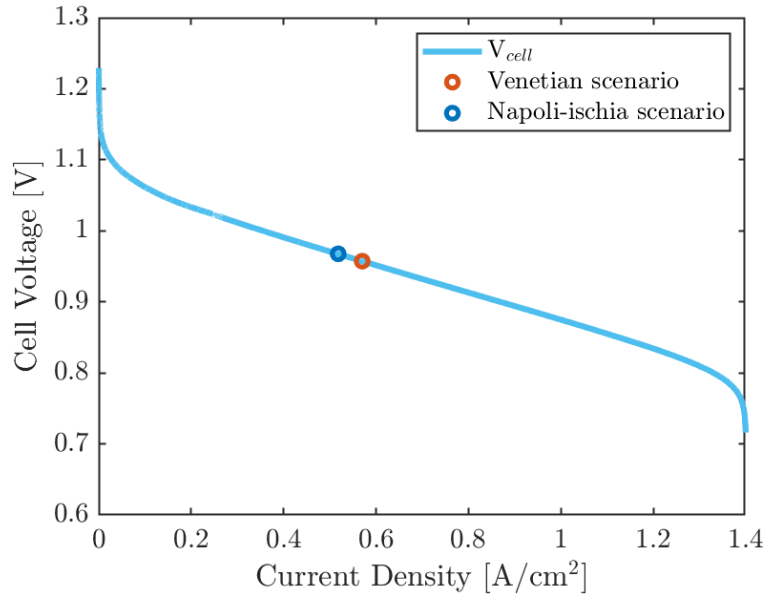

Figure 4.13: Mean operating points of the two scenarios

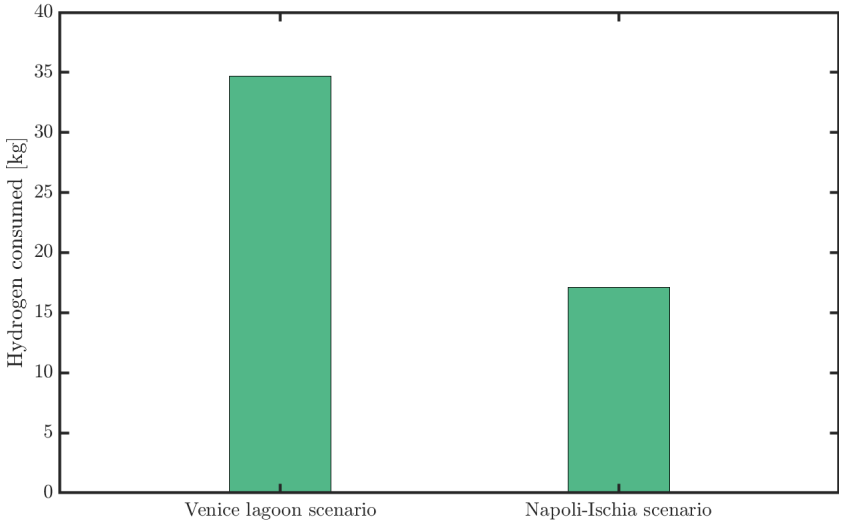

Figure 4.14: Average daily hydrogen consumed

fact is remarked in figure 4.15, in which is shown clearly the differences in the amount of energy involved in a daily operation.

What really matters in this case are the hydrogen refueling considerations. Hydrogen refueling is a critical point in this type of transportation, due to safety

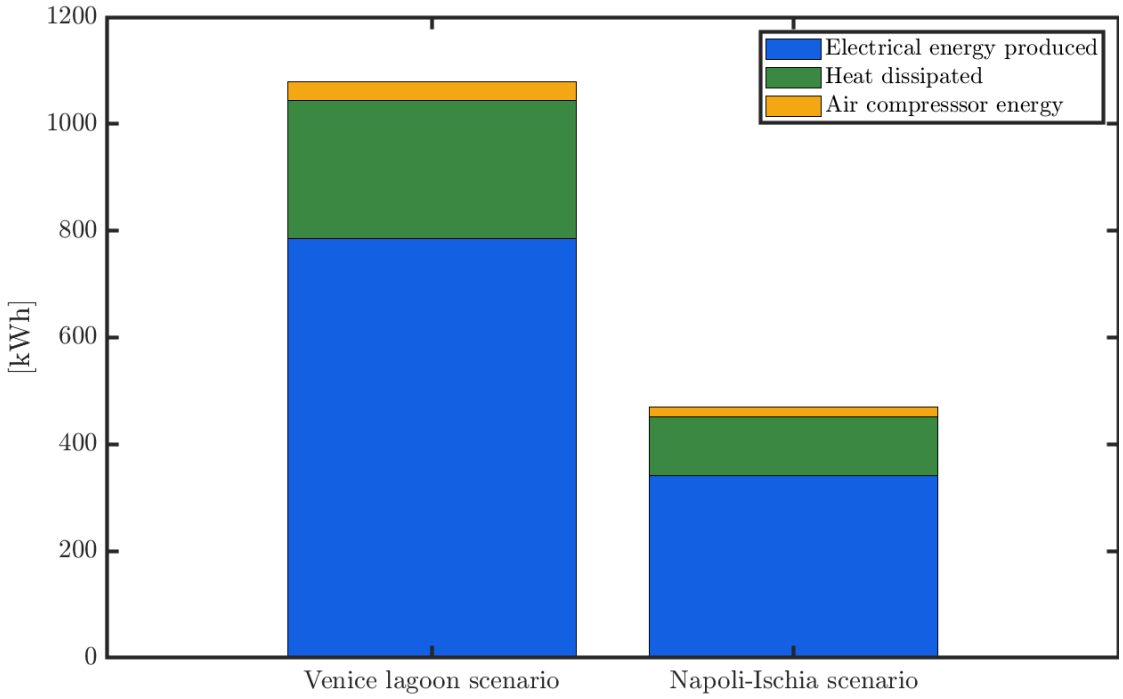

Figure 4.15: Relevant energies for a daily operation

issues and lack of infrastructures. In these simulation is considered that the hydrogen in stored in both situation in a 70 MPa 800 l tank. This way, it could be easier to understand which are the daily consumption and the necessary refueling.

In figure 4.16 are reported the daily time history of the hydrogen tank pressure and the residual hydrogen in the tank, for both scenarios.

The graph reveals that in the Venice's lagoon scenario, using a tank of this dimension is necessary for storing the required hydrogen. Indeed, days with peak of passengers, the consumption are even higher. Moreover, the tank pressure drops below 10 MPa, that is the around the minimum pressure tolerable. Indeed, the hydrogen tank valve control chosen is not able to handle lower pressures. The stack pressure would drops below the setpoint pressure of 0,16 MPa, leading to a performance drop.

Whereas, in the second scenario the hydrogen tank volume is even too big for the required operation. At the end of the day, the tank remains about 60% full.

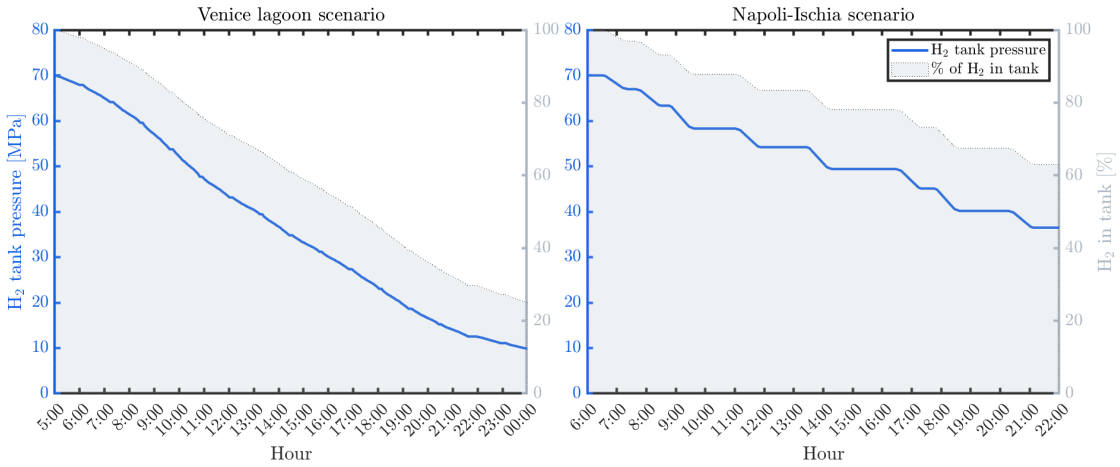

Figure 4.16: H_2 tank pressure and H_2 residual in the tank

Also the tank pressure is still high enough.

Hence, considering the Venetian scenario, since the passengers ferry up time is almost all the day, is necessary an high volume and high pressure hydrogen tank that must be refueled every night. On the other hand, the Napoli-Ischia scenario provides much more logistic flexibility. Firstly, the tank can be refueled around one time every two days, if considering a tank with the previous dimensions. Moreover, since between one travel to another there is always enough time for a refueling in the Napoli's port, a suitable alternative is to employ a smaller tank and/or a lower pressurized tank. This much more worthwhile, in terms of weight, efficiency, reliability and safety.

As final comparison, it's presented a straightforward economical analysis of the feasibility of employing a fuel cell in one scenario rather than another. This analysis is carried considering the daily number of passengers that exploit the service. Using the data in [1], it's retrieved the the total daily income from ticket sales. Then, its assumed that only about the 5% of the revenue is profit that can be used to recoup the investment and that only a little part of it is actually used, since the ACTV's fleet is constituted of several ferries. Thus, it's obtained an income of 864,6 € per day.

For the second scenario, it's directly evaluated the economic resources by considering the total daily number of passengers that travel using the hydrogen powered ferry. This way, is retrieved the total daily income and then is considered that, as in the first case, only the 5% of it is actually available. This value is 233,2€ per day.

Concerning the fuel cell system costs, according to [**?**], the mean cost of the whole system (fuel cell stack and auxiliaries) is 2659€/kW, that is 292460€ in total. Then, is considered a 50% overhead. The operation and maintenance costs are evaluated as the 5% of the system cost [**?**]. Lastly, the cost of hydrogen is 4,6€/kg.

Using these data, two cost functions are constructed that describes the total costs of the system during the years and the earnings that arise. These are shown in figure 4.17. As shown, the goal is to find which is the break-even point for the two scenarios, that is the point at which the total cost of the investment equals the total revenue generated. For both graphs, the blue lines represent the total costs (initial investment and hydrogen cost) while the green lines represent the income through the years.

The analysis shows that for the Venice's lagoon scenario, the break-even point occurs after 629 day, that is about 1,7 years. Whereas, for the Napoli-Ischia scenario it occurs after 2650 days, that is 7,3 year. The difference is very clear and it reflects the characteristics of the two situations. In the first scenario, the fuel cell would be employed in one of the most visited city in the world, that guarantees a high amount of tickets sold during all the year. Moreover, since it's assumed that in both scenario the fuel cell is characterized by the same output power, in the second scenario, in which the ferry reaches a much higher cruise speed, the total number of passengers is significantly reduced, as the incomes. In addition, the mean ticket price is very similar, 17,3€ in the first scenario and 22,5€ in the second. This small difference cannot compensate the difference in the number of sold tickets.

It worth noticing that if in the second scenario a more powerful cell were employed, it would be more cost-effective. Since would lead to more paying people, thus a earlier break-even point. Moreover, as shown the fuel cell would work in a point of the characteristic with a slightly higher efficiency, that becomes relevant in the long run.

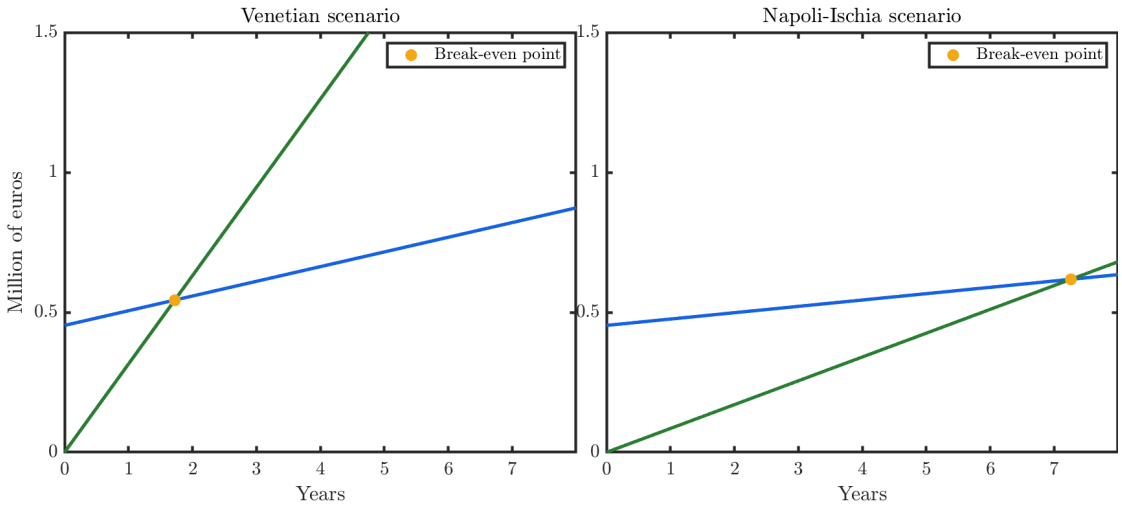

Figure 4.17: Break-even point for the two scenarios

Chapter 5

Conclusion

This work presented a Simulink© model of a Proton exchange membrane fuel cell for shipping industry. This model relies on many sizing parameters that define the whole system layout. These parameters can be easily changed according to the requirements to be respected, i.e. output power, system pressure, stack temperature, hydrogen consumed. This capability is reached thanks to the total developed dynamic modelling, that ensure a very high level of fidelity.

The system building blocks encompass auxiliary components as compressor, humidifiers and cooling system. This way, this model can be used to simulate fuel cell system from few kW to thousands of kW. By tuning the parameters and undergoing an optimisation procedure, the model can be adapted to the required application.

To evaluate the validity of the model, it is compared to the 110 kW PEM Fuel Cell model proposed by Mathworks, Inc employing the same sizing parameters. Thousands of simulation were carried in different possible maritime scenarios and the proposed comparison is made over every single building block. The obtained results shows an overall mean accuracy of about 98,5%. Whereas, considering the most relevant variables of the system, such as output voltage, power, efficiency, stack temperature, hydrogen consumed, hydrogen tank pressure and air

compressor power, the system reaches an accuracy of about 99,5%. Moreover, the simulation times are drastically reduced, since the model runs five time faster than the Mathworks model. Finally, the model ensures a simplified parameters handling and design changes, making definitely the model a perfect candidate for propulsion projects in a wide range of applications.

The model description was accompanied by two possible case study that served the purpose to provide an example of model application. The goal was to discover which scenario could be the most suitable for employing a PEM fuel cell as primary energy source. The results reveals that for an entire year operation the fuel cell works on average at the same operating point, consequently values such as efficiency, output power, and hydrogen consumption are similar. What really discriminates the two scenario are refueling considerations and economic considerations. Indeed, having the possibility to store on board the hydrogen into small tank is always preferable, in terms of weight, reliability and safety. Furthermore, employing a fuel cell system is convenient if it is economically feasible. This is strictly related to the income derived from the paying people that benefit from the service.

Bibliography

[1] Assessorato Al, Turismo Assessore, Simone Venturini, Francesco Bortoluzzi, A Cura Di, Tania Bettiol, Elena Marini, and Sara Rossi Coordinamento. Annuario del turismo, dati 2022, Citta' di Venezia. Technical report, 2022.

[2] Matteo Cavo, Eleonora Gadducci, Massimo Rivarolo, Loredana Magistri, Andrea Dellacasa, Matteo Romanello, Gerardo Borgogna, and Christian Davico. Thermal integration of PEM Fuel Cells and metal hydrides storage system for Zero Emission Ultimate Ship (ZEUS). In *E3S Web of Conferences*, volume 334. EDP Sciences, 1 2022.

[3] Y.A. Cengel. Heat and Mass Transfer-A Practical Approach. 3rd Ed. 2007.

[4] Qin Chen, Zhiqiang Niu, Hongkun Li, Kui Jiao, and Yun Wang. Recent progress of gas diffusion layer in proton exchange membrane fuel cell: Two-phase flow and material properties, 2 2021.

[5] Dung Van Dao, Ganpurev Adilbish, Thanh Duc Le, In Hwan Lee, and Yeon Tae Yu. Triple phase boundary and power density enhancement in PEMFCs of a Pt/C electrode with double catalyst layers. *RSC Advances*, 9(27):15635–15641, 2019.

[6] Martin Dostál, Karel Petera, and Stanislav Solnař. Gnielinski's correlation and a modern temperature-oscillation method for measuring heat transfer coefficients. *EPJ Web of Conferences*, 269:01009, 2022.

[7] Sandip Dutta, Sirivatch Shimpalee, and J. W. Van Zee. Numerical prediction of mass-exchange between cathode and anode channels in a PEM fuel cell. *International Journal of Heat and Mass Transfer*, 44(11):2029–2042, 4 2001.

[8] E4tech. The Fuel Cell Industry Review 2021. Technical report, 2021.

[9] Talal Elammas. Hydrogen fuel cells for marine applications: Challenges and opportunities. *Article in International Journal of Advanced Research*, 2023.

[10] Fuel Cells Bulletin. First fuel cell passenger ship unveiled in Hamburg. Technical report, 2008.

[11] Carlos Fustero Martinez, Paolo Delzano, and Politecnico Di Torino. Hybrid and Fuel Cell Powertrains: two projects for small vessels. Technical report, 2516.

[12] Gabriele G. Gagliardi, Ahmed Ibrahim, Domenico Borello, and Ahmad El-Kharouf. Composite polymers development and application for polymer electrolyte membrane technologies-a review, 2020.

[13] L. Grand-Clement, V. Ruiz, and J. Ihonen. DELIVERABLE 2.4 MARANDA-Marine application of a new fuel cell powertrain validated in demanding arctic conditions. Technical report, 2020.

[14] K. Gurbinder. PEM Fuel Cells. Technical report, 2022.

[15] Alexander Kabza. Just another Fuel Cell Formulary. Technical report, 2016.

[16] Shahram Karimi, Norman Fraser, Bronwyn Roberts, and Frank R. Foulkes. A review of metallic bipolar plates for proton exchange membrane fuel cells: Materials and fabrication methods, 2012.

[17] Lars Langfeldt and Dnv Gl. Maritime Fuel Cell Applications Technologies and ongoing developments. Technical report, 2018.

[18] Meng Li, Jiahao Lu, Yunfeng Hu, and Jinwu Gao. Oxygen Excess Ratio Controller Design of PEM Fuel Cell. In *IFAC-PapersOnLine*, volume 51, pages 493–498. Elsevier B.V., 1 2018.

[19] Weisong Li, Xuezhe Wei, Jiayuan Wang, and Xueyuan Wang. Construction of Nitrogen Content Observer for Fuel Cell Hydrogen Circuit Based on Anode Recirculation Mode. *World Electric Vehicle Journal*, 14(5), 5 2023.

[20] Inc Mathworks. PEM Fuel Cell System, 2023.

[21] Robert A Meyers, Timothy E Lipman, and Adam Z Weber. Encyclopedia of Sustainability Science and Technology Series Editor-in-Chief: Fuel Cells and Hydrogen Production A Volume in the Encyclopedia of Sustainability Science and Technology, Second Edition. Technical report, 2019.

[22] Abd El Monem AA and Ahmed M Azmy. Dynamic Modelling of Proton Exchange Membrane Fuel Cells for Electric Vehicle Applications. *Journal of Petroleum & Environmental Biotechnology*, 5(2), 2014.

[23] E. Moukheiber, G. De Moor, L. Flandin, and C. Bas. Investigation of ionomer structure through its dependence on ion exchange capacity (IEC). *Journal of Membrane Science*, 389:294–304, 2 2012.

[24] Marika Muto, Mayumi Nagayama, Kazunari Sasaki, and Akari Hayashi. Development of porous Pt electrocatalysts for oxygen reduction and evolution reactions. *Molecules*, 25(10), 5 2020.

[25] Trine Nerem. Assessment of Marine Fuels in a Fuel Cell on a Cruise Vessel Trine Nerem Assessment of Marine Fuels in a Fuel Cell on a Cruise Vessel. Technical report, 2018.

[26] E. Planes, L. Flandin, and N. Alberola. Polymer composites bipolar plates for PEMFCs. In *Energy Procedia*, volume 20, pages 311–323. Elsevier Ltd, 2012.

[27] Jay T. Pukrushpan, Anna G. Stefanopoulou, and Huei Peng. *Control of Fuel Cell Power Systems*. Advances in Industrial Control. Springer London, London, 2004.

[28] Annett Rabis, Paramaconi Rodriguez, and Thomas J. Schmidt. Electrocatalysis for polymer electrolyte fuel cells: Recent achievements and future challenges, 5 2012.

[29] Gholam Reza Molaeimanesh and Farschad Torabi. Fuel Cell Modeling and Simulation: From Microscale to Macroscale. Technical report, 2023.

[30] Shuaiba Samad, Kee Shyuan Loh, Wai Yin Wong, Tian Khoon Lee, Jaka Sunarso, Seng Tong Chong, and Wan Ramli Wan Daud. Carbon and non-carbon support materials for platinum-based catalysts in fuel cells, 4 2018.

[31] Colleen Spiegel. PEM Fuel Cell Modeling and Simulation Using MATLAB ®. Technical report, 2008.

[32] T E Springer, T A Zawodzinski, and S Gottesfeld. Technical In-formation Bulletins 465-223,465-225, 465-246. 6. P. Wagner. Technical Report 8, 1991.

[33] Jean St-Pierre and Shangfeng Du. Proton Exchange Membrane Fuel Cells (PEMFCs). Technical report, 2022.

[34] T Tronstad, H.H. Astrand, G.P. Haugom, and L. Langfeldt. Study on the use of fuel cells in shipping. Technical report, 2017.

[35] Federico Ustolin, Alessandro Campari, and Rodolfo Taccani. An Extensive Review of Liquid Hydrogen in Transportation with Focus on the Maritime Sector, 9 2022.

[36] L. van Biert, M. Godjevac, K. Visser, and P. V. Aravind. A review of fuel cell systems for maritime applications, 9 2016.

[37] Berend Van Veldhuizen, Lindert Van Biert, Purushothaman Vellayani Aravind, and Klaas Visser. Solid Oxide Fuel Cells for Marine Applications, 2023.

[38] Xiaoyu Wang, Jianzhong Zhu, and Minfang Han. Industrial Development Status and Prospects of the Marine Fuel Cell: A Review, 2 2023.

[39] Yun Wang. Porous-Media Flow Fields for Polymer Electrolyte Fuel Cells. *Journal of The Electrochemical Society*, 156(10):B1134, 2009.

[40] F.M. White. Fluid Mechanics. 7th Ed. Technical report, 2011.

[41] D. F Young, B. R. Munson, T. H. Okiishi, and W. W. Huebsch. A brief introduction to fluid mechanics. 2011.

[42] Yong Zhang and Zhengkai Tu. Flow-field design of the bipolar plates in polymer electrolyte membrane fuel cell: Problem, progress, and perspective. *Applications in Energy and Combustion Science*, 17, 3 2024.